An Insight into ββ-Enolase Deficiency: Functional Significance of Amino Acid 376

Songping Zhao

A Thesis

in

The Department

of

Chemistry and Biochemistry

Presented in Partial Fulfillment of the Requirements
for the Degree of Master of Science at
Concordia University
Montreal, Quebec, Canada

September 2006

Your file Votre référence
ISBN: 978-0-494-20729-1
Our file Notre référence
ISBN: 978-0-494-20729-1

Abstract

An Insight into ββ-Enolase Deficiency: Functional Significance of Amino Acid 376

Songping Zhao

Enolase, a dimeric enzyme, interconverts 2-phosphoglyceric acid to phosphoenolpyruvate in glycolysis. Due to its catalytic significance, deficiency in this pathway is rare. In year 2000, a male patient was identified with the first case of ββ-enolase deficiency. It was later determined that his β-enolase gene (ENO3) carried two missense mutations changing two conserved amino acids: G156D and G374E. The authors who identified this disease suggested that the stability of the enzyme might have been altered.

Our research focuses on one of the mutations (G374E), which was introduced into yeast enolase. The yeast enzyme was utilized due to its high sequence identity with the human enzyme, multiple known crystal structures bearing conserved structural characteristics and easy laboratory manipulation. The purified G376E protein is folded but nearly inactive. The subunit dissociation constant was increased by 1000-fold. Although the chemical and thermal stability of the enzyme was not greatly altered, the susceptibility towards proteolytic digestion was significantly high due to weaker dimer stability. Furthermore, our kinetic study shows greatly altered catalytic ability and affinity towards metal ion and substrate.

Aside from the original mutation, smaller polar and/or charged amino acids were substituted to examine the cause of the changes observed above. The results indicate that although not directly participating in catalysis or subunit interaction, amino acid 376 plays an important role in subunit interaction and catalytic activity.

Acknowledgments

I would like to extend my sincere gratitude to my research supervisor Dr. Judith Kornblatt for her supervision, consultation and availability. I would also like to gratefully thank my examining committee members Dr. Joanne Turnbull and Dr. Christopher Wilds for their suggestions, time and effort in following the progress of my work. A special thank to Dr. William Zerges who suggested the proteolytic susceptibility experiment. Another special thank to Dr. Peter Ulycznj of the Concordia Center for Structural and Functional Genomics for running my numerous analytical ultracentrifugation sample. Also I would like to thank Alain Tessier, a technician at Concordia University Mass Spectroscopy Center, who has trained me on the Q-ToF instrument and ran samples for me. I would like to thank my colleagues Shujun Liu, and Bonny Choy for support, encouragement and discussion. Another thank you goes to colleagues in the Chemistry and Biochemistry Department, Jiang Heng, Biao Shen, John Manioudakis, Jean-Francois Roy, Julie Bonvin, Yu Lei, Mengwei Ye, Xuying Shan, for their moral support and suggestions. Finally I would to thank my family members, who have selflessly supported me through out my life.

Table of Contents

List of Figures

List of Tables

Abbreviations

Ala	alanine
AUC	analytical Ultracentrifugation
Arg	arginine
CD	circular dichroism
Glu	glutamic acid
Gly	glycine
His	histidine
ITC	isothermal titration calorimetry
KOAc	potassium acetate
$NaClO_4$	sodium perchlorate
NaOAc	sodium acetate
OD	Optical Density
PEP	phosphoenolpyruvate
PhAH	phosphonoacetohydroxamate
Phe	phenylalanine
PGA or 2-PGA	2-phosphoglyceric acid
Pro	proline
Ser	serine
TAE	Tris/Acetic acid/EDTA
TE	Tris/EDTA
TLCK	Na-Tosyl-L-lysine chloromethyl ketone hydrochloride
UV	ultraviolet
Val	valine

Chapter 1 Introduction

1.1 General overview of enolase protein

Enolase, a dimeric enzyme (Figure 1.0), (2-phospho-D-glycerate hydrolyase, EC 4.2.1.11) catalyzes the interconversion of 2-phosphoglyceric acid (2-PGA) and phosphoenolpyruvate (PEP) in glycolytic pathway and gluconeogenesis pathway. It requires two divalent metal cations to catalyze the reaction and the binding order is first metal ion, substrate, then second metal ion. Enolase is a very common enzyme that is found in almost all organisms that metabolize sugars (*1*) and it was first isolated and purified from yeast as early as 1942 (*2*). There are three genes in mammals that encode for three different enolase isozymes. They are α, β, and γ isozymes; α-isozyme is found in major organs and various tissues; β-isozyme is expressed in muscle tissues; γ-isozyme is neuronal specific. Although the enolase does not have any regulatory properties (*3*), they are tissue specific in many species. Furthermore, due to the overlap of expression system, both homo- and hetero- dimers are found. The first mammalian enolase (from rabbit muscle) was sequenced by Chin in 1990 (*4*).

On the other hand, there are two genes coding for enolase isozymes in *Saccharomyces cerevisiae*: ENO1, and ENO2. ENO1 gene encodes for enolase 1. The amino acid sequence was first obtained both by sequencing of the protein and the gene in 1981 (*5-7*). ENO2 gene encodes for yeast enolase 2. The expression of these two isozymes are under metabolic and developmental control (*8*). The study confirms the expression of two enolase genes in yeast. Furthermore, it was found that by altering the growth condition (ex. in ethanol vs. in glucose) different amount of yeast enolase 1 and yeast enolase 2 were expressed (*8*).

Most of the enolases isolated to date are dimeric proteins, with the exception of enolase from thermophilic bacteria and a few other bacteria, which are octameric. (*9*) Although the specific metabolic advantage of having an octamer over a dimer is still unknown, C.K. Brown's group has proposed that the octameric structure contributes to the higher thermal stability (*9*). The dimeric enolase molecular weight ranges from 80 to 100k daltons. Yeast enolase 1 isozyme is 436 amino acids long and weighs 46671 daltons (*6*). Enolase is the only enzyme that catalyzes the dehydration reaction in glycolysis, and among different species, most characterizations were carried out on yeast enolase (*10*).

Enolase's amino acid sequence is conserved enzymes among different species. Yeast enolase 1 and human β-isozyme share approximately 63% of protein sequence identity and 79% of sequence similarity, whereas β-isozyme from rabbit muscle and human are almost identical with a high 97% sequence identity.

There are multiple crystal structures obtained from different species, including yeast (*11, 12*), lobster (*13*), *E. coli* (*14*), and even human γ-isozyme (*15*). When superimposed, yeast, lobster and *E. coli* enzyme showed great similarity in terms of tertiary structure, which suggests that the quaternary structure may also be conserved. The active site topology and key residues involved in catalysis are all well conserved as well (*14*).

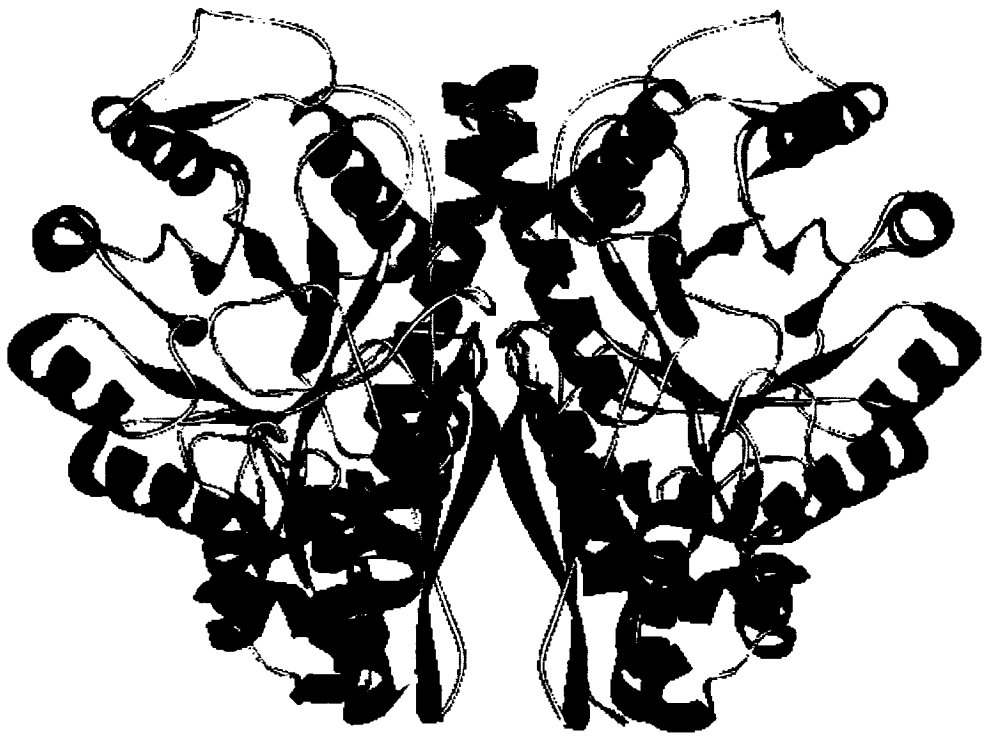

Figure 1.0: Yeast enolase structure. The secondary structures were highlighted (helix: red; sheets: blue). The picture was generated by WebLab ViewerLite software using 1one.pdb from RCSB Protein Data Bank. (http://www.rcsb.org).

1.2 Enolase structure

1.2.1 Secondary and tertiary structure of enolase

As mentioned earlier, enolase, in most organisms, is a dimeric protein of two identical subunits. Each subunit is composed of one continuous polypeptide chain. To date, there are over 20 high-resolution crystal structures described and available from different species and with different substrates or analogues and metals bound. These structures have provided a great deal of information regarding enolase such as conservation of secondary and tertiary structure, structure of the catalytic site, cofactor and substrate orientation in active site and inhibition, and possible asymmetry of two subunits.

Currently, all enolases reported have similar structural characteristics. All subunits consist of two domains. A smaller N-terminal domain, extending from amino acid 1 to 142 (in yeast), contains four β-sheets and three α helices. This domain is mainly responsible for interaction with the other subunit and contains a mobile loop. The loop contains a serine residue that interacts with the second metal upon loop closure over the active site. The rest of the chain (143-436) is the main catalytic domain, which has a shape of a barrel consisting of 8 β-sheets surrounded by 8 α-helices. Although the α/β-barrel is a commonly seen secondary structure feature among catalytic enzymes such as triosephosphate isomerase, all enolases adopt a slightly unusual $\beta\beta\alpha\alpha(\beta\alpha)_6$ topology (*11*). This topology layout is illustrated in Figure 1.1 (*14*). The major mobile loops of the enolase are between S3-H1, S4-S5, and S6-H7. The domain boundary is also shown on the Figure 1.1 (*14*).

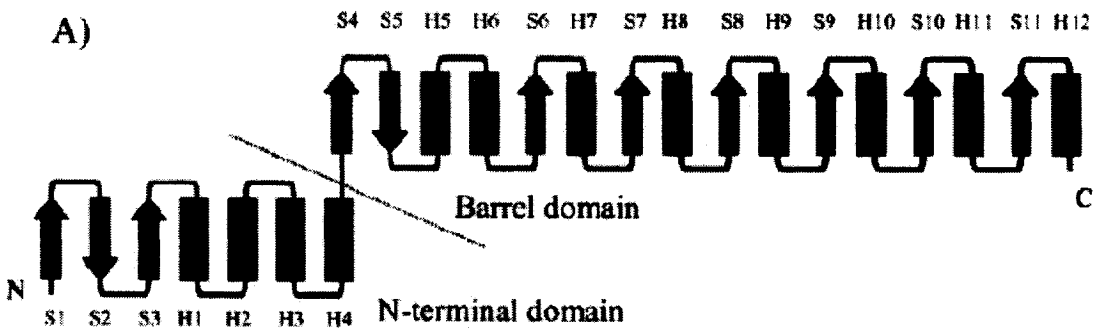

Figure 1.1: Enolase topology of $\beta\beta\alpha\alpha(\beta\alpha)_6$. Here α-helices are shown in solid bars with an H notation, β-sheets are shown in arrows with S notation (*14*).

Name	Secondary Structure Label	Amino Acid Residues
Anti-Parallel β meander	Strand S1	5-13
	Strand S2	17-25
	Strand S3	29-35
Helices of N-terminal domain	Helix H1 (L)	61-80
	Helix H2 (K)	86-96
	Helix H3 (J)	107-125
	Helix H4 (I)	128-136
8-fold α/β-barrel	Strand S4	150-153
	Strand S5	168-172
	Helix H5 (H)	179-200
	Helix H6 (G)	221-235
	Strand S6	241-247
	Helix H7 (F)	275-288
	Strand S7	293-296
	Helix H8 (E)	303-312
	Strand S8	316-320
	Helix H9 (D)	327-336
	Strand S9	341-345
	Helix H10 (C)	352-365
	Strand S10	368-373
	Helix H11 (B)	382-389
	Strand S11	394-397
	Helix H12 (A)	404-419

Table 1.1 Yeast enolase in pieces: amino acid residues within different secondary structural elements (*11, 14*). Letters in brackets (A, B, C, D...etc), are the helix assignment used in Figure 1.2.

The active site is located at the bottom of the β-barrel (*16*). The active site residues are on the barrel strands, with their polar side chain pointing towards the interior of the barrel. Figure 1.2 shows this feature. The active site residues are highly conserved, and thus have similar spatial orientations among different species (*11, 13, 14*).

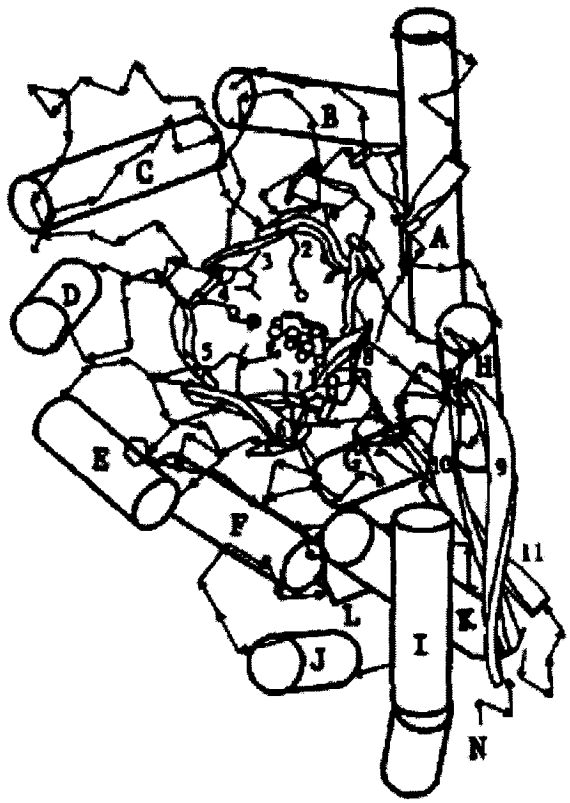

Figure 1.2: View of the enolase subunit along the barrel axis. "The active site is located in the bottom of the barrel cavity. The barrel is surrounded by helices, and the side chains from the barrel are pointing towards the interior of the barrel (*17*)."

1.2.2 Significance of loops in enolase

The loops of enolase play an important role in catalysis and tertiary and quaternary structure as well. The enolase loops contain approximately half of the overall amino acid residues, which includes many aromatic residues (*11*). Also, a few key loops are also associated with specific movement and positioning upon metal and substrate binding. Furthermore, loops are also contributing to the subunit interface (*17*). The movements of the loops therefore would be observed by spectroscopic techniques as the aromatic residues' environment changes. This allows us to probe the changes in structure.

There are three major loops that have attracted special attention in yeast enolase: Pro35-Gly60, Val153-Phe169, and Ser247-Gly275. The first loop is from the N-terminal small domain, and it is known as the active site loop because it covers the active site once metal cofactor and substrate are bound (*17*). There have been extensive studies done on residues of this loop to determine their role in enolase function (*18, 19*). For instance, site-directed mutagenesis was done on Ser39, and found it was necessary for catalysis. The closure of the first loop is an absolute requirement for enolase catalysis as it brings the Ser39 into proximity with the second metal cofactor (see Figure 1.3). This allows the carbonyl and hydroxyl oxygen group of Ser39 to chelate the metal ion and closes the entrance to the active site (*18*). Other studies centered on in residues near the beginning of the first loop, which are responsible for loop flexibility. Two glycine residues at position 37 and 41, which form a hinge, maximize the flexibility of this loop (*20*). Furthermore, this long loop extends from the active site to the subunit interface. The backbone N of Trp56 on this loop is also hydrogen bonded to the side chain oxygen of a glutamate on the other subunit (*16*). The other two loops are from the larger C-terminal

domain. Although the movement of Val153-Phe169 loop is also associated with metal and substrate binding, its motion is more limited compared to the active site loop (*17, 20, 21*). However, this loop contains His159, which is situated in the active site (see Figure 1.5), and is believed to be involved in both structuring the active site and participating in catalysis (*22, 23*). The last loop that extends from Ser247-Gly275 forms a hydrophobic core in the large domain, which helps the larger domain to keep its unique structure (*20*).

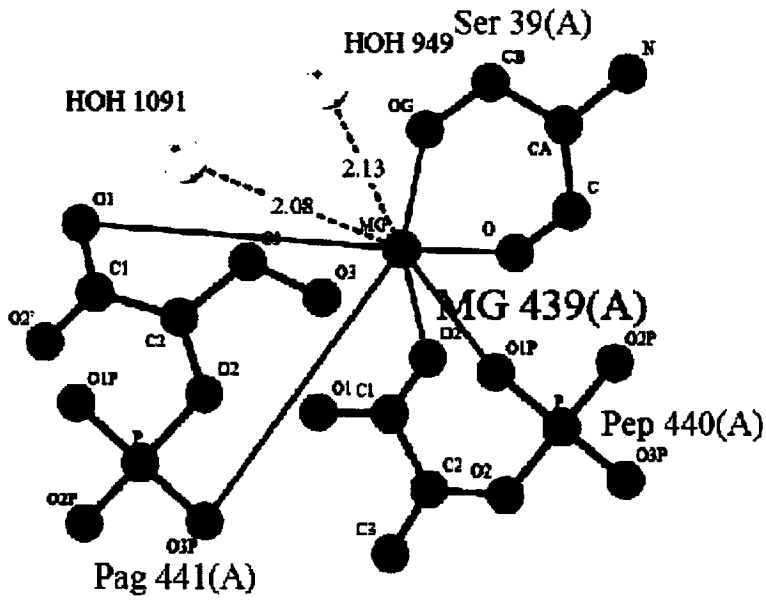

Figure 1.3: Second metal cofactor interaction with yeast enolase and substrate. The PAG is 2-phospho-D-glyceric acid, PEP is phosphoenolpyruvate and Mg is magnesium ion. (A) refers to chain A of the yeast enolase dimer. Reference from RCSB Protein Data Bank and EBI PDB sum: Ligand/metal interaction related to1one.pdb. (http://www.rcsb.org) & (http://www.ebi.ac.uk/thornton-srv/databases/cgi-bin/pdbsum/GetPage.pl?pdbcode=1one&template=ligands.html&o=METAL&l=1.2)

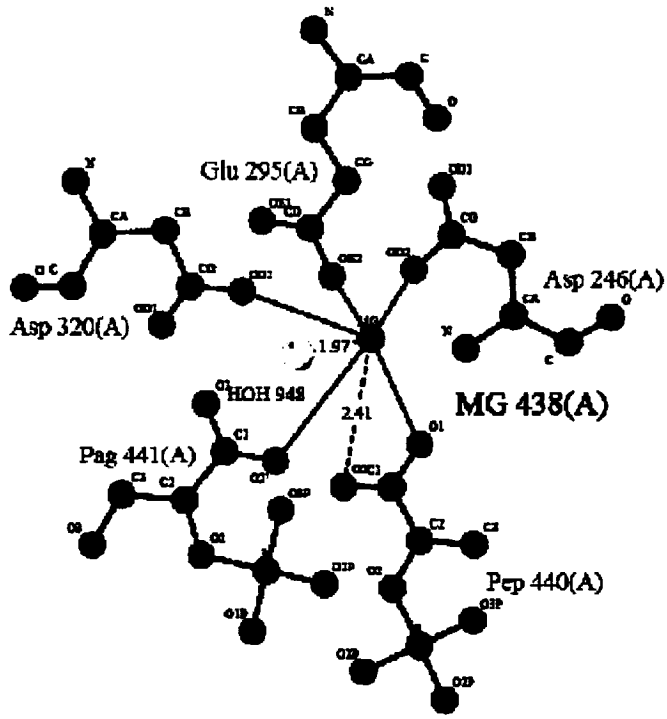

Figure 1.4: First metal cofactor interaction with yeast enolase and substrate. The PAG is 2-phospho-D-glyceric acid, PEP is phosphoenolpyruvate and Mg is magnesium ion. (A) refers to chain A of the yeast enolase dimer. Reference is from RCSB Protein Data Bank and EBI PDB sum: Ligand/metal interactions related to1one.pdb. (http://www.rcsb.org) & (http://www.ebi.ac.uk/thornton-srv/databases/cgi-bin/pdbsum/GetPage.pl?pdbcode=1one&template=ligands.html&o=METAL&l=1.1)

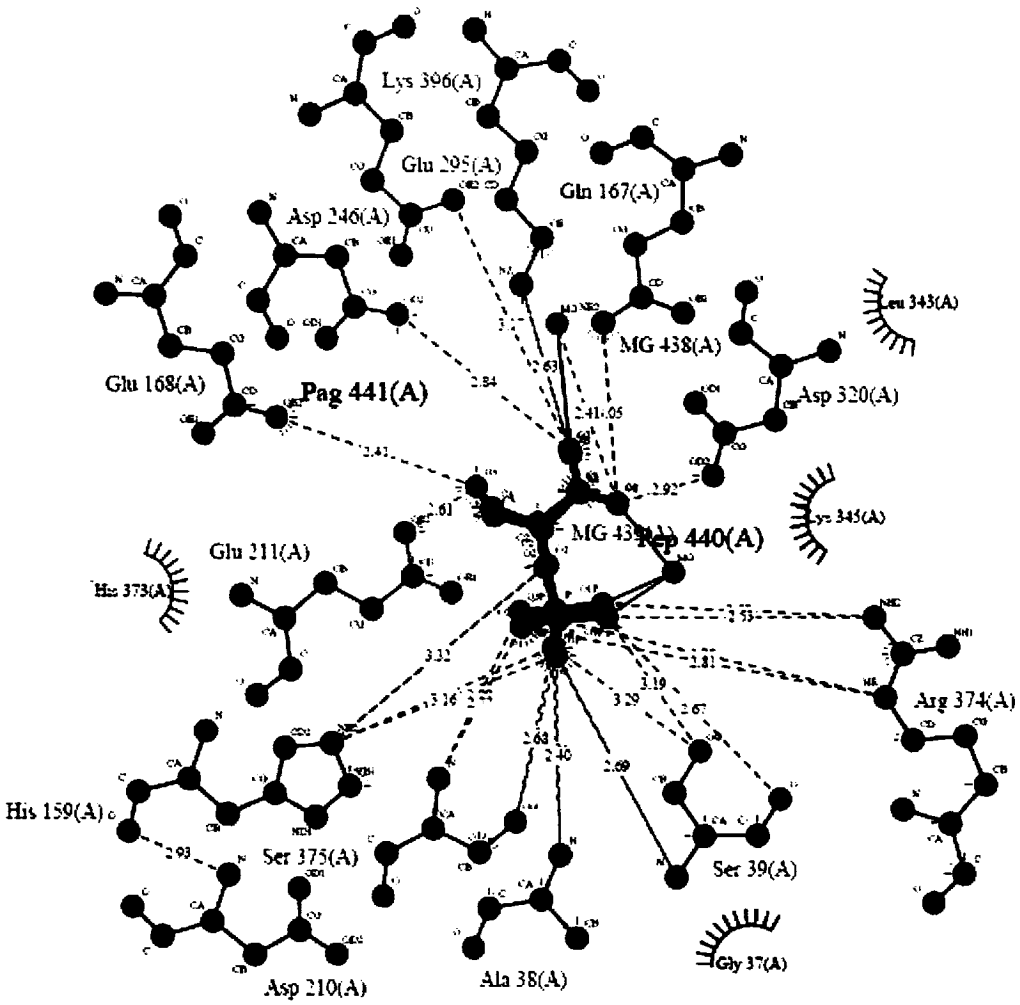

Figure 1.5: Substrate interaction with metal cofactors and yeast enolase. The PAG is 2-phospho-D-glyceric acid, PEP is phosphoenolpyruvate and Mg is magnesium ion. (A) refers to chain A of the yeast enolase dimer. Reference is from RCSB Protein Data Bank and EBI PDB sum: Ligand/metal interactions related to1one.pdb. (http://www.rcsb.org) & (http://www.ebi.ac.uk/thornton-srv/databases/cgi-bin/pdbsum/GetPage.pl?pdbcode=1one&template=ligands.html&l=1.1)

1.2.3 Subunit interface of enolase

Similar to the other important regions of enolase structure, the residues at the subunit interface are highly conserved as well (*13, 14*). In the presence of Mg^{2+}, yeast enolase is a dimer of two identical subunits (*1*). The major types of interactions at the interface are hydrogen bonding and ionic interactions (see Table 1.2, 1.3) (*16*); most of these interactions are between the smaller domain of one subunit and the catalytic domain of the other subunit. The residues at the interface are mostly polar, the ratio of charged residues to hydrophobic residues is approximately 3:2 for *E. coli* enolase (*14*). This results a relatively hydrophilic surface between the subunits (*16*). This may explain the dependency of dimerization on solvent ionic strength in *E. coli* enolase.

Residue of subunit A	RA(+)~~~~(-)RB	Residue of subunit B
Arg8	Nε-Oε2	Glu417
Arg8	NH2-Oε1	Glu417
Arg414	Nε-Oε1	Glu20
Arg414	NH2-Oε2	Glu20

Table 1.2: Ionic interaction pairs at subunit interface (*16*). Columns 1 and 3 indicate the residues involved in the interaction. Column 2 shows which atom is involved in the actual interaction. N represents nitrogen, O represents oxygen atom. The numbering of the atoms was done with respect to the alpha carbon of the amino acid backbone of each residue.

Residue of subunit A	RA(+)~~H~~(-)RB	Residue of subunit B
Glu417	Oε2-OH	Val2
Asn410	Nδ2-Oε1	Glu379
Asn410	Nδ2-O	Tyr11
Asn410	Oδ1-N	Tyr11
Glu404	Oε1-N	Ser403
Glu188	Oε1-N	Trp56
His191	Nε2-O	Arg14
Val208	O-N	Val208

Table 1.3: Hydrogen bonding interaction pairs at subunit interface (*16*). Columns 1 and 3 indicate the residues involved in the interaction. Column 2 shows which atom is involved in the actual interaction. N represents nitrogen, O represents oxygen atom. The numbering of the atoms was done with respect to the alpha carbon of the amino acid backbone of each residue.

1.3 Enolase catalysis mechanism

1.3.1 Enolase mechanism overview

Enolase catalyzes a β-elimination reaction that removes a water molecule from 2-PGA to form PEP (*24*). Figure 1.6 shows the general reaction catalyzed by enolase. The free energy change in this reaction is relatively small (~1kcal/mol). This reaction is the only dehydration reaction in glycolytic pathway (*25*), and it occurs in a stepwise manner: a base on the enzyme removes a non-acidic proton from C2 of 2-PGA to form a carbanionic intermediate, followed by the elimination of OH^- from C3 and then the formation of double bond between C2 and C3 occurs to yield PEP (*24, 26, 27*) (see figure 1.7 (*28*)). This mechanism was supported by kinetic isotope effect experiments in 1994 (*29*). In the same study, it was also proposed that the proton abstraction, OH^- elimination, and PEP release were the rate-limiting steps in enolase catalysis. However, a new study carried out in 1996 disrupted such proposal and reported that the conformation change and release of product were both partially rate limiting at pH 7.1, and at pH 6.1 the proton abstraction becomes partially rate limiting as well (*30*). As early as 1970, it was proposed that the dehydration elimination reaction of enolase occurs in an anti- stereochemical manner, that is the H^+ and OH^- were removed from opposite sides of the substrate (*31*). This agrees with identification of the active site residues in 1996, which were situated on the either side of the substrate bound to the enzyme (*32*).

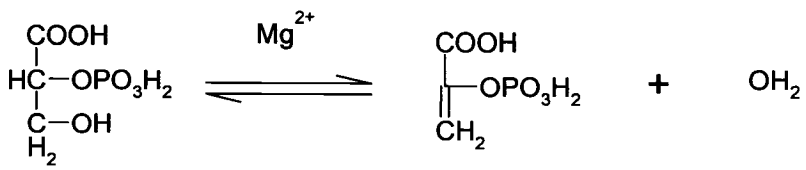

Figure 1.6: Enolase general reaction.

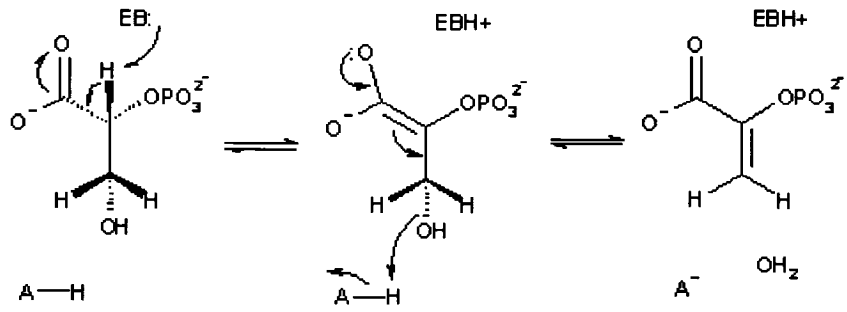

Figure 1.7: Detailed enolase reaction mechanism.

There have been several proposals as to which acid/base residues are involved in enolase reaction. Brewer in 1985 (*33*), and Lebioda and Stec in 1991 (*17*), proposed a water molecule between Glu211 and Glu168 as the catalytic base. This proposal was based on their crystal structure of enolase-Mg^{2+}-2PGA/PEP complex (*17*). In this proposal, the water molecule near C2 of 2-PGA was ionized by the carboxylic acid groups from Glu168 and Glu211. The ionized water molecule in turn acts as catalytic base in proton abstraction. The abstracted proton is then transferred onto Glu168, and then transferred to OH^- on C3 of 2-PGA to form water molecule (*17*). This mechanism was supported by site-directed mutagenesis studies carried out on E168Q on 1993 (*34*) and E211Q on 1995 (*25*). In both cases, the structural characteristics, stability of the enzyme and interaction with natural substrate were comparable to those of wild-type enzyme. However, severely decreased activity was observed for both cases (~0.01% of wild-type), thus identifying the importance of Glu168 and Glu211 in catalysis (*25, 34*).

Based on a crystal structure of yeast enolase with very tight binding inhibitor phosphonoacetohydroxamate (PhAH) (*20*), an inhibitor that mimics the structure of enolase carbanion reaction intermediate (*35*), Poyner *et al.* proposed Lys345 as the

catalytic base. Their work involved site-directed mutagenesis at positions 168, 211, and 345 (*32*). All three variants showed greatly decreased overall catalytic efficiency. Both E168Q and E211Q variants could catalyze the C2 proton exchange normally, but the K345A had lost that ability (*32*). This result contradicts the first proposal and identified the Lys345 as the catalytic base (*32*). However, when they used *(Z)*-3-chloro-2-phosphoenolpyruvate to test variants' ability to add OH^- and eliminate of Cl^- at C-3, a reaction mimics the addition of OH^- to C-3 of PEP in enolase reverse reaction, they found that the E211Q variant was affected the most. Thus confirms Glu211's interaction with OH^- at C3 (*32*), which matches the criteria of catalytic residues on opposite side of the substrate. This result is supported by the crystal structure of Wedekind *et al.* in 1994 (*20*), and it is in agreement with the first proposal as well. Moreover, this crystal structure showed a possibility of another residue's involvement in catalysis: His373 (*32*). His373's ε-nitrogen was only 2.9Å away from the water molecule between Glu168 and Glu211, and since this water molecule was suggested to participate in catalytic mechanism (*17*), they proposed that His373 may be involved in the elimination reaction of OH^- from substrate. But it was soon ruled out in 1997 by the study of Brewer's group (*36*) and another crystal structure (*21*). Brewer's group have made H373N and H373F mutants and found that their activity was severely decreased (*36*). Furthermore, the new crystal structure helped confirm His373's role in hydrogen-bonding network with Glu168, Glu211, and the bridging water molecule (*21*). It was then clear that the His373 was not directly involved in catalysis.

Another proposal postulated the imidazole group of His157 (His159 in yeast enolase) as the catalytic base in lobster enolase (*13*). This prediction was supported by

both the lobster enolase crystal structure and the work of yeast enolase by Vinarov *et al.* in 1999. It was found that the H159A yeast enolase mutant was unable to perform the deprotonation reaction at C2 of 2-PGA (*23*). However, in 2000, Brewer's group showed that H159A yeast enolase mutant possessed significant amount of activity, and so it is not the enzymatic base (*22*). Due to the contradiction, His159's role in catalysis is still to be determined.

Although some controversy remains, currently, Lys345 and Glu211 are generally recognized as the catalytic residues in the yeast enolase reaction. However, all investigators agree that the requirement for divalent metal cations is absolute.

1.3.2 Role of divalent metal cations in enolase catalysis

All known enolases to date require divalent metal cations to catalyze the interconversion reaction. The enolase activity is at its highest when the natural cofactor Mg^{2+} is used; this is possibly due to its high abundance. A metal ion must be bound at the active site in order for the substrate/product to bind. This binding is associated with some spectroscopic changes, which is probably due to the movement of the loops (*37, 38*). This metal ion will be referred as the first metal ion. The binding of substrate, which is accompanied by displacement of two water molecules from the active site, in turn allows the second metal ion to bind. The binding of substrate and second metal is accompanied by significant conformational changes (*11, 28*). This second metal is an absolute requirement for catalysis to occur. The catalysis, however, will not occur unless both metal ions are present, and the first metal ion must be an activating one (*39*).

Although the Mg^{2+} metal ion is the natural cofactor of enolase, many other ions can be substituted at the active site. In year 1983, Brewer's group conducted a study of active site metal ion using Sm^{3+}, Tb^{3+}, Co^{2+}, Ni^{2+}, Fe^{2+}, Zn^{2+} (*40*). They found that not all metal ions bound have the activating effect and nor does binding affinity correlate with activity (*40*), i.e. some metal ions bind tighter than Mg^{2+} but result in lower activity. Since then, many of the activating metal ions have been studied (*41-48*), and various activating metal ions were classified by their level of activity: $Mg^{2+} > Zn^{2+} > Mn^{2+} > Fe^{2+} > Cd^{2+} > Co^{2+} > Ni^{2+}$ (*10*).

Many studies show that at high concentrations of Mg^{2+} (*39*), Mn^{2+}(*49*), Cu^{2+}, Zn^{2+} etc. (*50*) enolase activity is significantly inhibited. There are two hypothesises: one proposes the presence of a third metal binding site, which, once occupied, inhibits

activity; the other proposes that the inhibition is due to kinetic substrate/product inhibition. The latter, in case of enolase, the activity is decreased as metal concentration increase, but the inhibition was never 100%. This may suggest that at high enough concentration of metal cofactor, the closure of active site loops is affected or, due to the abundance metal ions, the departure of second metal upon reaction completion is impeded. In most of the crystal structures to date, the inhibitory site is not observed, however, da Silva Giotto *et al.* claim to have observed such a site (*51*). In the crystal structure of enolase from *T.brucei* they have observed a Zn^{2+} ion bound near the active site at His156, blocking the active site loop from closing (*51*). They claim that the metal ion affinity at the inhibition site is relatively low and is therefore not observed in other structures. However, others counter this finding by claiming the observation was due to the high abundance of Zn^{2+} ions in the crystal (~10 mM). This debate between inhibition site and kinetic inhibition effect is still on going. Furthermore, some monovalent cations such as Na^{+}, Li^{+}, (*52*) and K^{+} (*53*) were also found to inhibit enolase activity.

1.4 Subunit dissociation

Enolase is known to lose its activity when two subunits dissociate. The active site of enolase is well contained within each subunit; it does not share any catalytic residues with another subunit. The question of what has changed during dissociation such that enolase becomes inactive has been occupying investigators for many years, as many have failed to isolate active enolase monomers.

Many different types of studies have been conducted on enolase subunit interface. Although investigators first believed that the subunit interaction was hydrophobic (*54*),

the successfully crystallized enolase structure revealed that the interactions were ionic and hydrogen bonding.

In 1969, Brewer's group showed that yeast enolase subunits dissociate in the absence of Mg^{2+}, in excess amount of EDTA and 1 M KCl. Even in the absence of KCl (a chaotropic salt), removal of Mg^{2+} allowed enolase subunits to dissociate readily (*55*). Although the dissociated protein lost most of its activity, the effect of dissociation was not irreversible. The study demonstrated the metal cofactor's role in stabilizing the form of dimeric enolase, and revealed that monomeric/dimeric forms can exist in equilibrium since the dissociation process is reversible (*55*). On the contrary, when a kosmotropic salt was used (KOAc), the dimeric form of enolase was favored (*56*). Using salts to maintain dimeric or monomeric enolase has been popular since then. The use of the chaotropic salt or the kosmotrope NaOAc favors the monomeric or dimeric form respectively (*57, 58*).

To date, there have been many attempts to create active monomers. In one of such efforts, the temperature was used to dissociate of enolase (*59, 60*). At 35-40 °C and a protein concentration of 1 μg/mL, Keresztes-Nagy's group claimed to have isolated active monomers (*59*). In more recent studies, hydrostatic pressure was one of the more successful tools used to generate active enolase monomers (*61*). It dissociates enolase by changing the hydration state of the molecular surfaces, and the process is reversible as well (*62*).

1.5 Current Project

1.5.1 Origin of mutation

In year 2001, a new glycolytic pathway deficiency, β-enolase deficiency, was discovered in Europe. This is the first case of human β-enolase deficiency (Glycogenosis type XIII) to date. The patient was a 47-year-old Italian male, who had two symptoms: exercise induced myalgias and generalized muscle weakness. Results from Immunohistochemistry and immunoblotting showed that the patient's muscle β-enolase level was dramatically reduced, while α-enolase level was normal (see Figure 1.8 (*63*)). Since β-enolase accounts for over 90% of enolase activity in muscle tissues, the patient's ability to metabolize sugar in muscle is greatly hindered. When the patient's ENO3 gene (gene for β-subunit) was sequenced, it was found that he was a heterozygous carrier of two missense mutations: G467A and G1121A. The changes in the DNA sequence resulted in mutations of two amino acid residues: G156D and G374E (human β-enolase number system). Both of these residues are in highly conserved regions of enolase. Although the father had passed away at the age of 86 due to an unspecified cause, his mother, an 85-year-old woman with hypertension, was identified as a heterozygous carrier of the G374E substitution. His 50-year-old sister was a heterozygous carrier of G156D, therefore, he must have inherited one mutation from each of his parents.

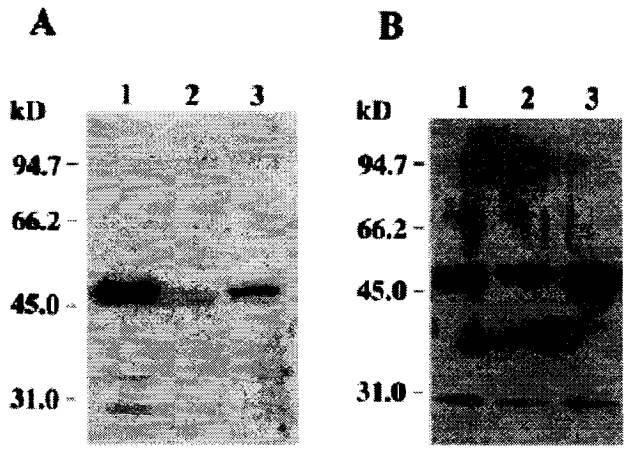

Figure 1.8: Western blot analysis of α- and β-enolase (*63*). (A) β-enolase. Lane 1 is control muscle, a 46-kDa band. Lane 2 shows a faint doublet of immunoactivity is present in the patient. Lane 3 is another control using purified muscle enolase. (B) Immunoblot using rabbit α-enolase antibodies. Lane 1 and 3 are controls. Lane 2 is a sample from the patient, where the lower band, a cross-reaction product with β-enolase, has disappeared.

1.5.2 Thesis premise

Proper positioning of substrate and metal ions, and dimer interface stability are crucial in enolase activity. A substitution at amino acid position 376 (yeast numbering) lies in a turn of the molecule and may have modified the enzyme's secondary structure (*63*). However, we believe that it may have altered the orientation of substrate and/or metal ions at the active site, as well as weakening hydrogen bonding at the subunit interface. Gly376 is located on a short loop between helix H10 and strand S10 of the $\beta\beta\alpha\alpha(\beta\alpha)_6$ topology (*11*). Upstream of this residue are Ser375 and Arg374, both of which are involved in substrate interaction. Furthermore, the backbone oxygen is hydrogen bonded to Ser36, which is within a loop of Pro35-Gly60. Not only does this loop extend from active site to subunit interface, it also contains Ser39, the only residue interacting with second metal ion. Moreover, three residues downstream of Gly376 is Val379, a residue involved in subunit interaction, and within 6Å of the Gly376, there are more

residues that are either directly associated with hydrogen bonding or adjacent to hydrogen bonding residues: Ser13 and Arg14 are close to Tyr11, and Arg405 is next to Glu404, Ser403, Arg402. Therefore up to six out of nine hydrogen bonding pairs at the interface may be affected (see Table 1.3). Although the amino acid 376 is not directly participating in the function of the enzyme, Glu376 may perturb nearby residues, resulting in serious problems. Thus, it is postulated here that, depending on the orientation of Glu376, more than one aspect of function may be affected by this mutation.

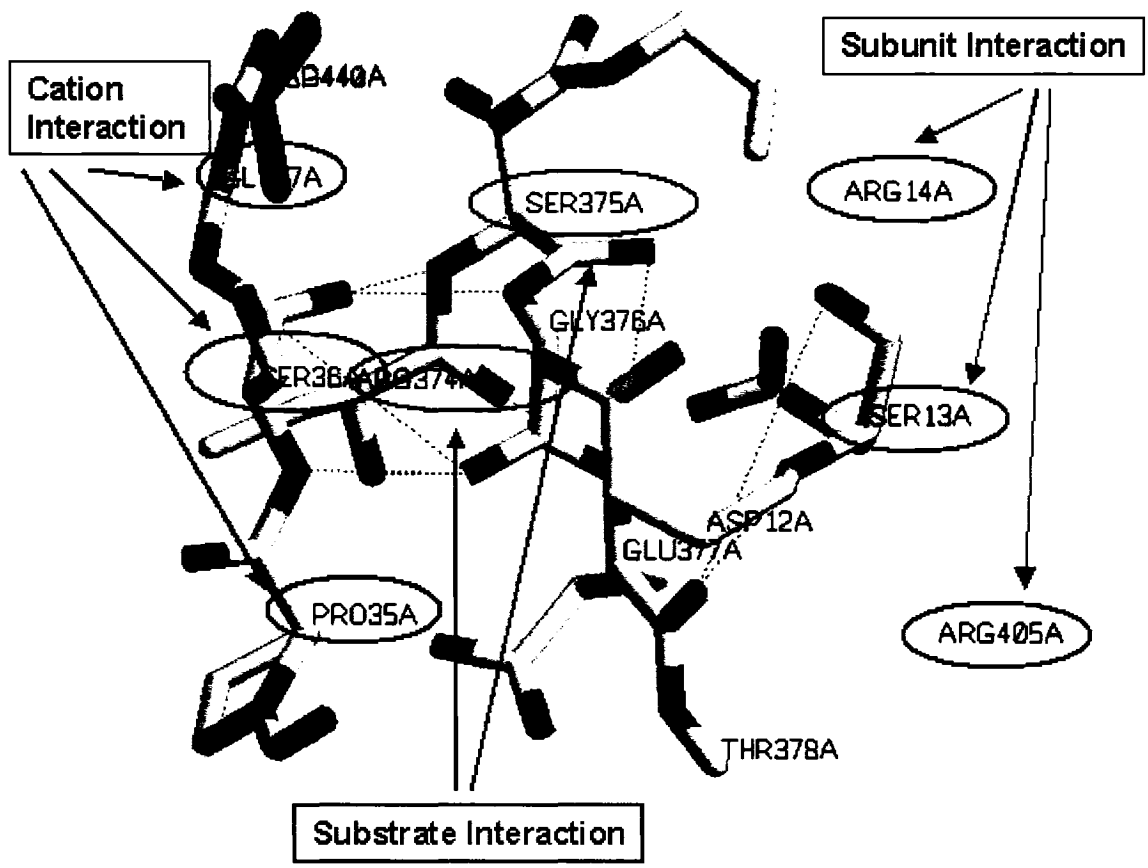

Figure 1.9: Amino acids within 6 Å of Gly376. The diagram was generated using Rastop molecular viewing software and 1one.pdb from RCSB Protein Data Bank (http://www.rcsb.org).

1.5.3 Research approach

In order to verify the postulate stated above, some structural characteristics, stability, and enzyme activity are examined separately. The human G374E mutation was introduced into yeast enolase 1, becoming G376E. The wild-type yeast enolase will be used as a control for comparison. To determine the possible changes stated above, a wide variety of spectroscopic techniques will be used to compare the spectroscopic characteristics of the variant and wild-type enzymes. The enzyme's chemical and thermal stability and proteolytic susceptibility will also be tested. Furthermore, the kinetic parameters will be determined using Mn^{2+} as metal cofactor and 2-PGA as substrate. The metal ion binding constant and substrate binding constant will be determined using isothermal titration calorimetry. Lastly, to determine whether it is the position, size, or charge that is affecting the variant's structure, stability and activity, a series of mutations will be introduced, varying size, and charge from the original glutamate substitution to the smallest residue possible. A total of six amino acid substitutes were introduced using site-directed mutagenesis: G376E, Q, I, D, N, A.

1.5.4 Project goals

The goals set for this project were as follows:

A) To perform the work stated in 1.3.3, substitutions at position 376 must be introduced by mutations of the wild-type plasmid using site-directed mutagenesis. Efficient purification procedures must be developed. Although Alessandra Padovani, a graduated M.Sc. student, developed the purification scheme of recombinant wild-type yeast enolase (*64*), modifications were needed for the new variants and wild-type enzyme.

B) The variant enzymes will be characterized using optical spectroscopic techniques to determine structural differences.

C) The stabilities of the variants will be compared to that of the wild-type.

D) The catalytic parameters of the variants will be compared to those of the wild-type enzyme to determine which aspect of catalytic function is altered.

Chapter 2 Methods and Materials

2.0 Various buffers

In this project, the most commonly used buffers are as follows:

TEM buffer : 50 mM Tris, 1 mM $Mg(OAc)_2$, 0.1 mM EDTA pH 7.4. This buffer was used in protein purification and various spectroscopic studies.

MME buffer : 20 mM Mes, 2 mM $Mg(OAc)_2$, 0.2 mM EDTA, pH 6.0. This buffer was used in protein purification.

MT buffer : 25 mM Mes-Tris, pH 7.1. This buffer was used in activity assays and ITC experiments.

EAB buffer : 50 mM imidazole, 1 mM $Mg(OAc)_2$, 0.1 mM EDTA, 250 mM KCl, pH 7.1. This buffer was used in preliminary activity assays.

Tris base, $Mg(OAc)_2$, $MnCl_2$, KCl and imidazole were from Fisher Scientific. MES and EDTA disodium salt dehydrate were obtained from Fluka.

2.1 Oligonucleotide design

The primers used in site-directed mutagenesis were designed using PC Gene and NEB Cutter (New England Biolabs Inc.). The primers were designed keeping the GC content, melting temperature, and poly GC ending in mind. They contain the amino acid substitution at amino acid 376, as well as a silent mutation that either introduced a *Cla*I or removed a *Bgl*II restriction site. The *Cla*I restriction site silent mutation was not utilized in mutations other than G376E because the design failed to take the restriction enzyme's DNA methylation sensitivity into account.

Oligonucleotides were purchased from BioCorp Inc. Their sequences were as follows:

Name	Oligonucleotide Sequences (complimentary sequence are not shown)
Wild-type	5'-GG-GGT-GTT-ATG-GTT-TCC-CAC-AGA-TCT-GGT-GAA-ACT-GAA-GAC-3'
G376E	5'-GG-GGT-GTT-ATG-GTT-TCC-CA**T**-**C**GA-TCT-**GAA**-GAA-ACT-GAA-GAC-3'
G376Q	5'-GG-GGT-GTT-ATG-GTT-TCC-CAC-AGA-TC**C**-**CAG**-GAA-ACT-GAA-GAC–3'
G376I	5'-GG-GGT-GTT-ATG-GTT-TCC-CAC-AGA-TC**C**-**ATT**-GAA-ACT-GAA-GAC-3'
G376D	5'-GG-GGT-GTT-ATG-GTT-TCC-CAC-AGA-TC**C**-GAT-GAA-ACT-GAA-GAC-3'
G376N	5'-GG-GGT-GTT-ATG-GTT-TCC-CAC-AGA-TC**C**-**AAT**-GAA-ACT-GAA-GAC-3'
G376A	5'-GG-GGT-GTT-ATG-GTT-TCC-CAC-AGA-TC**C**-GCT-GAA-ACT-GAA-GAC-3'

Table 2.1: The list of oligonucleotides used in this project. The underlined code is amino acid 376. Bold letters represent the bases that were changed from wild-type.

The minimum standard for ordered oligonucleotides was OPC grade; G376D, N and A oligonucleotides were HPLC grade.

DeoxyNTP mixture (10 mM of each dNTP) and *Pfu* polymerase (2.5 U/μL) were purchased from MBI Fermentas in Montreal. *Pfu* buffer was supplied with the polymerase package. The recombinant yeast enolase DNA was previously ligated into *Nde*I and *Bam*HI restriction sites of pET-3a plasmid. pET-3a (Novagen) was supplied by Dr. Elizabeth Cadieux of Concordia University.

2.2 DNA extraction

Mini-preps were performed based on protocol listed in BioTechniques 22:404-406 (1997) at earlier stage of the project. Later, to facilitate the screening and extraction procedures, the Wizard® Plus Minipreps DNA Purification System was used. The protocol used was based on the manual provided along with the system. For each small scale preparation, 10 mL of culture were grown overnight and used to extract plasmid DNA. For sequencing, a 100 mL bacteria culture was grown overnight. The protocol used for large scale DNA extraction was obtained from Dr. Paul Joyce of the Chemistry and Biochemistry Department of Concordia University. This protocol was modified based on a protocol by Drs Paul Kreig and Doug Melton of Harvard University(*65*).

Wizard® Plus Minipreps DNA Purification System was purchased from Promega. Bovine pancreas RNase A was purchased from Boehringer Mannheim. It was prepared as 10mg/mL stock solution followed by heat inactivation. PEG 800 was from Fisher Scientific and was prepared as 30% stock solution. TE buffer (pH 7.4, 10 mM Tris-Cl, 1 mM EDTA) used to dissolve DNA was prepared according to Maniatis (*66*). Sucrose and glucose were from Fisher Scientific. Lysozyme was purchased from Boehringer Mannheim.

2.3 Site-directed mutagenesis

The oligonucleotides purchased from BioCorp Inc. were suspended in appropriate amount of distilled water (150-250 μL). The concentrations were determined based on number of bases and OD_{260}. OD value of 1 is approximately 50 μg of double stranded DNA or 33 μg of oligonucleotides. The site-directed mutagenesis was carried out using the QuickChange method (Stratagene). Each incubation contained 200-350 ng of double stranded wild-type recombinant yeast enolase DNA, 250-400 ng of oligonucleotides, 2 μL of 10 mM dNTP solution, and 10 μL of 10X *pfu* buffer, in a final volume of 100 μL. This reaction mixture was covered by ~200 μL of mineral oil. The *pfu* polymerase (5 units per reaction) was added after the first denaturation cycle. A minimal 16 PCR cycles were performed using the following parameters:

1) Denaturation : 95 °C, 30 seconds
2) Annealing : 54 °C, 60 seconds
3) Extension : 72 °C, 14 minutes.

Upon completion of the PCR cycles, the reaction mixture was removed from PCR tubes and 20 units of *Dpn*I restriction enzyme were added. The reaction mixture was incubated at 37°C for at least 1 hour to digest the methylated wild-type DNA.

The presence of amplified DNA was then confirmed by electrophoresis with a 1% agarose gel containing ethidium bromide; the DNA was visualized under ultraviolet (UV) light.

The digested PCR products were then transformed into XL-1-Blue *E. coli* cells. The transformation procedure is described in section 2.4. A couple of colonies were selected and inoculated into 5-10 mL of LB media containing ampicillin (0.1 mg/mL).

The plasmid DNA was then extracted using DNA mini preparation methods described in section 2.2. To verify if the mutation was introduced, the DNA plasmid were digested using *Bgl*II restriction enzyme, and migration pattern of the digests of mutant DNA were compared to *Bgl*II digestion of wild-type DNA.

Yeast enolase plasmids were maintained in XL-1-Blue *E. coli*; glycerol stocks were stored at –86°C. XL-1-Blue strain was also used for site-directed mutagenesis as well. BL-21 (DE3) *E. coli* strain was used in expression of the yeast enolase proteins.

*Bam*HI, *Nde*I, *Dpn*I and *Bgl*II (all 10 units/μL) were purchased from MBI Fermentas. The digestion buffers and BSA solution were supplied with the different restriction enzymes.

TAE buffer was prepared as 50X stock solution according to Maniatis (*66*) and was diluted to 1X prior to use (final concentration is 0.04M Tris-acetate, 0.001M EDTA). Glacial acetic acid was from EMD. Agarose was from ICN Biomedicals Inc. λ-DNA marker (*Eco*RI/*Hind*III digest, 50 μg/mL) was from Promega.

2.4 Transformation

Competent cells (100 μL) were incubated with the DNA plasmid (DNA plasmid volume depends on concentration) on ice for 40 minutes. Then the cells were heat shocked at 42 °C for 90 seconds. The cells were then grown on a 37 °C shaker for 90 minutes at 225-RPM rotating speed. 2 5-50 μL aliquots o f the cultures were then plated on LB + agar + ampicillin (0.1 mg/mL) plate and grown overnight at 37°C.

2.5 DNA sequencing

Large-scale DNA preparations were carried out to obtain the mutant plasmid in large quantity (see section 2.2.2). The DNA inserts between the T7 and T7t sites were sequenced by Bio S&T Inc. The resulting sequence was aligned (using BLAST) with the wild-type sequence to ensure the mutation was present, and that no other mutations had been introduced during the process.

2.6 Protein expression and purification

Wild-type or mutant DNA plamid were transformed into BL-21 (DE3) *E. coli* cells. The colonies on one plate were suspended in 5.0 mL of LB media; 200 μL of this suspension was used to inoculate 50 mL of growth media containing peptone, yeast exact, M9 salts (*67*) and ampicillin (400 mg/L). Cells were then grown at 37°C, 225 RPM until an OD_{600} of approximately 0.5 was reached. The amount of time required to reach this value varied depending on the number of colonies on the plate, but in general, the growth level was reached within two to three hours. Ten mL of the above sample is then induced into 1L of growth media containing M9 salts, 1.6% α-lactose and 400 μg/mL of ampicillin. The cells were grown at 37°C, 225 RPM for 14 hour, and then harvested by centrifugation in Beckman J2-HS centrifuge with a JA-10 rotor at 5K RPM, 4°C.

The cells are then weighted and suspended in 20-35 mL of TEM buffer. A small volume of 200 mM phosphonoacetic acid (final concentration is approximately 1 mM) was added to stabilize enolase protein during purification. A pinch of DNaseI and RNase was also added to reduce the nucleic acid material in purified enzyme. The cells were well suspended using a 10 gauge needle on a 10 mL syringe. The cells were lysed using a

Branson 250 Sonifier while on ice, using bursts of 30 seconds, with a 30 second cooling period between bursts. The output setting is 3.0, and meter reading is between 40-60. Six bursts were used per 10g of wet cell weight. The pH of lysed cell solution was checked with pH paper and adjusted to approximately 7.2, if necessary, using 1M Tris. The lysed cell solution was centrifuged at 16 K RPM, 4°C, for 30 minutes; the supernatant was transferred to a fresh tube and recentrifuged. Salting out technique was then carried out for the supernatants. For wild-type, G376Q, G376I, G376N, and G376A, the first cut was 0 – 40% ammonium sulfate concentration, followed by a 40 – 85% cut. Enolase protein was precipitated in the 40 – 85% cut (confirmed using activity assay and SDS-PAGE). For G376E and G376D, the salting out concentration was changed to 0 – 50% followed by 50 – 85% precipitation, the desired protein was found in 50 – 85% precipitate. The desired precipitate was collected by centrifugation. The protein pellet was suspended using a small volume of TEM buffer or MME buffer depending on the protein. The suspended protein solution was then dialyzed against TEM or MME buffer, the dilution factor was at least 100-fold. Buffer was changed after 2-3 hours of dialysis with constant stirring, and dialysis was continued overnight. The total dilution factor is over 1000-fold.

On the following the day, the protein solution was applied to the first ion exchange column. For wild-type, G376Q, G376I, G376N and G376A, the protein solution was applied to a ~150 mL Q-Sepharose fast flow column equilibrated with TEM buffer, and eluted using TEM buffer with a flow rate of ~1 mL/min; for G376E and G376D protein, it was applied to CM-Sepharose fast flow column and eluted with a 0-0.25M gradient of KCl in MME with a flow rate of ~0.33 mL/min. OD_{280} and OD_{260} were recorded for selected fractions, and activity assay was also carried out for active

enzymes. The activity assay here was performed in enolase assay buffer using phosphoenolpyruvate (PEP). For inactive enzymes, the fractions containing enolase were monitored using SDS-PAGE. The fractions containing enolase were then pooled and precipitated using 85% ammonium sulfate. The pellet was collected by centrifugation, suspended in the corresponding buffer, and dialyzed for 2 hours followed by another overnight dialysis for second ion exchange column.

On the third day, the wild-type, G376Q, G376I, G376N or G376A enzyme were applied to a CM-Sepharose fast flow column and eluted as described above, whereas G376Q and G376D proteins were applied to a small (~1.5 mL) Q-Sepharose fast flow column equilibrated with TEM buffer and then protein were eluted with TEM containing 0.1M NaCl. The fractions containing the desired protein were selected and pooled as described above. The protein was then precipitated again using 85% ammonium sulfate and stored at 4°C for long-term storage.

The purified protein concentration was determined from the absorbance at 280 nm; the extinction coefficient was 0.89 $(mg/mL)^{-1}$.

Tryptone and/or Peptone, yeast extract powder, α-Lactose, and the Na_2HPO_4, NaCl, NH_4Cl, and KH_2PO_4 in M9 salts were all purchased from Fisher Scientific. Ampicillin used in growth control and screening was from Fisher Biotech. Agar was purchased from ICN Biomedicals Inc. and Becton Dickinson.

The M9 salt solution was prepared as 5X concentrate solution; 200 mL were added to 800 mL of growth media. Ampicillin was prepared as 100 mg/mL stock solution by filter sterilization using a 0.45 μm Nalgene syringe filters.

DNase I was from Roche and RNase was purchased from Boehringer Mannheim. Phosphonoacetic acid was purchased from Aldrich Chem Co. It was prepared as 200 mM stock solution and was stored at -20°C. Q-Sepharose and CM-Sepharose fast flow resins were from Amersham Biosciences. $(NH_4)_2SO_4$ used in protein precipitation was from MP Biomedicals LLC. NaCl and KCl used in column washing were from Fisher Scientific.

2.7 SDS-PAGE

Twelve percent resolving, 4% stacking gel SDS-PAGE was performed according to Mini-PROTEAN®II Dual Slab Cell instruction manual. The solutions required were also prepared according to the instruction manual. Samples containing loading dye and approximately 10 μg of protein were prepared. They were boiled for 90 seconds to denature the protein. Twenty μL of sample were subjected to electrophoresis at 200V for approximately 1 hour. The gel was stained with coomassie brilliant blue for approximately 30 minutes, followed by 2 hours of distaining.

Acrylamide, bis-acrylamide, SDS, TEMED, Coomassie Brilliant Blue R-250, 2-mercaptoethanol, ammonium persulfate and low range SDS-PAGE standards were all from BIO-RAD. Acrylamide stock solution was prepared as 30% solution using acrylamide and bis-acrylamide (29:1) and was stored at 4°C. SDS was prepared as 10% stock solution and was stored at room temperature. Ammonium persulfate stock was prepared as 10% solution and was stored at -20°C. A 12% resolving gel was used, with a 4% stacking gel. Electrophoresis running buffer was made in 5X solution with Tris base,

glycine and SDS. Glycine used was from Fluka. HCl used to adjust pH was from Fisher Scientific.

2.8 Q-ToF mass spectroscopy

The Q-ToF mass spectroscopy was used to determine the molecular mass of wild-type and variant enolase enzymes. The sample was dialyzed overnight in TEM and then buffer exchanged into 50% acetonitrile, 0.2% formic acid. The direct spray method was used for molecular mass determination. It was also used to determine the protein fragment size in a later stage of the project. Alain Tessier, a technician at Concordia University Mass Spectroscopy Center did most of the equipment setup and manipulation.

The acetonitrile was from EMD. The formic acid was from Anachemica. The Microcon centrifuge filter devices used for buffer exchange (with 30000 dalton cut-off and 10000 dalton cut-off) were purchased from Millipore.

2.9 Spectroscopic analysis

The wild-type dimer and monomer were prepared using TEM with 0.3 M NaOAc, or 0.3 M $NaClO_4$ respectively. The spectroscopic characteristics of the variants were compared with that of the wild-type enzyme. All experiments were performed in TEM buffer, or TEM buffer containing different salts at 15 °C.

1) Far-UV circular dichroism (CD): the spectra were collected using Jasco J-710 spectrophotometer. A 0.1 cm quartz (QS) cuvette was used. The parameters were: 260-200 nm range, 0.2 nm step resolution, 0.25 second response time, 1.0 nm bandwidth and

50 nm/minute scan speed with 5 accumulations. The protein concentration was approximately 1 mg/mL. Corresponding buffer spectra were also collected using the same parameters. Buffer subtraction and noise reduction was done using Jasco Standard Analysis software.

2) Fourth derivative ultraviolet spectroscopy: the scans were obtained using either a Varian Cary 1 or Varian Cary 100 UV-visible spectrophotometer. The cuvette used was quartz (QS) and volume capacity was 1 mL, and path length was 1 cm. The parameters were: 260-305 nm range, average time 1.0 second, 0.1 nm data interval and 6.0 nm/minute scan rate. Each sample was scanned once, including the corresponding buffers. Buffer subtraction and calculation of the fourth derivative was performed using Sigmaplot 8.0. The quantitations were done based on peak ratios: (second peak minus second minima)/(first peak minus first minima).

3) Near-UV CD: the spectra were collected using the same instrument as far-UV dichroism. The cuvette used was also quartz with 3 mL volume capacity and 1 cm path length. The parameters used were: 350-250 nm range, 0.2 nm step resolution, 1 second response time, 1.0 nm bandwidth and 20 nm/minute scan speed with 4 accumulations. The protein concentration was the same as far-UV CD experiment. The analysis was done in the same manner as well.

In effort to shift the monomer-dimer equilibrium of the variant enzymes, the samples were incubated in different conditions (specified in result section) at 15 °C. Near-UV CD spectra were then recorded. For some cases, the sample was subjected to analytical ultracentrifugation (AUC) experiment to ensure more accurate results. The procedures involved in AUC experiment are described below.

NaOAc and $NaClO_4$ were from Fluka. Both stock solutions were prepared as 3M with final TEM buffer concentration of 1X. These stock solutions were stored at 4°C. The dialysis tubing used to desalt and buffer exchange was from Bio Design Inc. The dialysis tubes were boiled in distilled water twice, and stored in 0.1 mM EDTA solution prior to use.

2.10 Analytical ultracentrifugation (AUC)

The sedimentation comparison was carried out at protein in TEM buffer containing 0.3 M sodium acetate (NaOAc) or 0.3 M sodium perchlorate salt ($NaClO_4$). The protein concentration was 1 mg/mL. The experiment was performed at 15 °C, 400 μL of buffer vs. 390 μL of protein sample.

The subunit dissociation experiment was carried out in the same manner as above. The samples were in TEM plus varying concentration of NaOAc, KOAc and $NaClO_4$. The variant proteins were in TEM buffer containing 0.3M NaOAc. Sedimentation coefficients were determined at 4 different protein concentrations: 13 μM, 4 μM, 1.3 μM, and 0.4 μM. The 13 and 4 μM sample were monitored at 280 nm, whereas 1.4 μM and 0.4 μM sample were monitored at 230 nm.

For each case, the scans were collected continuously, the experiment ended when all protein were settled at the bottom of the cells which usually takes approximately 100 scans (time needed vary from 4-5 hours to overnight depending on the temperature of the experiment). The data were then analyzed using DCDT+ analysis software using the

corresponding density and viscosity. The solvent density and viscosity were estimated using Sednterp software.

2.11 Chemical denaturation

Urea was purchased from Fluka. The stock solution of 10M was prepared with a final TEM buffer concentration of 1X and pH adjusted to ~7.4. This solution was stored at room temperature. The protein was incubated in varying concentrations of urea (0M to 8M) for at least 20 hours. The final samples all contained the same concentration of enzyme at 1mg/mL, and the same concentrations of TEM buffer. Far-UV CD spectra were collected for each sample after the incubation was complete. The data were then smoothed and a graph of CD signal change at specific wavelength (222 nm) vs. urea concentration was constructed. The CD signals were converted to percentage denatured using the following equation:

$$\% \text{ Denatured} = ((CD_{xM} - CD_{8.0M}) / (CD_{0.0M} - CD_{8.0M})) * 100$$

The CD_{xM} stands for CD signal at 222 nm of a specific urea concentration; the $CD_{8.0M}$ stands for CD signal at 222 nm at 8.0 M urea concentration; the $CD_{0.0M}$ stands for CD signal at 222nm at 0.0 M urea concentration.

The tertiary structural changes were monitored at a few urea concentrations using near-UV CD. The samples were prepared as 1 mg/mL, and incubated as above. The near-UV CD spectra were collected and the change in tertiary structure was analyzed using CD signal at 283 nm.

The quaternary structural changes were also examined. The sedimentation coefficients of wild-type and G376E proteins were determined at urea concentration less

than 1.2 M. The sample concentration were 1 mg/mL, the procedure used to set up the instrument was the same as described in AUC section. The analysis was carried out the same way as well.

2.12 Temperature denaturation

Protein samples were 1mg/mL in TEM buffer. Far-UV CD signal at 222nm was monitored as the temperature increased. The following parameters were used in this part of the experiment: signal tracking wavelength was 222 nm, temperature range 35 to 70°C, step resolution 0.2°C, 2 minutes wait time, 0.25 seconds response time, 1 nm bandwidth, 200 mdegree sensitivity, and the rate of temperature change was 15°C per hour. By assuming at 35°C there is 100% native protein and the denaturation is complete at 70°C, the CD signal was converted to percentage denatured using the following equation:

$$\% \text{ Denatured} = ((CD_{xT} - CD_U) / (CD_F - CD_U)) * 100$$

The CD_{xT} represent the CD signal at a specific temperature; the CD_U is CD signal at 70 °C, and the CD_F is the CD signal at 35 °C.

The temperature stability of rabbit ββ-enolase was also tested in same manner.

2.13 Proteolysis susceptibility

Samples of mutant protein and dimeric wild-type enolase, 1 mg/mL, were prepared in TEM buffer. Wild-type monomeric enolase, 1 mg/mL, was prepared by incubating the enzyme in TEM buffer + 0.3M $NaClO_4$ for approximately 2 hours. The volume of all samples was 100 μL. To each sample, a small volume of trypsin protease (diluted in TEM buffer) was added so that the final mass/mass ratio between protein and

protease was 1000:1 respectively. The samples were well mixed and incubated at 15°C. At specific time intervals of 10, 20, 30 and 60 minutes, 10 μL of the incubation sample was removed and added to 2 μL of 10 mM TLCK trypsin inhibitor (in water), followed by addition of 2X loading dye. The sample was then well mixed, and was incubated in boiling water for 120 seconds to denature protein and protease. Finally SDS-PAGE was used to monitor the progress of proteolysis. Proteolytic susceptibility of rabbit ββ-enolase monomer was also tested in the same manner, using longer incubation times.

To determine the size of the proteolytic fragment, Q-ToF mass spectroscopy was used. The G376E sample was digested for 60 minutes. Then a small volume (3 μL) was applied to Q-ToF ion trap. It was then washed with 5% acetonitrile for 5 minutes, and eluted with a 5-90% acetonitrile gradient over 20 minutes.

To determine the fragment sizes from wild-type yeast enolase, a much higher concentration of protein was used. Over 5 mg/mL of wild-type enzyme (100 μL) was first dissociated using 0.3M $NaClO_4$, and an overnight incubation at 15 °C was carried out. Trypsin was added the next morning (final ratio of trypsin to enolase was 1:1000) and the sample was incubated for another 60 minutes. Ten μL of 10 mM TLCK trypsin inhibitor was added. The final mixture was diluted 50- and 25-fold into 50% acetonitrile, 0.1% formic acid and analyzed by mass spectroscopy as described above. The rest of the procedures are the same as G376E protein.

To determine the rate of the trypsin digestion, the wild-type enolase was incubated in different $NaClO_4$ concentrations. The trypsin-digested samples were collected at 5, 10, 15, 30, 60 minutes intervals. The SDS-PAGE results at three

concentrations of $NaClO_4$ were analyzed using GeneSnap software from SynGene. Graphs of relative band intensity vs. time were constructed.

Furthermore, in an effort to determine the scale of the exposed site, a variety of proteases were used: chymotrypsin, elastase, endoproteainase glu-c, pepsin. These proteases exhibit different amino acid specificity for the cut sites (*68*). The samples were incubated for 60 minutes at 15 °C, followed by denaturation and electrophoresis analysis.

Trypsin from bovine pancreas containing TPCK inhibitor used in limited proteolysis experiment was purchased from Sigma. Na-Tosyl-L-lysine chloromethyl ketone hydrochloride (TLCK) was purchased from Fluka.

2.14 Kinetic analysis

The kinetic experiments were performed in metal free 25 mM Mes-Tris buffer containing 0.25M KOAc pH 7.1. Free metal ion was removed by passing the buffer through a chelex column (after chelex the pH was approximately 7.3). Dialysis of protein was done in 25 mM Mes-Tris buffer containing 1 mM $MnCl_2$, two dialyses of at least 100 fold was carried out. After dialysis, protein was diluted with metal free assay buffer to give final concentration 1 mg/mL (G376E, Q, N, A), 2 mg/mL for G376D and 0.1 mg/mL (wild-type). The final metal concentration was taken into account when calculating the Km value. There were two aspects of the kinetic activity inspected here: a) the Mn^{2+} metal ion dependence, and b) the PGA concentration dependence. The assay parameters were as follows: 1) assay buffer, 1 mM of synthesized PGA, enzyme and varying concentrations of metal, with a final volume of approximately 1 mL. 2) assay

buffer, a fixed concentration of $MnCl_2$ that was not inhibitory (based on part 1), enzyme, and varying concentrations of PGA with a final volume of approximately 1 mL. Different concentration of PGA solution was made using serial dilution with metal free assay buffer. The absorbance change at 240 nm was monitored over a period of two minutes in both cases to ensure the linearity of the assay curve. The ΔOD_{240} was converted to Δ[PEP] using PEP extinction coefficient (ε = 1.25 mM^{-1}). The rate of the reaction was plotted against the concentration of $MnCl_2$ or PGA. The result was fitted using Michaelis-Menten equation or modified substrate inhibition equation. The modified substrate inhibition equation is as follows:

$$y = ((V1*x)+(V2*x*x/Ki))/(Km+x+(x*x/Ki))$$

Where V1 is maximum velocity, the V2 is the limiting velocity, the Km is Michaelis constant, and the Ki is inhibition constant. The y is the rate of the reaction and x is the concentration of the metal ion or substrate.

The KOAc was from Fluka. It was added into 25 mM MT buffer to achieve a final concentration of 250 mM. Chelex 100 chelating resin was from BIO-RAD. The resin was washed extensively using distilled water. Buffers were passed through a column made of such resin slowly to remove free metal ions, and were then stored in a 20% nitric acid washed plastic bottle at 4°C. Nitric acid used to soak the glassware was from BDH. Substrate 2-PGA were synthesized from PEP using methods described by Sims *et al* (*69*). The PEP was purchased from Boehringer Mannheim.

2.15 Isothermal titration calorimetry (ITC)

A solution of an equilibrium mixture of PEP/PGA mixture was made by dissolving PEP in 5 mL of 25 mM MT buffer containing 1 mM $MnCl_2$. The concentration of the solution was determine from it absorbance at 240 nm. The extinction coefficient of PEP is 1.25 mM^{-1} at 240 nm. A 20 μL of concentrated wild-type yeast enolase was added (~0.2 mg), and solution was incubated at 4°C overnight to reach equilibrium. A stock solution of $MnCl_2$ was also made. The process was carefully manipulated to minimize concentration errors.

The protein samples were dialyzed against 25 mM MT buffer containing 1 mM $MnCl_2$. The ratio of enzyme to buffer of each dialysis was at least 1:100, with one buffer change. Using the dialysis buffer, the protein sample was diluted to 2.5 mL with approximately 100 μM concentration. The PEP/PGA mixture was diluted to 2-3 mM (depends on experiment) using dialysis buffer as well. The injection volume ranged from 3-4 μL, and total injection number was 60-80. The concentration of the protein is determined based on the protein left after the loading process is complete.

To make a protein solution with most of second metal cofactor absent, protein sample was passed quickly through a Chelex-100 column (2-3 mL of resin) that had been equilibrated with MT buffer. Then the protein was eluted with 25 mM MT metal-free buffer. The buffer volume used to elute the protein varies depending on the volume of protein sample loaded onto the column. Total volume was approximately 2.5 mL. To this protein solution, a small volume of 44 mM phosphonoacetohydroxamate (PhAH), a tight binding inhibitor, was added. The final concentration of the inhibitor is slightly higher than protein concentration. This sample was titrated with 2-3 mM of $MnCl_2$ (diluted

using metal free 25 mM MT buffer). The injection volume was 3-4 μL, and total injection number was 60-80.

For both experiment, the data obtained was fitted using Microcal Origin software using one or two site fitting options. This experiment was performed on wild-type and G376E, Q, D, N yeast enolase.

2.16 Instruments and software associated with this project

For 4th derivative UV analysis, kinetic assay, various OD readings, the Varian Cary 1 or Cary 100 UV-Visible Spectrophotometer was used. Jasco J-710 Spectropolarimeter was utilized for all CD related experiments. Reference correction and noise reduction was done with Jasco software. For experiments related to fluorescence, an Aminco Bowman Series 2 Luminescence Spectrometer was used. The analytical ultracentrifugation experiments were performed on a Beckman Optima^{TM} XL-1 Analytical Ultracentrifuge. The analysis of results was done using DCDT+, Sednterp, and Sedfit software. (Obtained from RASMB website: http://www.bbri.org/RASMB/) The mass spectroscopic experiment was performed on Micromass Q-ToF-2^{TM}. Kinetic data were analyzed using non-linear regression with EnzFitter version 2.0 (Biosoft). For the isothermal titration calorimetry experiment, Microcal Incorporated's VP-ITC MicroCalorimeter was used. The data analysis was done using Microcal Origin 5.0 software designed for ITC experiments. To determine the relative band intensity in the proteolysis susceptibility experiment, GeneGenius Bio Imaging System was used to collect the photos, and GeneSnap 4.0 was used in analysis. Both of these tools were from SynGene.

Chapter 3 Results

3.1 Site-directed mutagenesis

The complete wild-type recombinant plasmid DNA is approximately 6.0 kb long. This includes the yeast enolase gene insert, and pET-3a vector. The insert is between *Nde*I and *Bam*HI restriction sites, which has a size of approximately 1.3 kb, and the vector is approximately 4.7 kb long. The identification of the mutants was based on the loss of a *Bgl*II restriction site. The wild-type *Bgl*II digestion yields two fragments of size 4696 bp and 1222 bp. The mutant DNA removes one of the BglII sites which makes the digestion yield only one fragment of size 5918 bp. Figure 3.1 demonstrates this observation, and Figure 3.2 shows the digestion pattern for wild-type vs. G376I protein.

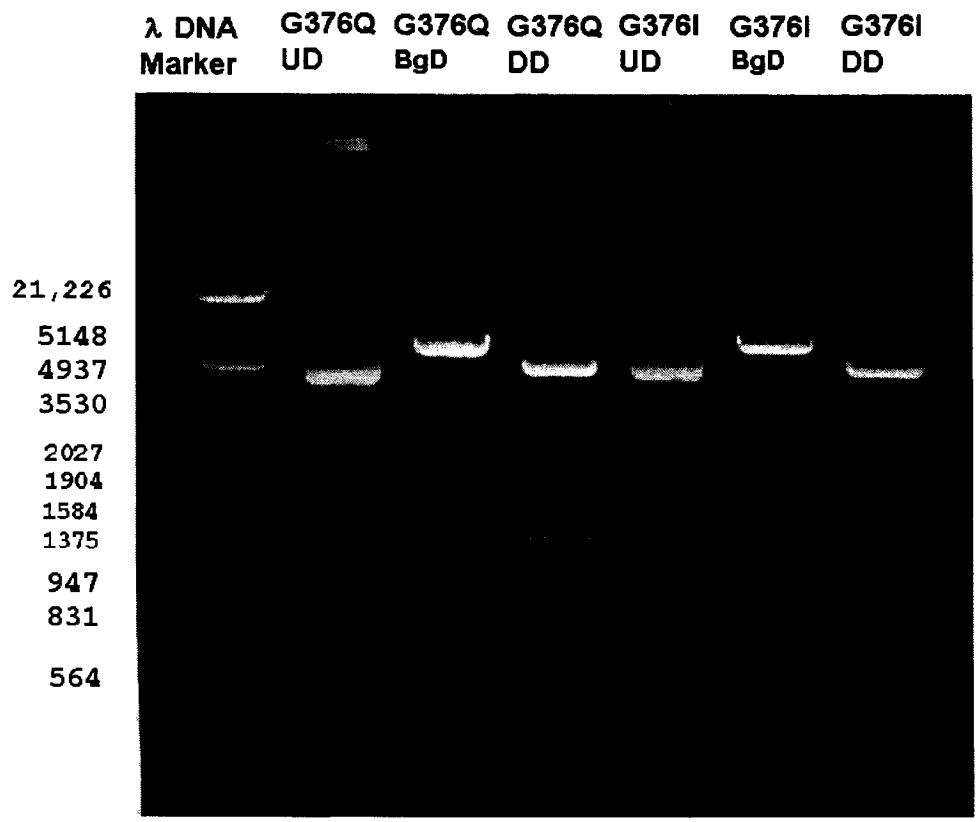

Figure 3.1: DNA gel for screening. UD = undigested, BgD = *Bgl*II digestion, DD = *Bam*HI, *Nde*I digestion. Units are in base pairs.

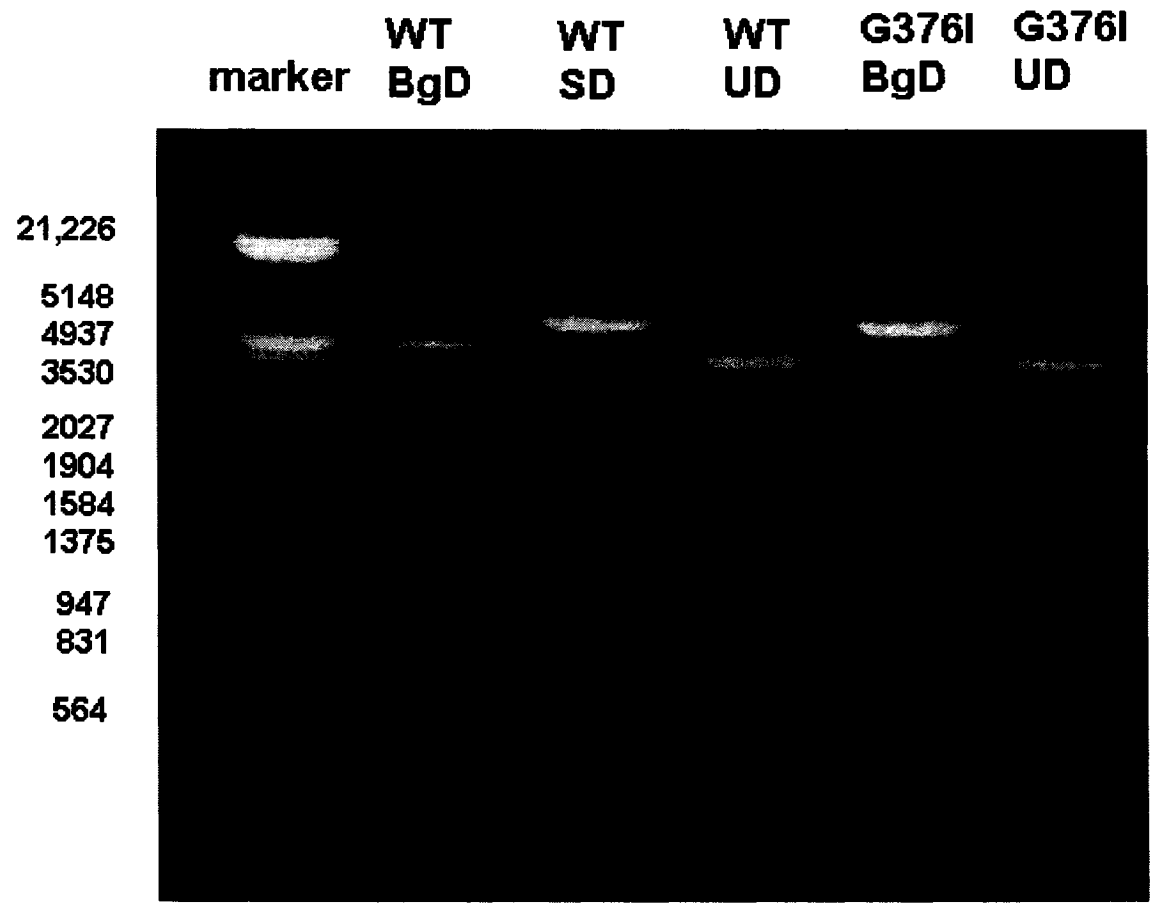

Figure 3.2: Agarose gel of digestion pattern comparison of wild-type DNA vs. G376I mutant DNA. UD = undigested, BgD = *Bgl*II digestion, SD = *Nde*I digestion. Units are in base pairs.

Following the large-scaled plasmid preparation, the DNA plasmids were sent to BioS&T Inc. (Montreal) for sequencing. The sequencing results revealed that there are three silent mutations present in the wild-type recombinant plasmid, which is carried over into all of the mutant plasmids. Moreover, the sequencing results has confirmed the presence of the substitution made, and that there were no other missense mutations introduced.

The purification schemes were revised based on the previous work (*64*). The salting-out and ion exchange columns were used to purify wild-type and variant proteins.

The wild-type and variants with the same overall charge (G376Q, G376I, G376N, G376A) were precipitated using 0-40% and 40-85% ammonium sulfate cuts. The enolase was precipitated in 40-85% salt cut. Q-Sepharose and CM-Sepharose ion exchange column purification was then carried out. The elution profile is shown in Figure 3.3. The mutants with one charge less than wild-type (G376E, G376D) were precipitated using 0-50% followed by 50-85% ammonium sulfate precipitation range. This was followed by CM-Sepharose, and a small volume Q-Sepharose column purification (~2 mL). The elution profiles of G376E mutant are shown in Figure 3.4. The elution profiles were very similar among the proteins with the same overall charge, and therefore the elution profiles of one protein were shown for each case. During the purification process, it was found that the catalytic abilities of the variants were significantly lower than that of wild-type. Elution of the variants was monitored based on the $OD_{280/260}$ ratio and SDS-PAGE results. The purification of wild-type enzyme is summarized in Table 3.1. The purification summary of the variant however, was not complete due to severely decreased protein activity, but the amount of protein obtained at each step is shown in Table 3.2. The SDS-PAGE of G376E purification process is shown in Figure 3.5.

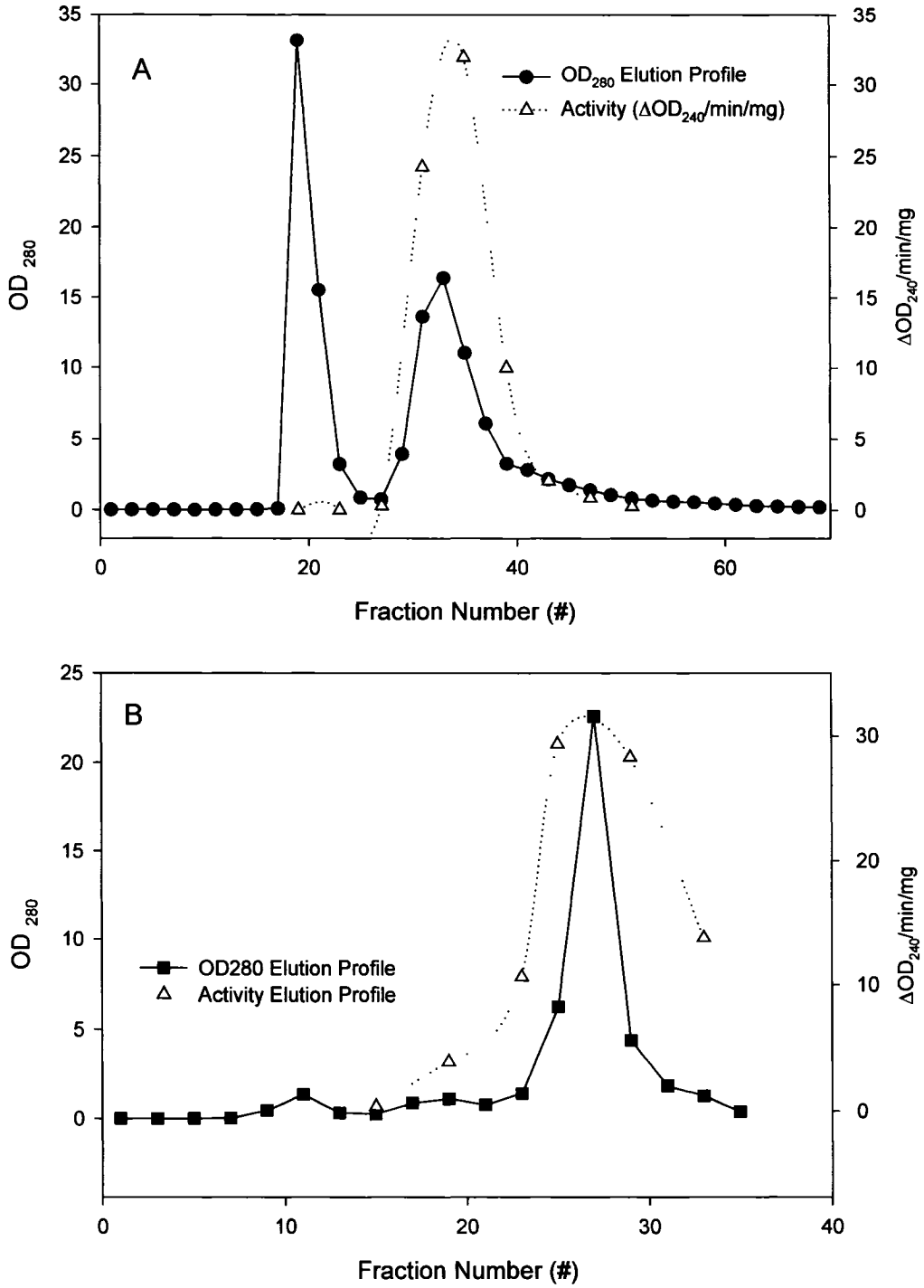

Figure 3.3: Wild-type A) Q-Sepharose elution profile, B) CM-Sepharose elution profile. The gradient started at fraction #13.

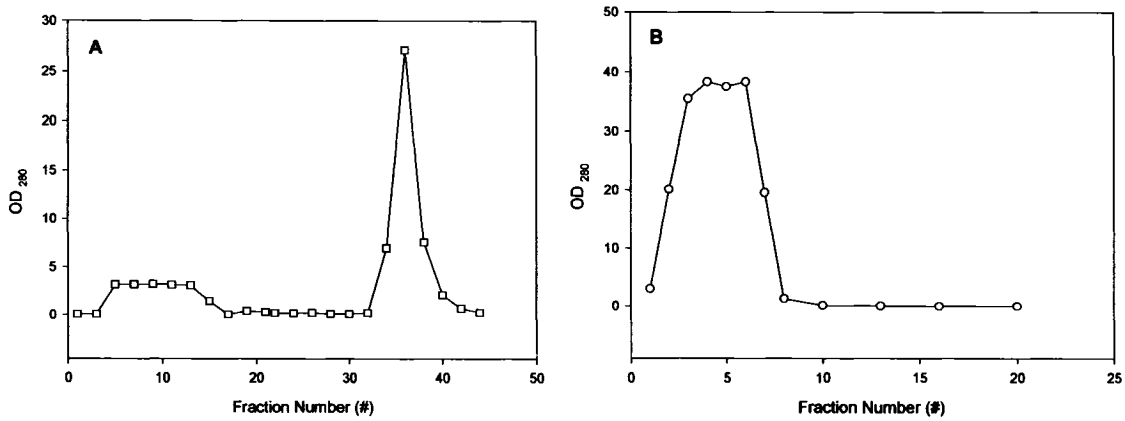

Figure 3.4: G376E A) CM-Sepharose elution profile, the gradient started at fraction #22, B) Q-Sepharose elution profile.

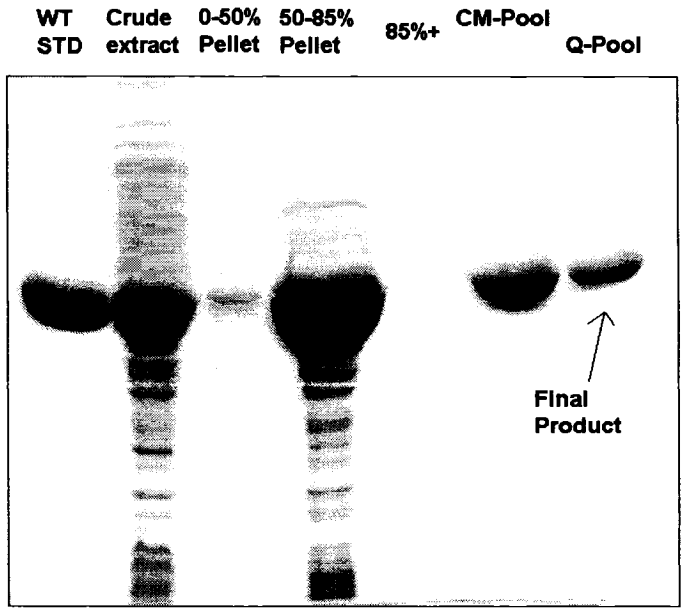

Figure 3.5: G376E purification SDS-PAGE.

	Volume (mL)	Total Activity (units)	Total Protein (mg)	Activity Yield (%)	Specific Activity (Units/mg)	Fold Purification
Crude extract	30.5	7823.25	10479.8	-	0.747	-
40% cut supernatant	26.0	7131.8	6892.6	91.2	1.035	1.38
85% cut pellet	13.0	4427.8	4053.4	56.6	1.092	1.46
85% cut supernatant	21.0	67.2	987.0	-	-	-
Q-Pool	32.0	6086.4	366.72	77.8	1.660	2.22
CM-Pool	25.8	4365.4	255.16	55.8	1.711	2.29

Table 3.1: Wild-type protein purification summary. Specific activity was calculated by dividing total activity by total protein. Fold purification was calculated by dividing the specific activity of each stage by crude specific activity. The units here are defined as ΔOD_{240}/min, the activity assays were done using phosphoenolpyruvate. The total protein was estimated using OD_{280} absorbance.

	Volume (mL)	Total Protein (mg)
Crude extract	30.0	12462.4
50% cut supernatant	26.0	4465.3
85% cut pellet	8.0	3770.8
85% cut supernatant	24.0	846.0
CM-Pool	25.5	313.1
Q-Pool	10.0	278.5

Table 3.2: G376E variant purification summary. The total protein was estimated based on OD_{280} absorbance.

Purified protein molecular mass was determined using Q-ToF mass spectroscopy. Each mutant's molecular mass was determined, and was compared to the result of wild-type protein. Mass spectrum of wild-type enzyme is shown in Figure 3.6. The experimental molecular mass of wild-type and variants were compared to the theoretical value in Table 3.3.

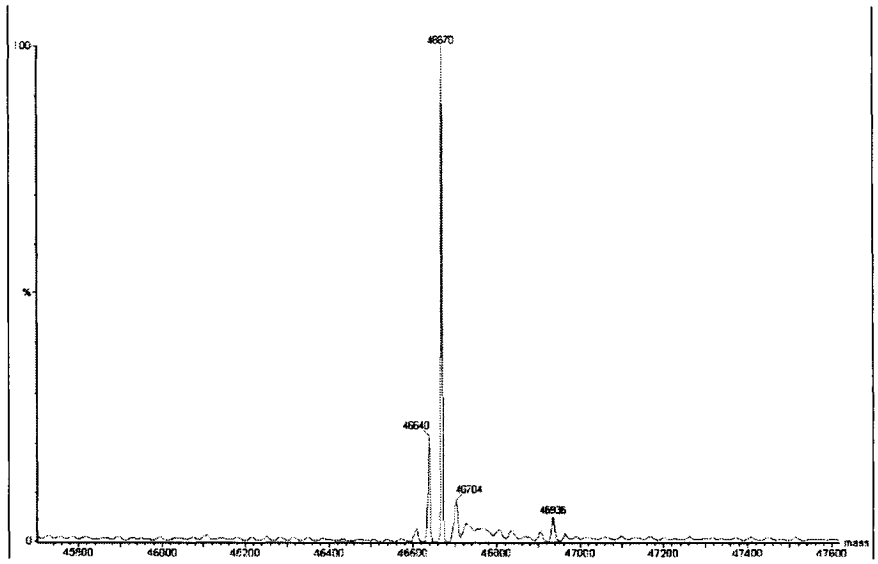

Figure 3.6: Q-ToF mass spectroscopy result of wild-type enzyme.

Name	Theoretical M.W. (Da)	Experimental M.W. (Da)	Difference (Da)
Wild-Type	46671	46670	1
G376E	46743	46743	0
G376Q	46742	46740	2
G376I	46727	46725	2
G376D	46729	46727	2
G376N	46728	46725	3
G376A	46685	46681	4

Table 3.3: Wild-type and variants' theoretical and experimental molecular weights.

3.2 Structural studies of variants vs. wild-type through spectroscopic techniques

3.2.1 Secondary structural characteristics comparison

To determine how the substitutions at amino acid 376 in yeast enolase would affect the overall secondary structure, far UV-circular dichroism (CD) was used. CD spectra were collected in range of 260-200 nm. In this region, the polarized light is absorbed by amide-amide interaction of the protein peptide backbones. Since there are

various types of secondary structure present in different proteins, each protein's polarized light absorption pattern is different. This property allows us to probe secondary structural differences between the wild-type and the variant enolases. Figure 3.7 shows that the wild-type and variants spectra have similar shape and minima at approximately 208 nm and 222nm, which correspond to α-helices absorption characteristics. Although not shown, the G376Q, G376N, G376I variants all yield similar far UV-CD spectra. Also the protein in TEM buffer with or without 0.3M NaOAc yield similar results, and at lower protein concentration, the spectra were nearly superimposable (See Figure 3.8).

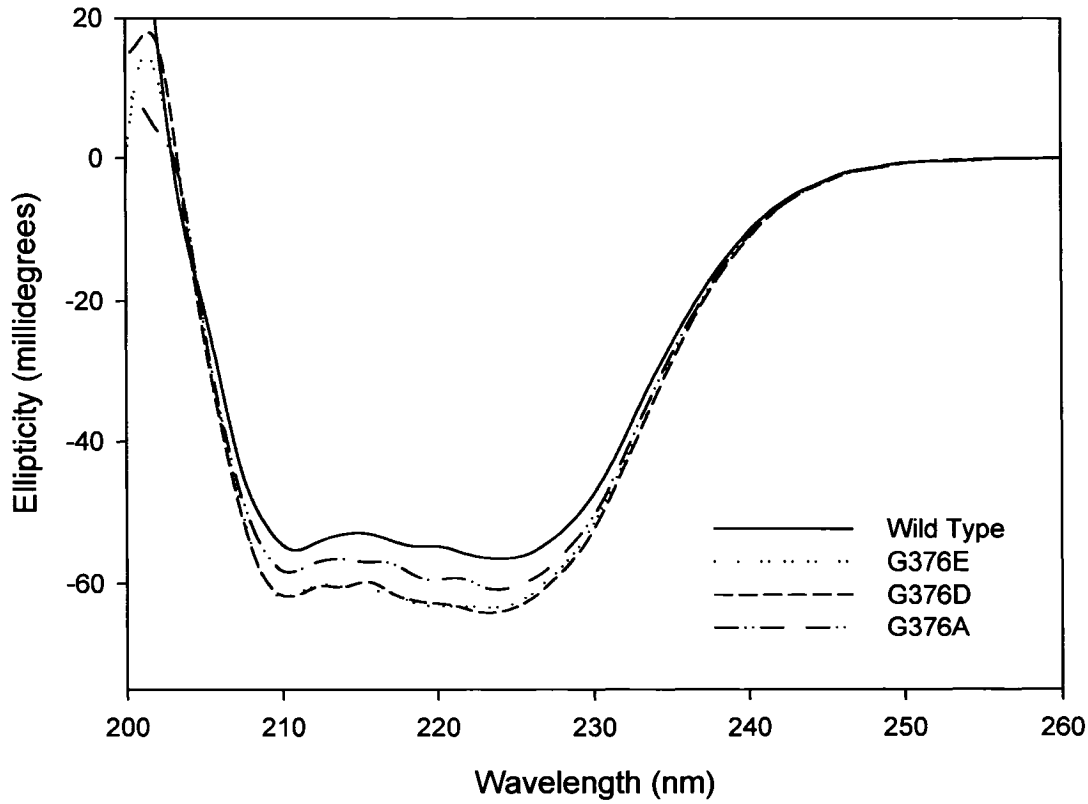

Figure 3.7: Far-UV CD spectra comparison of wild-type yeast enolase vs. G376E, D, A variants (all in TEM buffer). Each protein concentration was 0.5 mg/mL. Protein samples were scanned using 1 mm quartz (QS) cell at 15 °C.

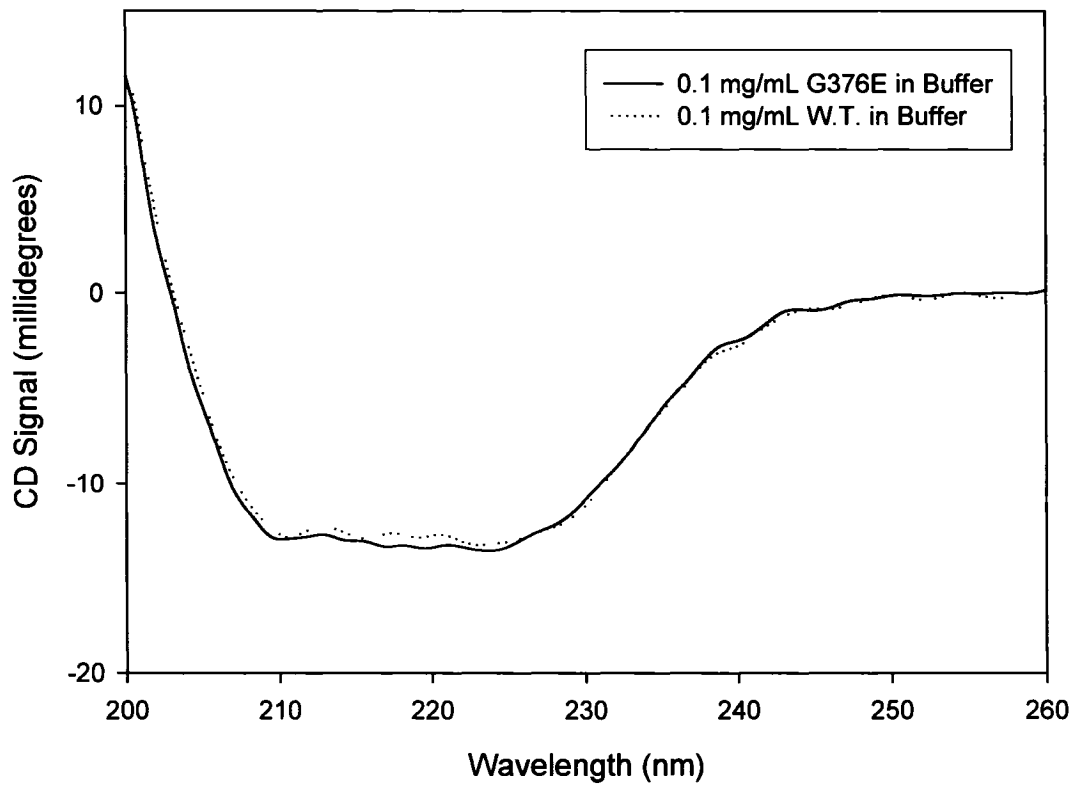

Figure 3.8: Far-UV CD spectra comparison of wild-type yeast enolase in TEM buffer vs. G376E enolase in TEM buffer. Each protein concentration was 0.1 mg/mL and the scan were done in 1 mm quartz (QS) cell at 15 °C.

3.2.2 Tertiary structural characteristics comparison

Yeast enolase has 5 Trp, 9 Tyr and 16 Phe (See Figure 4.0 in discussion), these amino acid residues can serve as chromophores for monitoring tertiary structural changes by 4th derivative UV and near UV CD. The results obtained by using these techniques are shown below. Using the salt described in the introduction, wild-type yeast enolase dimer (in 0.3 M NaOAc) and monomer (in 0.3 M $NaClO_4$) were made. Their spectra were used as the standards. The UV absorbance spectra were collected for wild-type monomer, dimer, and each variant protein in TEM buffer with/without 0.3M NaOAc. The 4th derivative UV spectra was calculated from the zero-order spectra using mathematical transformation described by Lange et al (*70*). Typical wild-type yeast enolase dimer and monomer 4th derivative UV spectra are shown in Figure 3.9A. The position of the maxima and minima, and their intensities allow us to probe the environment of the aromatic amino acids in a protein. Thus, it helps reveal the tertiary structural differences. To quantitate this difference, the ratio of maxima to minima is utilized.

Ratio = {second maxima – second minima}/{first maxima – first minima}

As found in previous studies, the shape of the 4th derivative UV spectra changes significantly when a dimeric yeast enolase becomes monomeric, due to the increased aromatic amino acid solvent accessibility. It is, therefore, used as a tool to probe yeast enolase subunit dissociation. The spectra comparisons of wild-type vs. variants are shown in Figure 3.9B-D. The quantitated data based on these spectra are presented in Table 3.4.

Similar to 4th derivative UV method, near-UV circular dichroism can be used to monitor the tertiary conformational change as well. Aromatic amino acids, phenylalanine, tyrosine and tryptophan, absorb in this region, and their absorption bands depend on the

environment of these residues. The combined absorption band of these three types of aromatic residues is unique for different proteins due to different amino acid composition and environments of the aromatic residues. In general, phenylalanine absorbs in range of 255-270 nm, while tyrosine absorbs in range of 275-282 nm, and lastly the tryptophan absorbs near 280 nm (*71*). In yeast enolase, when a dimer dissociates into monomer, the CD spectra in near-UV range is changed dramatically. When the spectrum of monomeric wild-type enzyme is subtracted from that of the dimer dimer, the difference resembles a tryptophan absorption spectrum (See Figure 3.10). The spectral differences were at their largest at approximately 283 nm. Ellipticity at 283 nm was therefore used to calculate the fraction of monomer present in each mutant protein (See Figure 3.11 and Table 3.5, 3.6).

Clearly, the 4^{th} derivative UV results and aromatic CD results are not in agreement with each other. This observation will be further discussed in the next chapter. In this section, the calculation was based on the assumption that the variant protein will have the same type of spectroscopic characteristics as the wild-type enzyme. Evidently, that assumption may be incorrect.

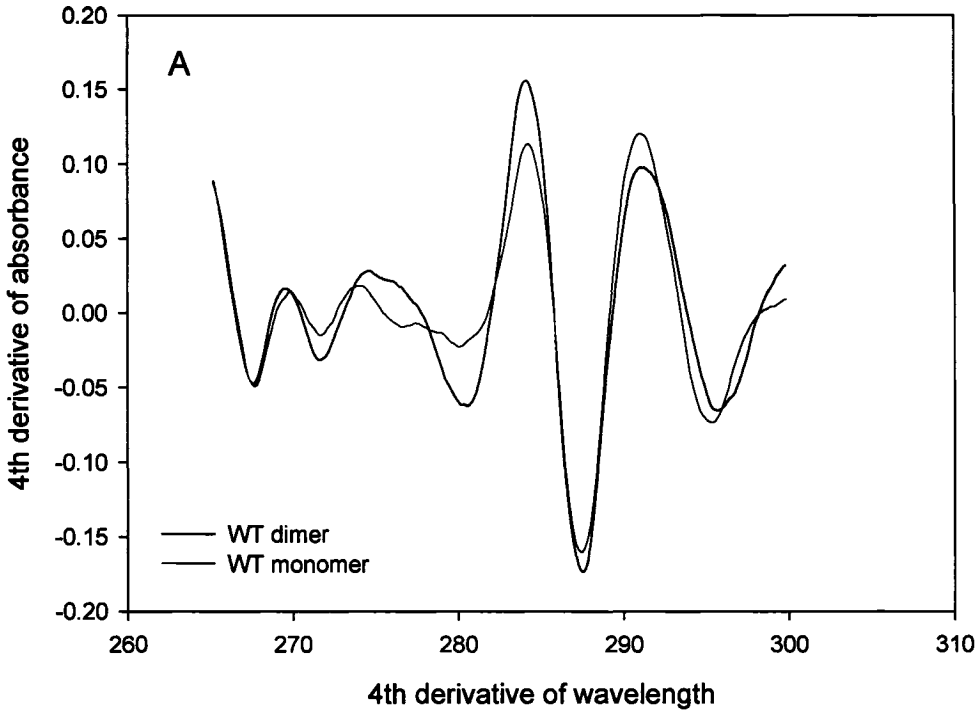
A
0.20
0.15
0.10
0.05
0.00
-0.05
-0.10
-0.15
-0.20
4th derivative of absorbance
WT dimer
WT monomer
260
270
280
290
300
310
4th derivative of wavelength

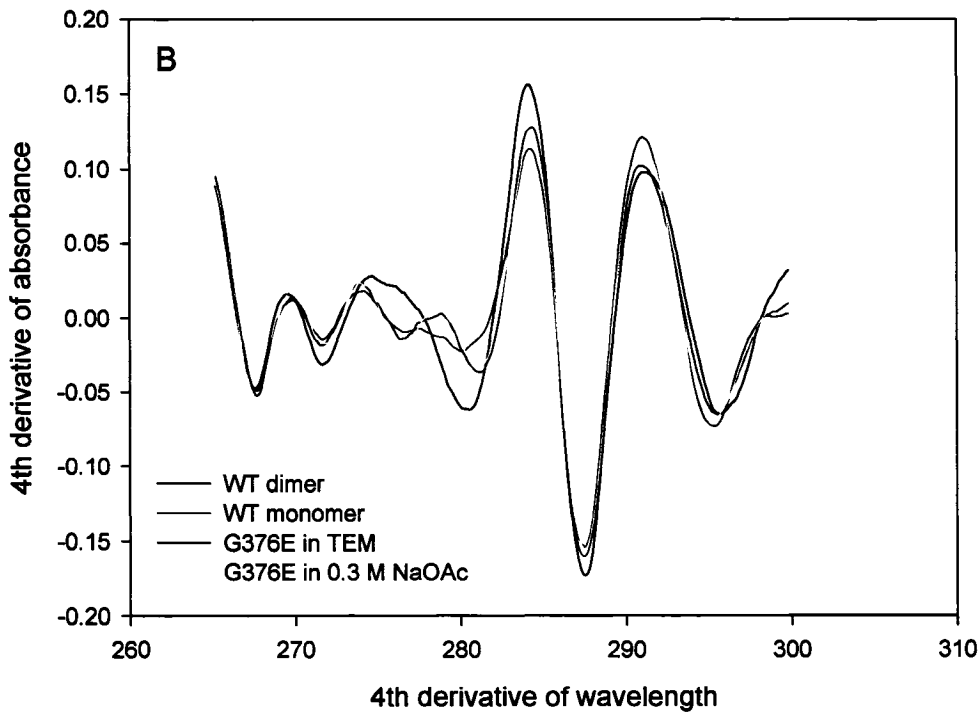
B
0.20
0.15
0.10
0.05
0.00
-0.05
-0.10
-0.15
-0.20
4th derivative of absorbance
WT dimer
WT monomer
G376E in TEM
G376E in 0.3 M NaOAc
260
270
280
290
300
310
4th derivative of wavelength

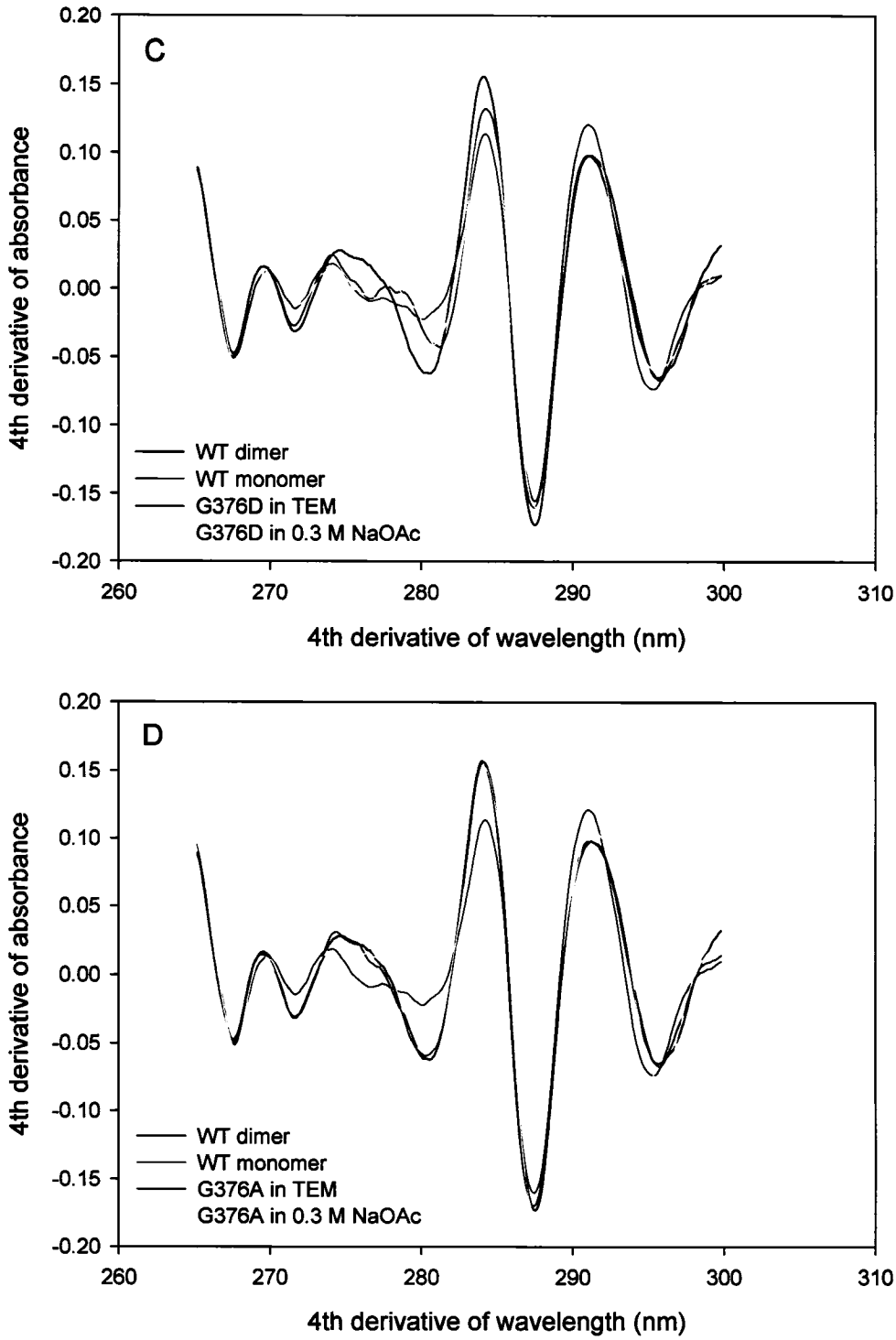

Figure 3.9: 4th derivative UV spectra of A) wild-type dimer, monomer; B) wild-type vs. G376E variant in TEM and 0.3 M NaOAc; C) wild-type vs. G376D in TEM and 0.3 M NaOAc; D) wild-type vs. G376A in TEM and in 0.3 M NaOAc. All sample concentration was 1.0 mg/mL; the scans were taken in 1 cm quartz (QS) cell at 15°C.

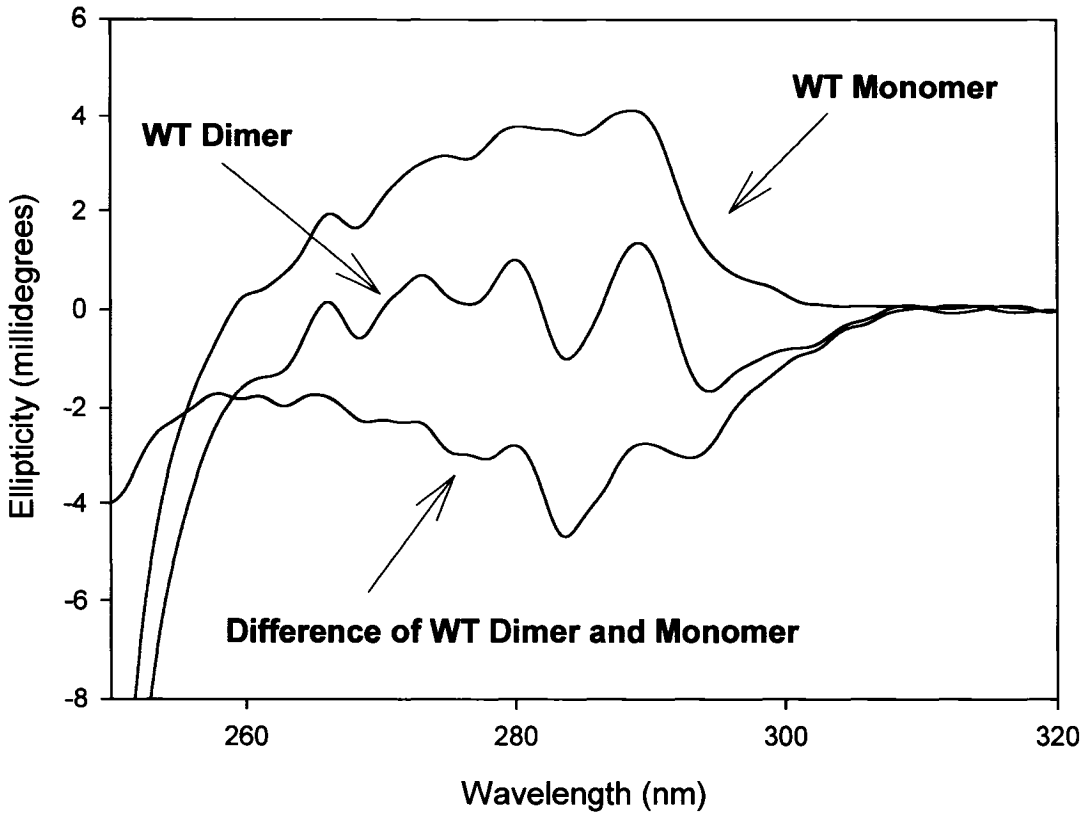

Figure 3.10: Near-UV CD spectra of wild-type dimer, monomer, and their difference. Protein concentration is 1 mg/mL (10.71 μM), the scans collected using 1 cm quartz (QS) cell at 15 °C.

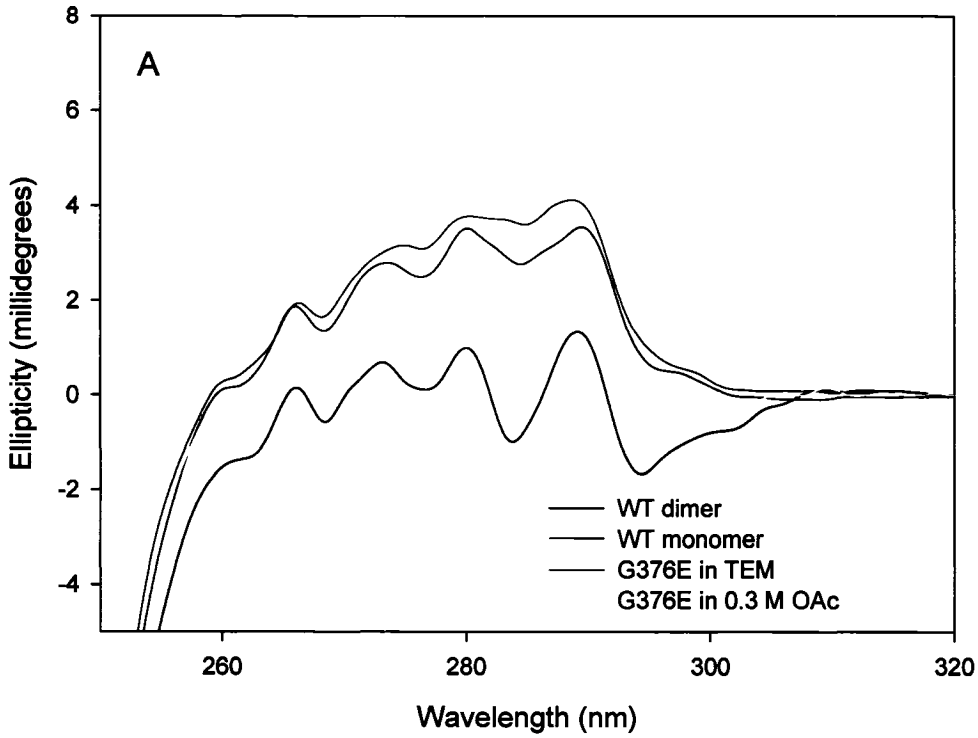
A
8
6
4
2
0
-2
-4
Ellipticity (millidegrees)
260
280
300
320
Wavelength (nm)
WT dimer
WT monomer
G376E in TEM
G376E in 0.3 M OAc

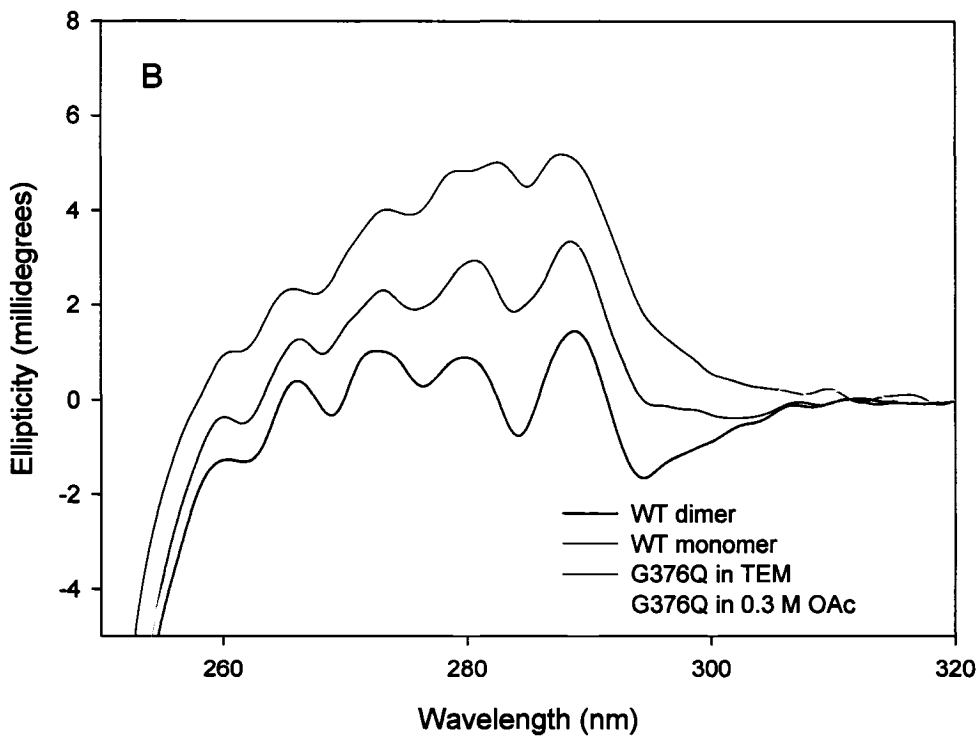
B
8
6
4
2
0
-2
-4
Ellipticity (millidegrees)
260
280
300
320
Wavelength (nm)
WT dimer
WT monomer
G376Q in TEM
G376Q in 0.3 M OAc

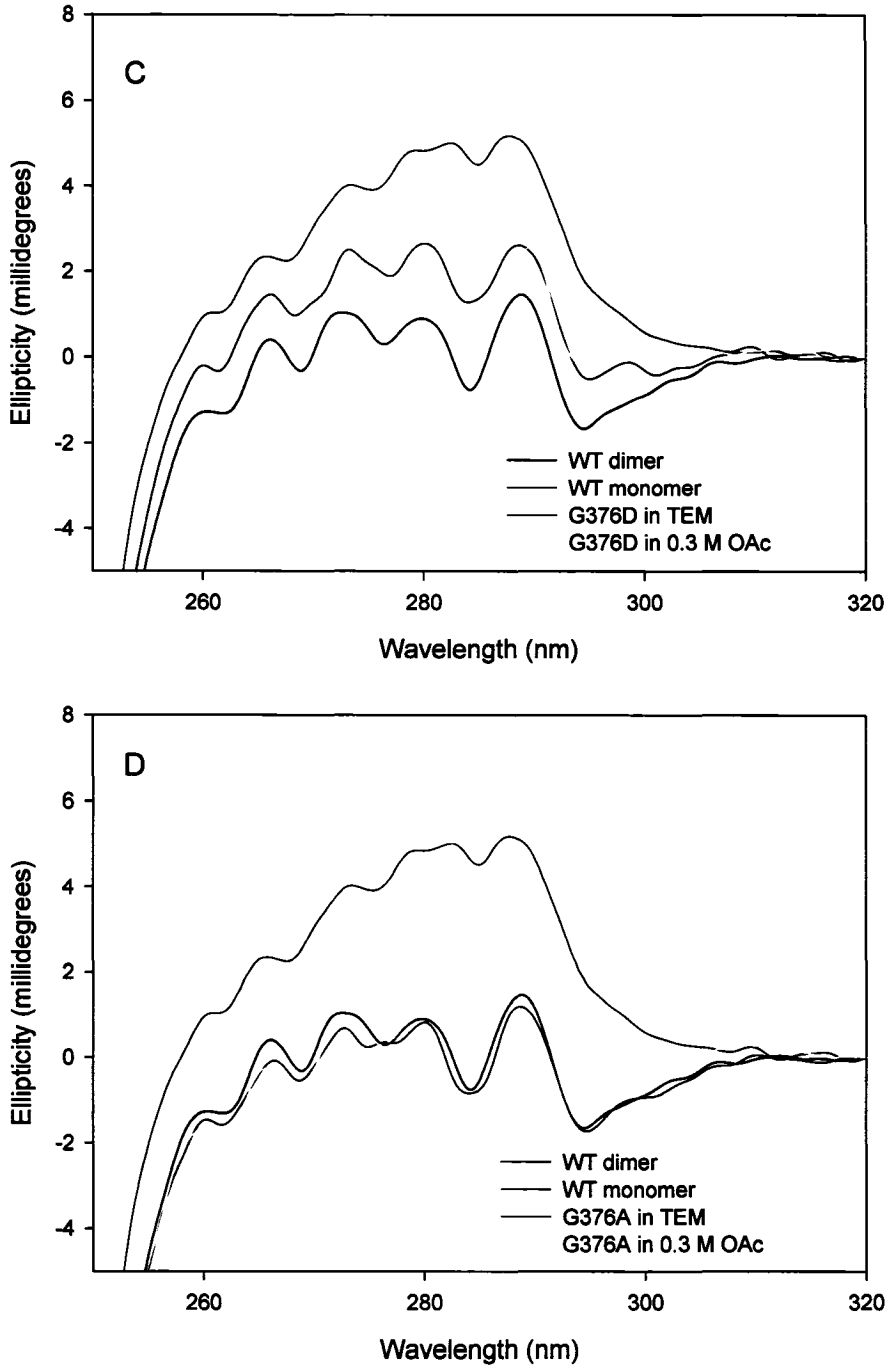

Figure 3.11: Near-UV CD spectra of A) wild-type monomer/dimer vs. G376E in TEM and 0.3 M NaOAc B) wild-type monomer/dimer vs. G376Q in TEM and 0.3 M NaOAc; C) wild-type monomer/dimer vs. G376D in TEM and 0.3 M NaOAc; D) wild-type monomer/dimer vs. G376A in TEM and in 0.3 M NaOAc. All sample concentration was 1.2 mg/mL, except G376E, whose concentration was 1 mg/mL. The scans were taken in 1 cm quartz (QS) cell at 15°C.

Name	Δ1	Δ2	Δ2/ Δ1	% Dissociated
Wild-type dimer	0.1629	0.3293	2.021	0 %
Wild-type monomer	0.1942	0.2740	1.411	100 %
G376E in buffer	0.1678	0.2816	1.672	57.2 %
G376E in OAc	0.1833	0.2772	1.512	83.4 %
G376Q in buffer	0.1829	0.2952	1.614	66.7 %
G376Q in OAc	0.1881	0.3012	1.601	68.9 %
G376I in buffer	0.1675	0.2687	1.604	68.4 %
G376I in OAc	0.1954	0.2739	1.402	101.5 %
G376D in buffer	0.1649	0.2880	1.747	44.9 %
G376D in OAc	0.1697	0.2873	1.693	53.8 %
G376N in buffer	0.1637	0.3067	1.874	24.1 %
G376N in OAc	0.1812	0.3003	1.657	59.7 %
G376A in buffer	0.1649	0.3272	1.984	6.1 %
G376A in OAc	0.1813	0.3289	1.814	33.9 %

Table 3.4: Quantitated values of 4th derivative UV results. Δ1={first maxima – first minima}; Δ2 = {second maxima – second minima}.

Name	CD signal @ 283 nm (millidegrees)	% Dissociated
Wild-type dimer	-0.7772	0 %
Wild-type monomer	3.7201	100 %
G376E in buffer	2.9981	84.7 %
G376E in OAc	2.2415	68.7 %

Table 3.5: Ellipticity at 283 nm of G376E variant. The percentage dissociation was estimated based on wild-type dimer and monomer values. Protein concentrations were 1 mg/mL.

Name	CD signal @ 283 nm (millidegrees)	% Dissociated
Wild-type dimer	-0.7054	0 %
Wild-type monomer	4.7610	100 %
G376Q in buffer	1.8577	46.9 %
G376Q in OAc	1.7185	44.3 %
G376I in buffer	3.1318	70.2 %
G376I in OAc	2.4937	58.5 %
G376D in buffer	1.3014	36.7 %
G376D in OAc	0.8277	28.0 %
G376N in buffer	0.5486	22.9 %
G376N in OAc	0.5922	23.7 %
G376A in buffer	-0.8309	-2.3 %
G376A in OAc	-0.2990	7.4 %

Table 3.6: Ellipticity at 283 nm of each variant protein. The percentage dissociation was estimated based on wild-type dimer and monomer values. Protein concentrations were 1.25 mg/mL.

3.2.3 Quaternary structural characteristics comparison

As observed above, the secondary structures of the mutants were likely to be intact, while some spectroscopic results suggested possibility of dissociated protein. The mutant proteins were subjected to analytical ultracentrifugation (AUC), and the sedimentation coefficients of the mutants were compared to that of wild-type enzyme. In contrast to the CD and UV spectroscopic techniques, instead of relying on chromophore environment, the sedimentation coefficients ($S_{20,W}$) depend on the average molecular weight and shape of the species present in a sample. This coefficient describes the velocity of a molecule per unit gravitational acceleration. It can provide more accurate insights on quaternary structure of a molecule, and even be used in monitoring dissociation (*72*). The G376E sedimentation coefficient was compared to that of wild-type dimer and monomer at ~1 mg/mL concentration. Figure 3.12 shows a snapshot comparison of the run. The G376E and wild-type dimer were in 0.3 M NaOAc, while wild-type monomer was in 0.3 M $NaClO_4$. The presence of salt is usually required in AUC runs in order to prevent primary charge effects that may cause the protein to sediment more slowly (*72*). In this experiment, it is evident that the mutant protein is sedimenting slower than the wild-type dimer, but faster than the wild-type monomer. The solvent density and viscosity corrected sedimentation coefficients are shown in Table 3.7. This experiment confirms the observation made in tertiary structure studies: the G376E mutant is partially dissociated. Based on previous experiment on commercially available yeast enolase, a fully dimeric yeast enolase protein has a sedimentation coefficient of 5.490 ± 0.165, while a fully monomeric yeast enolase protein has a sedimentation

coefficient of 3.353 ± 0.134. Using the following equation, the fraction monomer was calculated, and the values are shown in Table 3.7.

$$f_{monomer} = (S_{20,W(dimer)}-S_{20,W(sample)})/(S_{20,W(dimer)}-S_{20,W(monomer)})$$

Based on this experiment, G376E was found to be 42.7 % dissociated. Similarly, G376Q, I, D and N was also found to be partially dissociated. Their sedimentation coefficients are shown in Table 3.8. Clearly, the mutation at Gly376 affected the subunit interface stability.

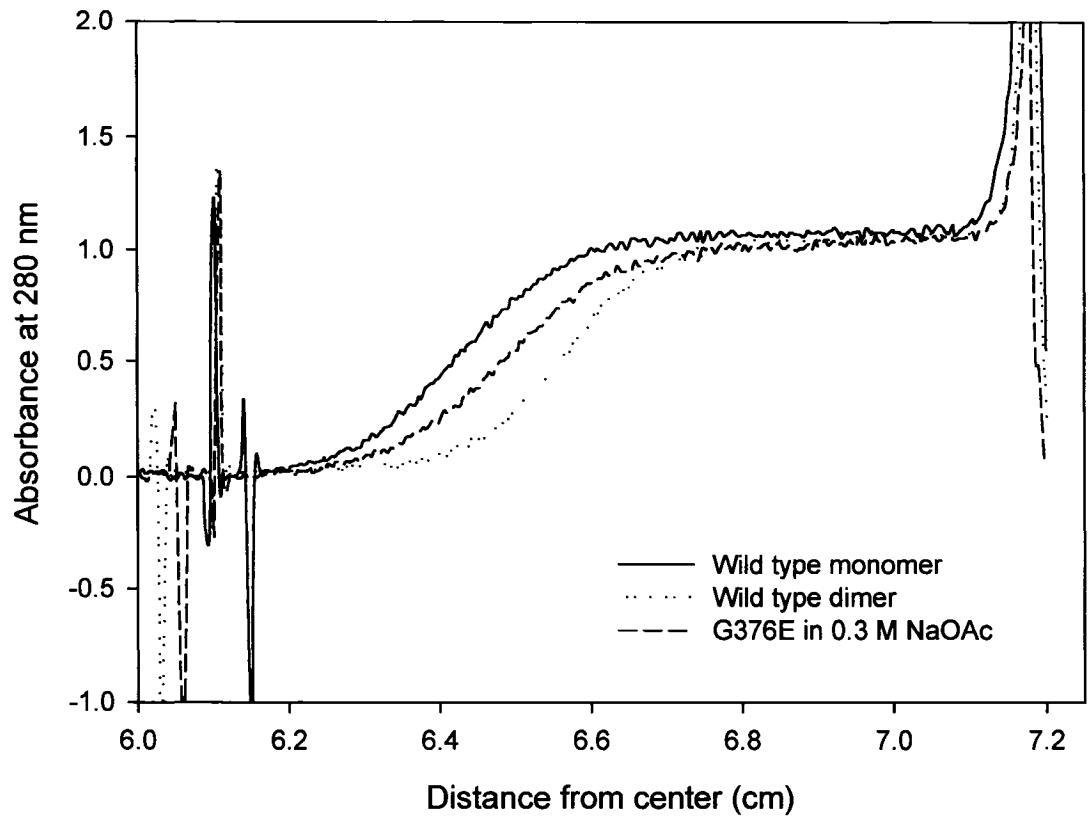

Figure 3.12: G376E vs. wild-type monomer, dimer AUC snapshot. The concentration of proteins were approximately 1 mg/mL for each, the snapshot was scan #30 at 15 °C.

Name	Sedimentation Coefficient ($S_{20,w}$)	Fraction monomer
Wild-Type Dimer	5.590 ± 0.004	0
Wild-Type Monomer	3.302 ± 0.007	1
G376E in 0.3 M NaOAc	4.612 ± 0.004	0.427

Table 3.7: Wild-type monomer, dimer sedimentation coefficients vs. G376E, and estimated fraction of monomer. The analysis was done using DCDT+ 2.0 software.

Name	Sedimentation Coefficient ($S_{20,w}$)	Fraction monomer
G376Q in 0.3 M NaOAc	4.628 ± 0.006	0.436
G376I in 0.3 M NaOAc	4.525 ± 0.006	0.482
G376D in 0.3 M NaOAc	4.996 ± 0.004	0.269
G376N in 0.3 M NaOAc	5.208 ± 0.004	0.173
G376A in 0.3 M NaOAc	5.623 ± 0.002	~ 0

Table 3.8: Sedimentation coefficients of G376Q, I, D, N, A. Concentration of G376Q, I were approximately 1 mg/mL; G376N, A concentration were approximately 1.26 mg/mL; G376D concentration was approximately 1.5 mg/mL. The scans were taken at 15 °C.

3.3 Dissociation studies of wild-type and variants yeast enolase

3.3.1 Determination of dissociation constant of wild-type vs. variants

As seen in the previous section, the mutations at Gly376 caused the protein to partially dissociate. To understand the severity of this observation, we carried out a study regarding the $S_{20,w}$ protein concentration dependency. Here, we are assuming that the dissociation is reversible and the $S_{20,w}$ value of the variants depend on the concentration of protein. In a situation of dimer-monomer equilibrium, the increase of protein concentration would result in increased fraction of dimer, while the decrease of protein concentration increase the fraction of monomer (*72*). Based on such properties, we aimed to determine the dissociation constant of each mutant protein. In this experiment, the protein concentration range was approximately 30-fold (0.4 μM to 15 μM for some case)

for selected mutants. For the remaining mutants, dissociation constants were from a single determination of $S_{20,W}$ at 1 mg/mL concentration from Section 3.2.3.

The dissociation constant was calculated based on fraction monomer, dimer and protein concentration using the following equation:

$$K_d = 4\ [\text{enolase}]\ (f_M)^2/(f_D)$$

Where f_M and f_D represents the fraction monomer and dimer.

The summary of this experiment is shown in Table 3.9 and 3.10. The wild-type dissociated constant was based on the dissociation studies of the wild-type in $NaClO_4$ from year 2002 performed Dr. Judith Kornblatt (unpublished data). The value obtained was based on multiple methods. The dissociation constants of five variants were increased by 1000-fold to 100-fold. The only variant remained as dimer was G376A.

Name	Sedimentation Coefficient ($S_{20,W}$)	Dissociation Constant (M)
Wild-Type	5.590 ± 0.004	1×10^{-8}
G376E 13 µM	4.574 ± 0.005	1.67×10^{-5}
G376E 4.4 µM	4.290 ± 0.009	1.26×10^{-5}
G376E 1.3 µM	3.818 ± 0.007	1.46×10^{-5}
G376E 0.4 µM	3.601 ± 0.018	1.08×10^{-5}
G376D 16.4 µM	4.996 ± 0.004	4.56×10^{-6}
G376D 5.1 µM	4.990 ± 0.004	1.46×10^{-5}
G376D 1.6 µM	4.597 ± 0.006	1.92×10^{-5}
G376D 0.5 µM	4.171 ± 0.009	1.99×10^{-6}

Table 3.9: Summary of dissociation constant of wild-type vs. G376E, D enzymes.

Name	Sedimentation Coefficient ($S_{20,W}$)	Dissociation Constant (M)
Wild-Type	5.590 ± 0.004	1×10^{-8}
G376Q	4.628 ± 0.006	1.17×10^{-5}
G376I	4.525 ± 0.006	1.59×10^{-5}
G376N	5.208 ± 0.004	8.59×10^{-7}
G376A	5.623 ± 0.002	$\sim 1 \times 10^{-8}$

Table 3.10: Summary of dissociation constant of wild-type vs. G376Q, I, N, A enzymes.

3.3.2 Efforts to shift monomer-dimer equilibrium towards dimer

Like many other equilibrium systems, monomer-dimer equilibrium of wild-type yeast enolase can be shifted depending on buffer conditions. Therefore, by finding the optimal conditions, the partially dissociated protein should be able to become fully dimeric once again. A combination of buffer conditions was tested to shift the mutant monomer-dimer equilibrium. Although many buffer conditions allow the near-UV spectra to become more dimer-like, none of the conditions by itself resulted a spectrum similar to that of wild-type dimer (See Figure 3.13). On the contrary, the monomer-like spectrum for G376E was obtained easily by adding varying concentrations of $NaClO_4$ (See Figure 3.14).

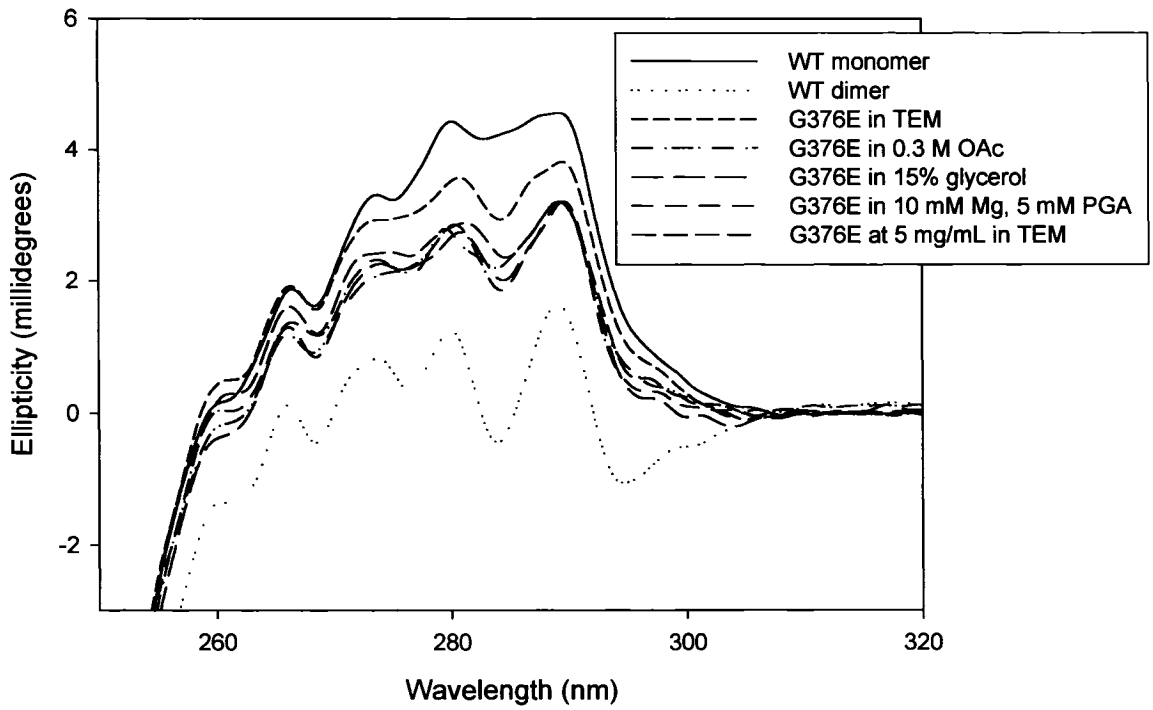

Figure 3.13: Near-UV CD spectra of G376E variant in different buffer conditions to shift monomer-dimer equilibrium towards dimer. All protein concentration was 1 mg/mL, except the 5 mg/mL sample. The scans were collected using 1 cm cell, at 15 °C. The 5 mg/mL sample scan was collected using 0.2 cm cell.

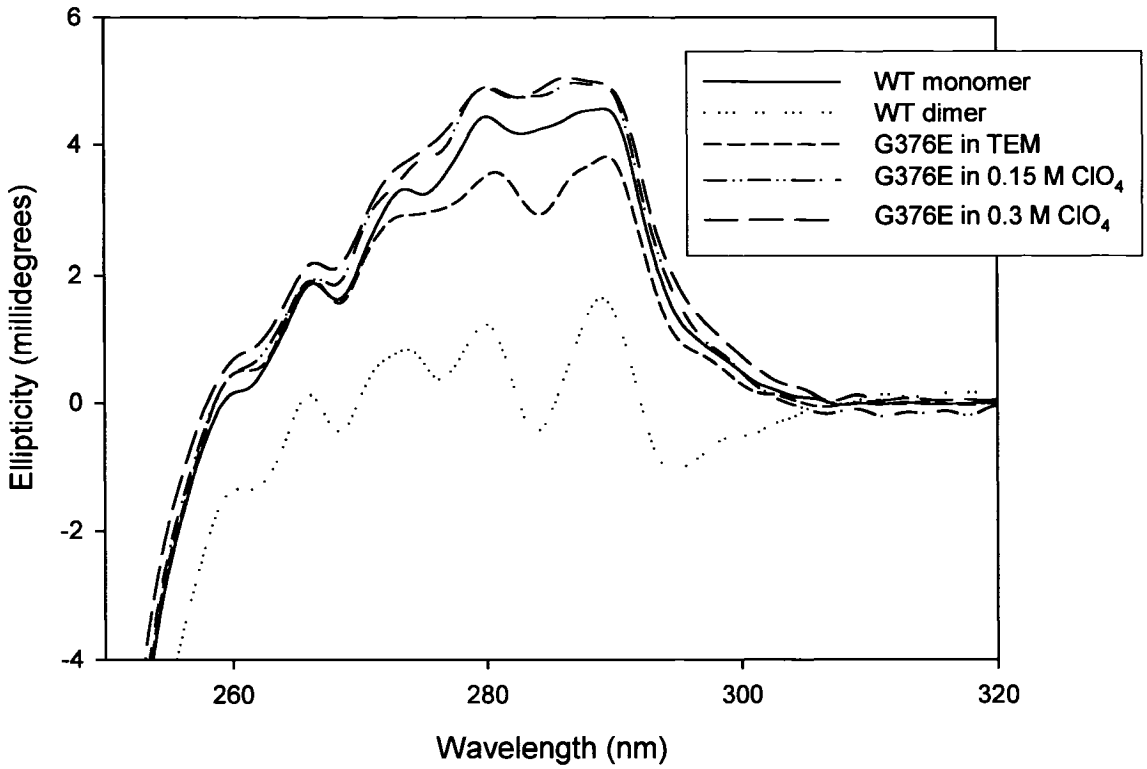

Figure 3.14: Near-UV CD spectra of G376E variant in different buffer conditions to shift monomer-dimer equilibrium towards monomer All protein concentration was 1 mg/mL. The scans were collected using 1 cm cell, at 15 °C.

During the process of determining condition for ITC experiments in the latter stage of the project, it was found that by replacing the natural metal cofactor Mg^{2+} with Mn^{2+}, the fraction monomer was decreased by approximately 25%. This observation was confirmed by both near-UV CD experiment and AUC experiment. Furthermore, by using higher protein concentration (~5 mg/mL), Mn^{2+} as the cofactor, and the presence of natural substrate PEP/PGA mixture, a dimer-like sedimentation coefficient and near-UV CD spectra were obtained for G376E (See Figure 3.15 and Table 3.11).

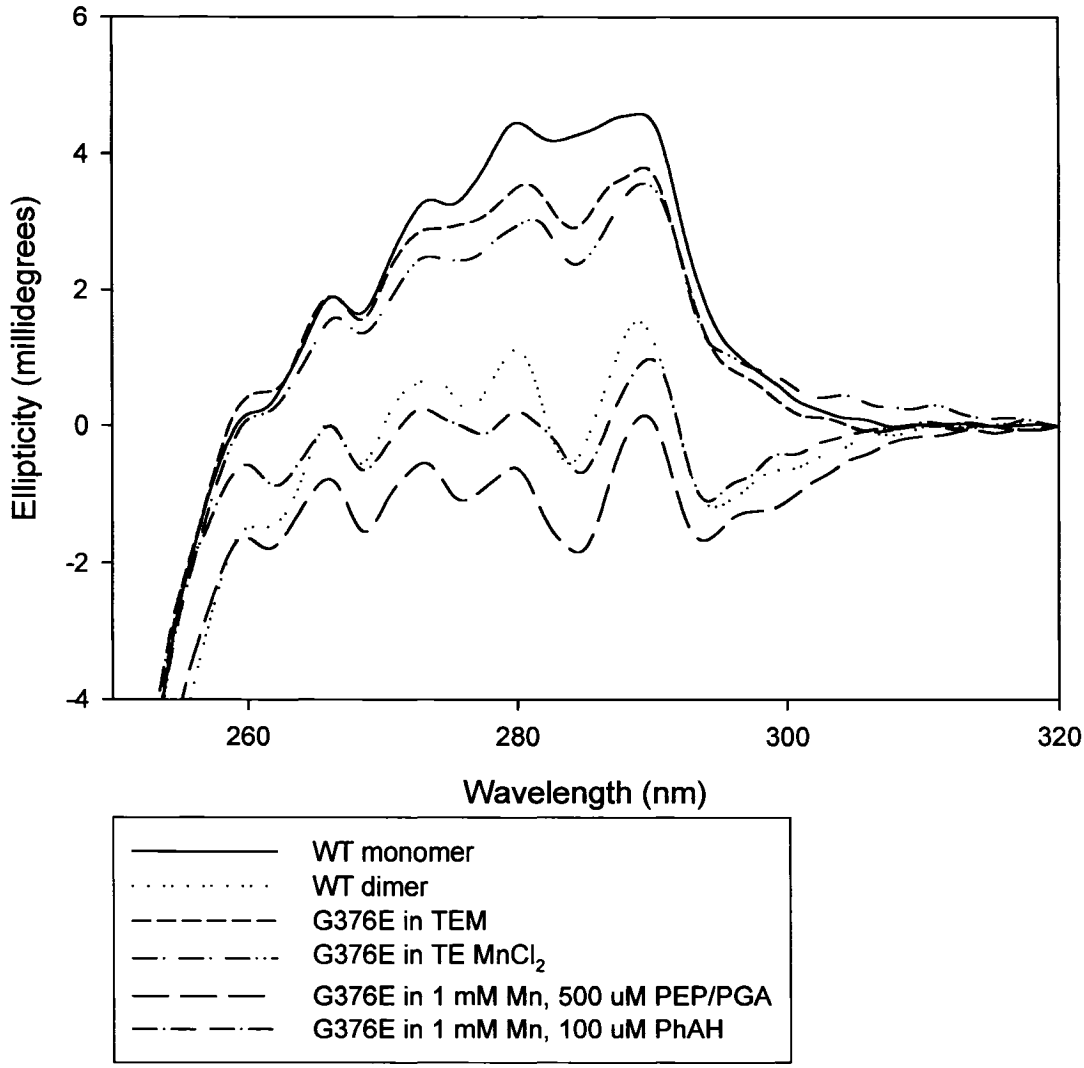

Figure 3.15: G376E near-UV CD spectra at different ITC experimental conditions.

Name	Sedimentation Coefficient ($S_{20,w}$)	Fraction Monomer
10.7 μM G376E in 1 mM Mg^{2+} + 0.3M NaOAc	4.411 ± 0.595	0.534
10.7 μM G376E in 1 mM Mn^{2+} + 0.3M NaOAc	4.890 ± 0.675	0.272
100 μM G376E in MT 1 mM Mn^{2+}	5.262 ± 0.034	0.149
100 μM G376E in MT 1 mM Mn^{2+}, 500 μM PEP/PGA mix	5.646 ± 0.034	~ 0
100 μM G376E in MT 1 mM Mn^{2+}, 100 μM PhAH	5.616 ± 0.032	~ 0

Table 3.11: Sedimentation coefficient of G376E at different buffer conditions.

3.4 Protein stability of wild-type vs. variants yeast enolase

3.4.1 Chemical stability of wild-type vs. variants

Could the differences in dissociation constants be due to differences in conformational stabilities of variants and wild-type protein? To determine whether the mutations at amino acid 376 affect the stability of overall structure, a urea denaturation experiment was performed. The urea disrupts the hydrogen bonding, and non-covalent interactions within protein structure. Often, the midpoint of urea concentration, $[urea]_{1/2}$, can be determined quite accurately regardless the of unfolding mechanism. On the contrary, the free energy involved in denaturation can be difficult to calculate for multi-stage denaturation profiles. Yeast enolase turns out to be one of the more complicated systems to analyze: the denaturation process is occurring while dissociating process is happening. The results shown here focus mainly on denaturation curve shape and $[urea]_{1/2}$.

The urea denaturation curved was constructed based on fluorescence and peptide CD results. The fluorescence data however, produced far more fluctuation than CD data. It is therefore not shown. The CD was used to monitor denaturation process by following the changes at 222 nm, a wavelength where α-helices structural change can be observed. The fraction denatured was calculated using the following equation and was plotted against the urea concentration to produce the denaturation curve.

$$f_U = (y_F - y)/(y_F - y_U)$$

Where f_U refers to fraction unfolded, y_F represents the value at folded state (0 M urea), y_U represents the value at unfolded state (8 M urea), and y represents values at different urea concentration.

Denaturation curves of wild-type and G376E enolases are shown in Figure 3.16. The basic curve shapes of the two are very similar, with the exception that G376E $[urea]_{1/2}$ is decreased by approximately 0.4 M. In the same fashion, G376Q and G376I urea denaturation curves were constructed and they were compared to curve for wild-type enzyme. Small differences were observed in these two mutants as well (See Table 3.12). The results suggest that the chemical stability of the mutants was slightly decreased.

Another important observation made here concerns changes in the tertiary and quaternary structure of G376E during urea denaturation process. Although the peptide CD showed that at low urea concentration (less than 1 M), the G376E was not unfolded, these samples were dissociated according to near-UV CD and AUC experiment. A plot of near-UV CD signal at 283 nm against the urea concentration is shown in Figure 3.17. The intensity at 283 nm is increased at first, and started to decrease as the urea concentration increased. Furthermore, the sedimentation coefficients of wild-type enzyme and G376E at low urea concentration are shown in Table 3.13. These two results solidify the fact that G376E is dissociated before denaturation. Therefore, G376E follows a different unfolding pattern than wild-type protein in terms of quaternary structure. The data were not fit to a simple 2-states model of unfolding to obtain thermodynamic parameters of the process. The unfolding pattern of yeast enolase most likely involves multiple states.

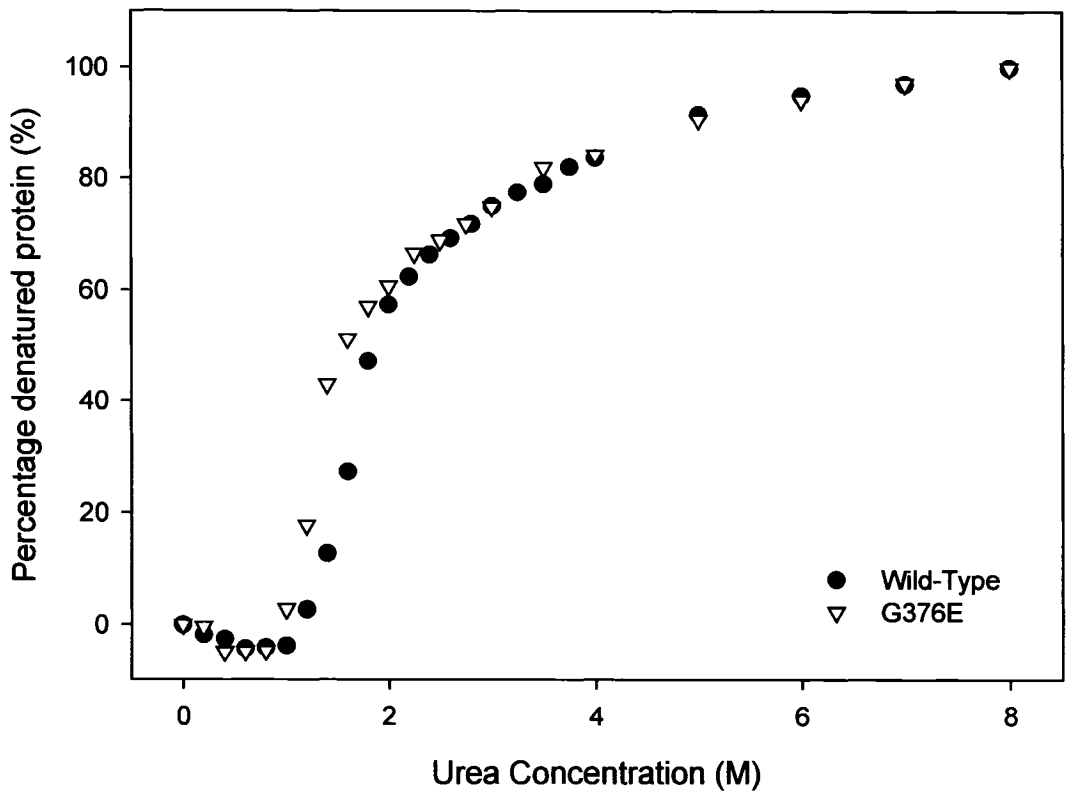

Figure 3.16: Urea denaturation curve of wild-type enzyme vs. G376E. The concentration of each sample was 1 mg/mL. The scans were collected in 0.1 cm quartz (QS) cell at 15 °C.

Name	$[Urea]_{1/2}$
Wild-Type	~ 1.9 M
G376E	~ 1.5 M
G376Q	~ 1.7 M
G376I	~ 1.8 M

Table 3.12: $[Urea]_{1/2}$ comparison of wild-type and variants.

Urea Concentration	Wild-Type ($S_{20,w}$)	G376E ($S_{20,w}$)
0.0 M	5.789 ± 0.002	5.069 ± 0.005
0.4 M	5.665 ± 0.003	4.426 ± 0.006
0.8 M	5.499 ± 0.005	3.932 ± 0.004
1.0 M	5.438 ± 0.006	Not determined
1.2 M	5.397 ± 0.007	Not determined

Table 3.13: Sedimentation coefficient comparison of wild-type enzyme vs. G376E at low urea concentration. Each sample concentration was 1mg/mL, the scans were collected at 15 °C.

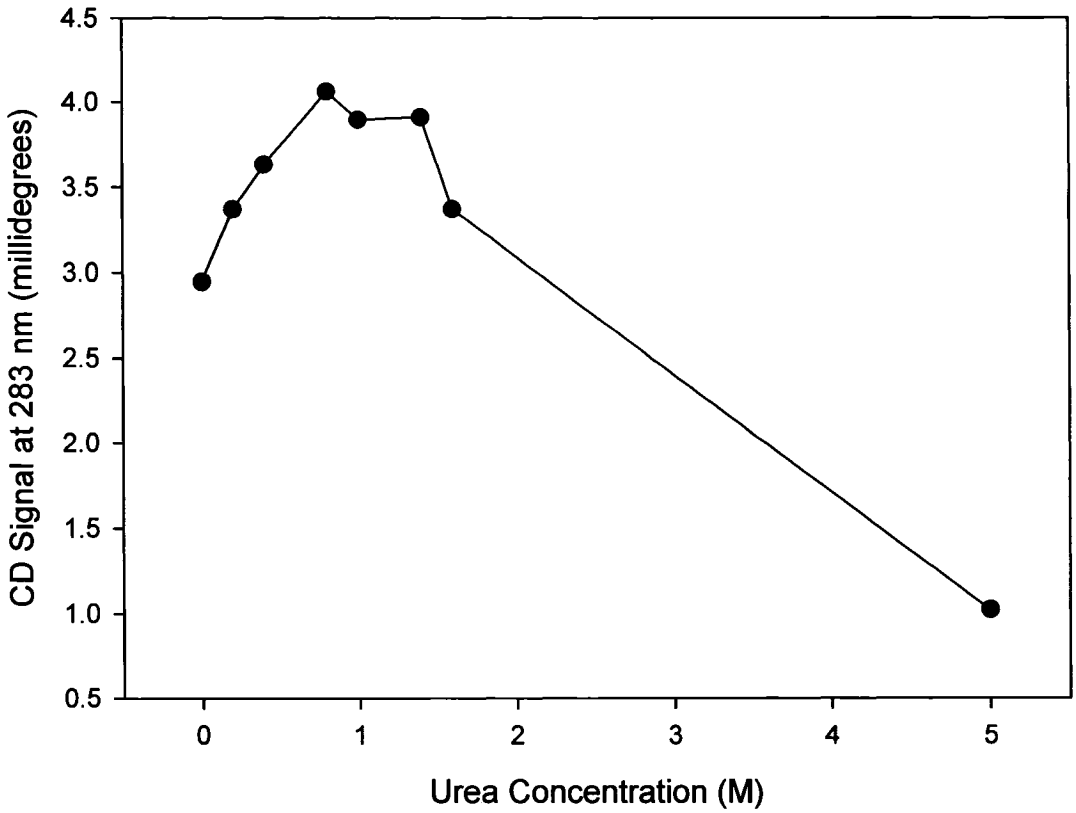

Figure 3.17: The near-UV CD signal of G376E at 283 nm vs. different urea concentration. The concentration of each sample was 1 mg/mL. The spectra were taken using 1 cm quartz (QS) cell at 15 °C.

3.4.2 Thermal stability of wild-type vs. variants

Similar to chemical stability experiment, the thermal stability experiment can also give insights into protein stability. Circular dichroism in the peptide region (222 nm) was used again to monitor the denaturation process. The changes in CD signal were recorded from 35 °C to 70 °C. The denaturation curve was normalized using the equation from chemical stability section. An example of yeast enolase thermal denaturation curve is shown in Figure 3.18. The ββ-rabbit muscle enolase was also tested as a control. The denaturation curves of proteins were all similar in shape. Vairant protein denaturation temperatures were compared to those of the wild-type and ββ-rabbit muscle enolase and are shown in Table 3.14. All variants denaturation temperatures were lower than that of wild-type yeast enolase and ββ-rabbit muscle enolase. There were no direct correlations between denaturation temperature (T_m) and dissociation constant.

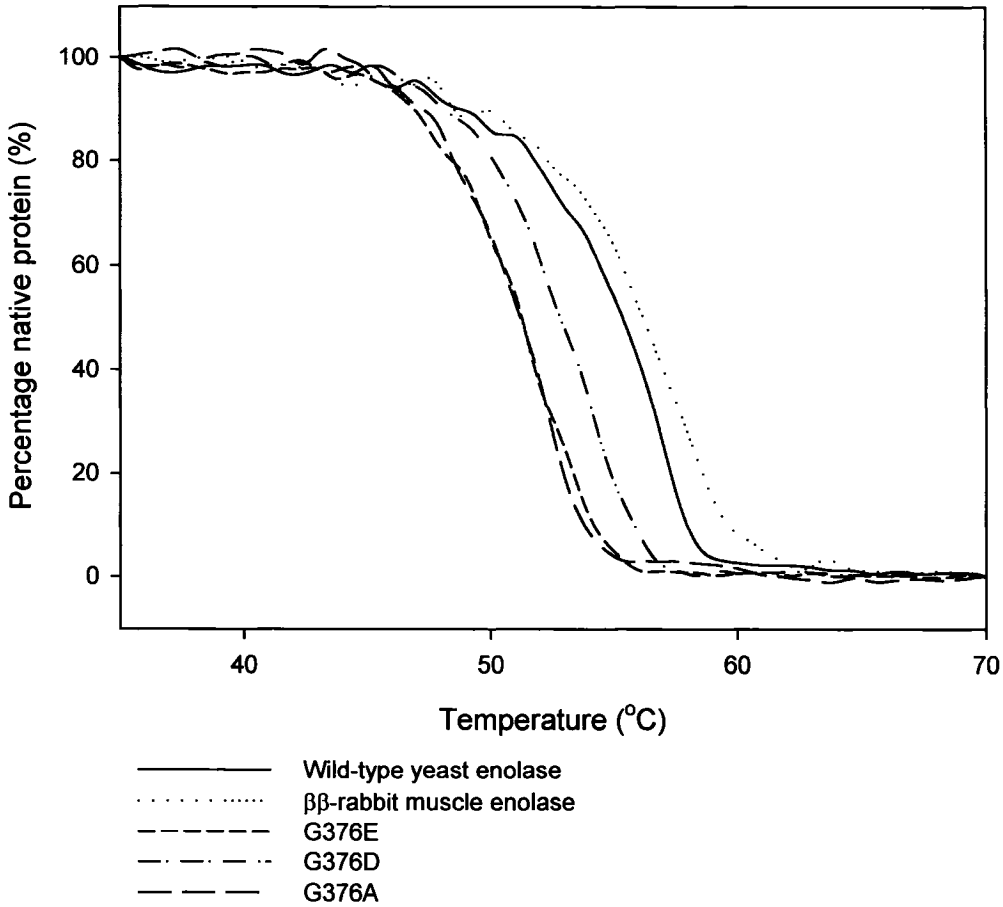

Figure 3.18: Thermal denaturation curve of wild-type, rabbit ββ- enolase, G376E, G376D, G376A. The concentration of each sample was approximately 1 mg/mL. The scans were collected in 0.1 cm circular quartz (QS) cells.

Name	Experimental T_m Value (°C)	Difference from wild-type (°C)
Wild-Type	55.4	-
ββ-Rabbit Muscle enolase	56.3	+ 0.7
G376E	51.2d	- 4.2
G376Q	48.8	- 6.4
G376I	50.0	- 5.4
G376D	52.9	- 2.5
G376N	49.5	- 5.9
G376A	51.3	- 4.1

Table 3.14: Summary of wild-type, ββ-rabbit muscle and variants enolases' T_m values.

3.4.3 Proteolytic susceptibility of wild-type vs. variants

When a protein remains in its native conformation, it is almost completely resistant to cleavage by low concentrations of protease (*68*). At low protease concentration, it is usually expected that only the most exposed or disordered region of protein will be cleaved. Therefore, the selection is very specific since the cleavage opportunity is limited. By determining the site cleaved, one can obtain some insights as to how the structure of a protein is altered in different states. The primary protease of choice for our experiment was trypsin, due to abundance of possible cleavage sites in yeast enolase protein. The digestion patterns of the variants were compared to wild-type enzyme. Figure 3.19 shows that after approximately 60 minutes of limited cleavage, G376E were cleaved into three major components. It is clear that the wild-type dimer remained intact while wild-type monomers were cleaved. The masses of different fragments were determined using Q-ToF mass spectroscopic technique. Based on the molecular mass of the fragments, the trypsin cleavage sites of G376E mutant and wild-type monomer were determined to be the same (See Table 3.15 and 3.16).

To determine the rate of the cleavage and if one site is more accessible than the other, the tryptic digestion patterns of wild-type enzyme were examined at three different $NaClO_4$ concentrations: 0.1 M, 0.2 M, and 0.3 M. Figure 3.20 shows an example of this experiment. The SDS-PAGE gel here was also used to determine the rate of cleavage. By using GeneSnap software and GeneGenius Bio Imaging System, the relative intensity of different bands was calculated, and plotted against time (See Figure 3.21). As shown in Figure 3.21, the bands corresponding to intermediate fragments slowly disappeared over 60 minutes period, and the intensity of the final fragment increased. However, there was

no evidence suggesting one site was more accessible then the other according to this experiment.

Furthermore, a series of other proteases were also used to determine the extent of the trypsin-exposed regions and to determine the existence of other exposed region on the protein. The results show that within the proteases selected for this experiment, only chymotrypsin was able to cleave G376E enolase (See Figure 3.22). The chymotrypsin cleavage site is still to be determined.

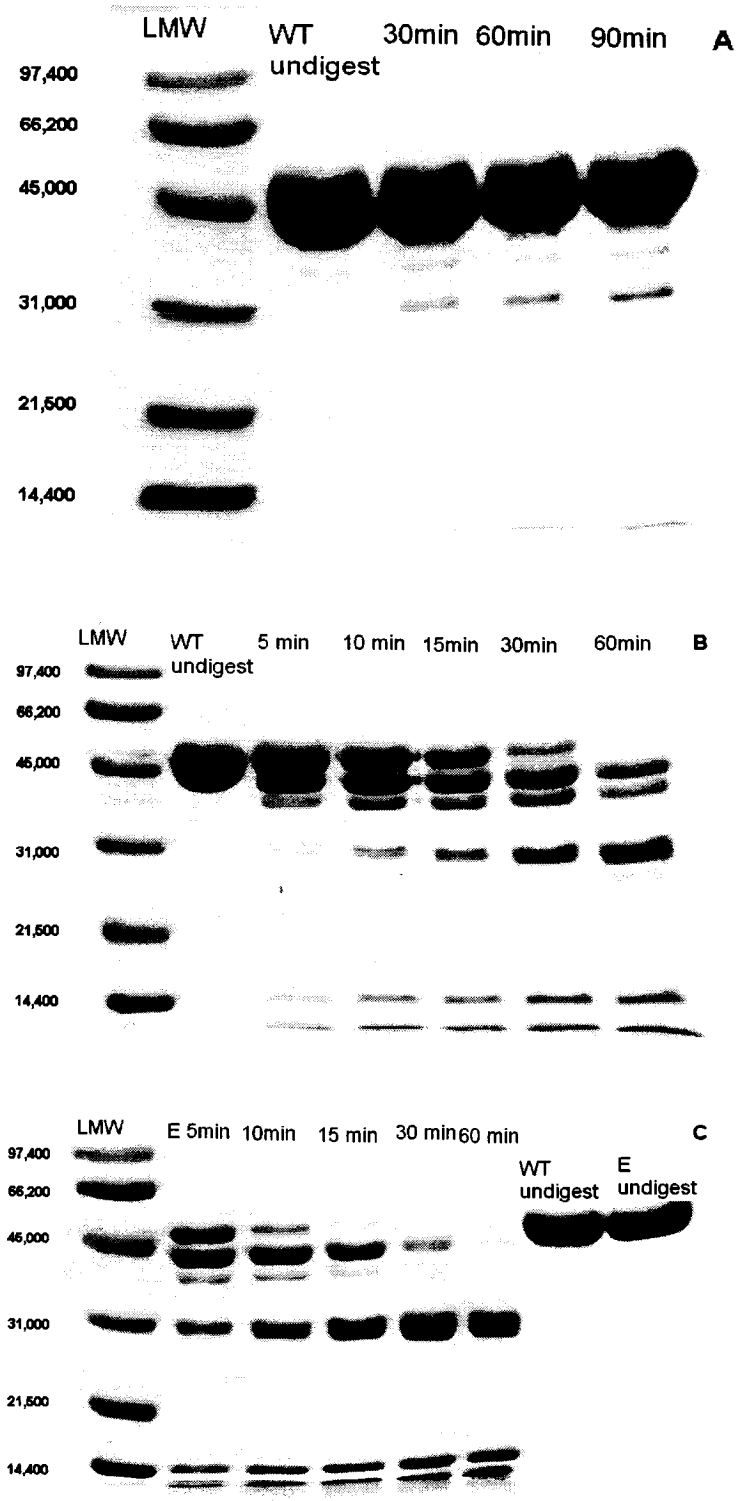

Figure 3.19: SDS-PAGE of trypsin digestions: A) wild-type dimer, B) wild-type monomer, C) G376E. Each sample was approximately 1mg/mL. All digestions took place at 15 °C.

Band Number	Experimental Mass	Amino Acid Fragment	Theoretical Mass
1	29982 Dalton	D50 – R329	29982.0 Dalton
2	11515 Dalton	I330 – L436	11515.0 Dalton
3	5282 Dalton	A1 – R49	5281.9 Dalton

Table 3.15: Estimated trypsin digestion site on G376E based on Q-ToF mass spectroscopic result.

Band Number	Experimental Mass	Amino Acid Fragment	Theoretical Mass
1	11442 Dalton	I330 – L436	11442.9 Dalton
2	5281 Dalton	A1 – R49	5281.9 Dalton
3. Logical Fragment	Could not be determined	D50 – R329	29982.0 Dalton

Table 3.16: Estimated trypsin digestion site on wild-type based on Q-ToF mass spectroscopic result.

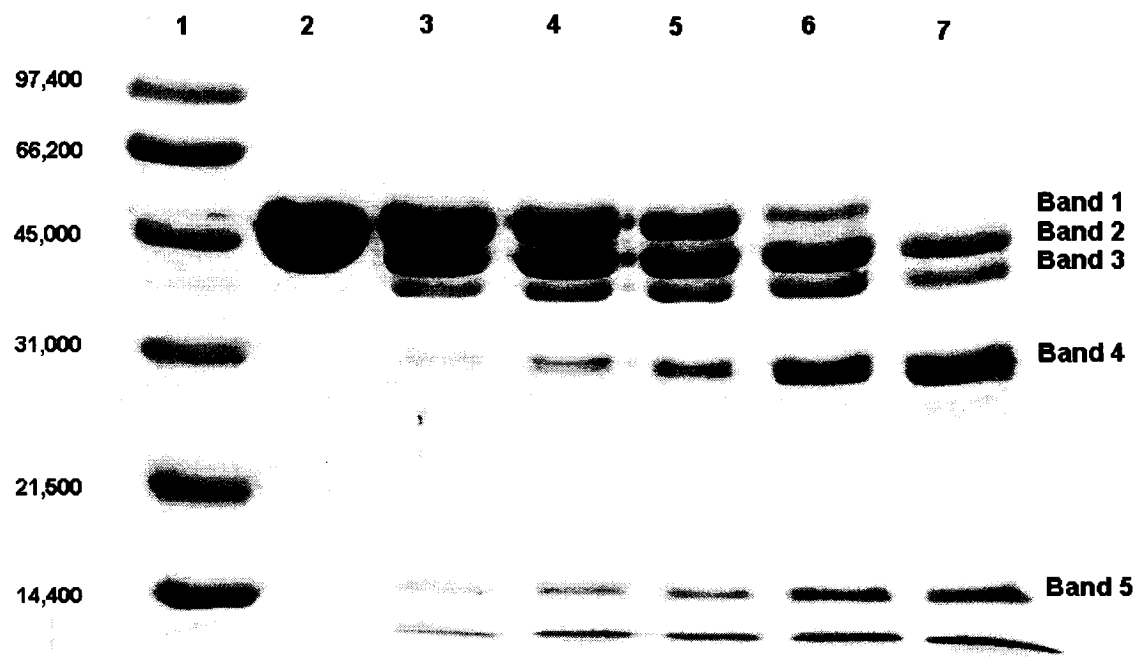

Figure 3.20: Trypsin digestion of wild-type yeast enolase in 0.3 M $NaClO_4$. Lane 1: Low range molecular marker; lane 2: undigested WT; lane 3: WT in 0.3 M $NaClO_4$ digested for 5 minutes; lane 4: WT in 0.3 M $NaClO_4$ digested for 10 minutes; lane 5: WT in 0.3 M $NaClO_4$ digested for 15 minutes; lane 6: WT in 0.3 M $NaClO_4$ digested for 30 minutes; lane 7: WT in 0.3 M $NaClO_4$ digested for 60 minutes. The incubations were done at 15 °C. Each lane contains approximately 10 μg of protein.

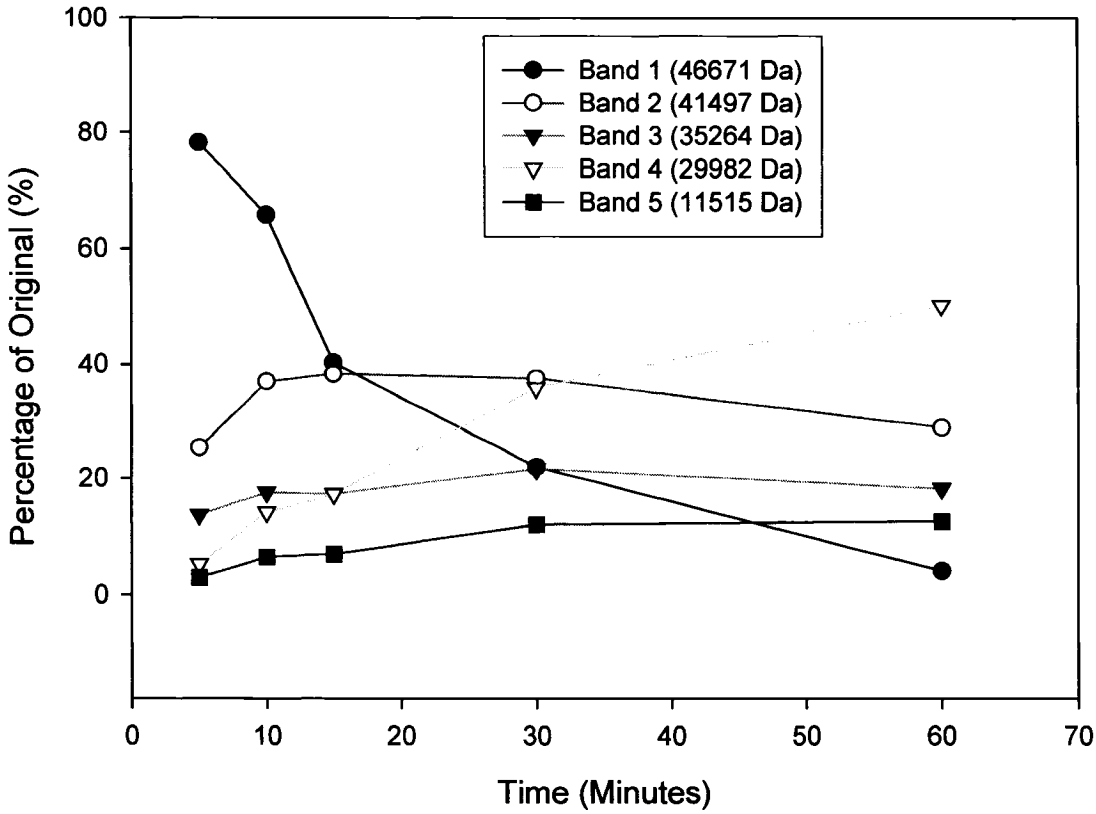

Figure 3.21: The relative intensity of SDS-PAGE bands of trypsin digested wild-type enzyme in 0.3 M $NaClO_4$. The band numbers are shown in Figure 3.20, the percentage was estimated using GeneGenius Bio Imaging System based on SDS-PAGE result.

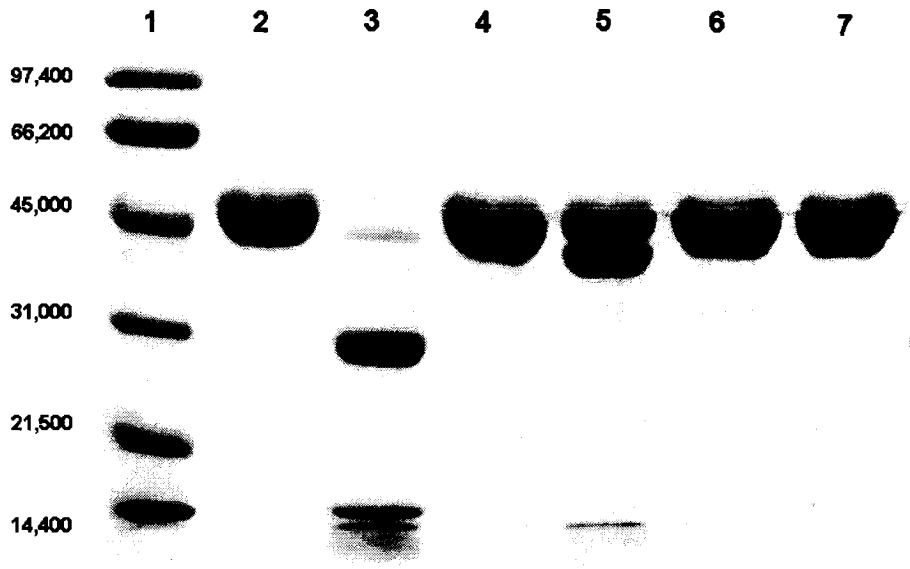

Figure 3.22: SDS-PAGE of different protease digesting G376E. Lane 1 is low range molecular marker; lane 2 is undigested G376E; lane 3 is trypsin digested; lane 4 is pepsin digested; lane 5 is chymotrypsin digested; lane 6 is endoproteainase glu-c digested; lane 7 is elastase digested sample. All samples were digested at 15 ℃ for 60 minutes.

3.5 Kinetic study of wild-type vs. variants

3.5.1 Determination of kinetic parameters

After completing the spectroscopic characterizations and stability characterizations, kinetic studies were performed on the variants and wild-type. The proteins were titrated with Mn^{2+} and PGA substrate, and the kinetic parameters of reactions catalyzed using the substrate and cofactor were determined. The natural metal cofactor Mg^{2+} was not used because in the presence of Mn^{2+}, a larger fraction of the protein was dimeric. The protein pre-assay condition was also tested by AUC; the proteins were still partially dissociated (See Table 3.17). Samples of kinetic graphs are shown in Figure 3.23 and 3.24. The results are summarized in Table 3.18 and Table 3.19. The results showed generally increased K_m for metal cofactor and substrate, and greatly decreased k_{cat} for most of the mutants. The only exception was G376A, which so far has shown similar properties to wild-type in most aspects. However, even for G376A mutant, the k_{cat} has decreased by nearly 50% and catalytic efficiency of G376A is less than half of wild-type enzyme. The decreased K_m values suggest possible weaker binding ability of metal ion and substrate. The lower k_{cat} suggests that the catalytic efficiency is depressed or dissociation induces lower activity. Furthermore, to effectively compare the catalysis ability of the active species, i.e. the dimeric protein, the k_{cat} were corrected using fraction monomer in pre-assay stock solution (See Table 3.20). There were no major differences observed between the corrected and the uncorrected k_{cat} values.

Name	Sedimentation Coefficient ($S_{20,w}$)	Fraction Monomer
G376E	4.696 ± 0.053	0.405
G376D	5.236 ± 0.024	0.160
G376N	5.187 ± 0.075	0.183

Table 3.17: Sedimentation coefficients of the variant proteins at pre-assay stock condition. At concentration of 1 mg/mL, the scans were taken at 5 °C to mimic condition on ice.

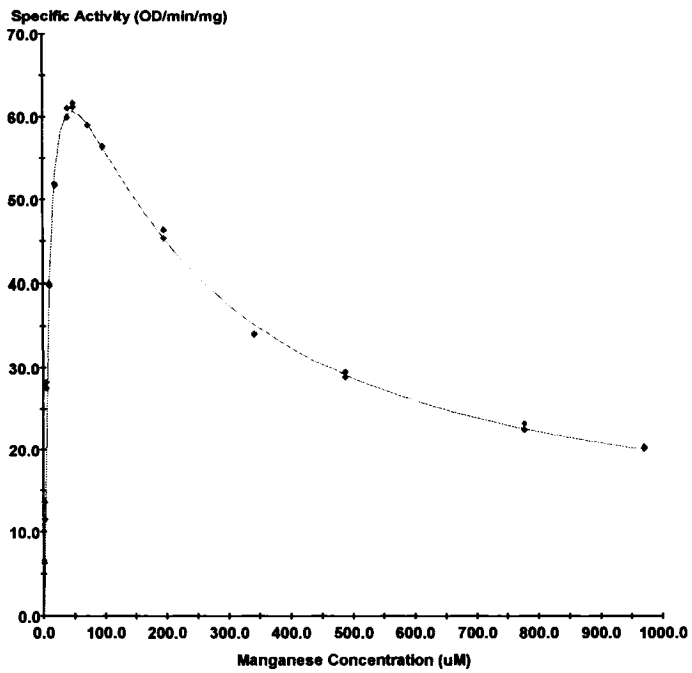

Figure 3.23: Wild-type Mn^{2+} substrate saturation curve.

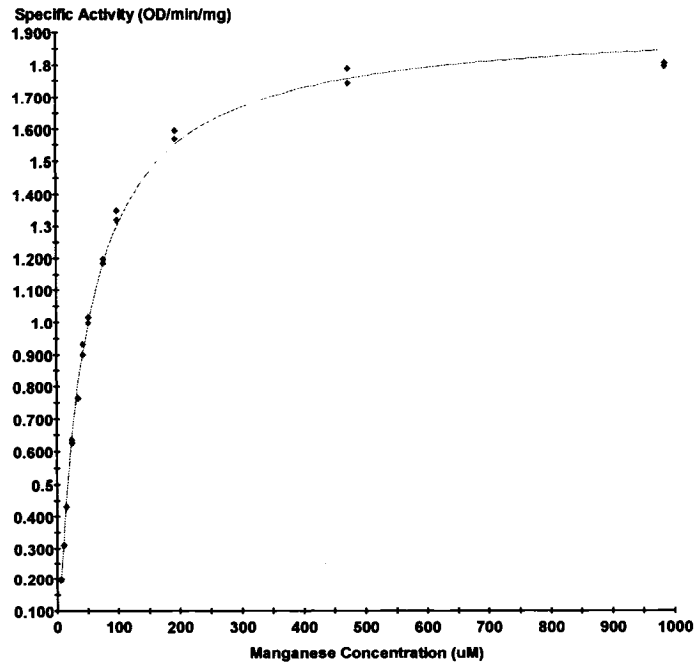

Figure 3.24: G376E Mn^{2+} substrate saturation curve.

Name	K_m (μM)	k_{cat} (s^{-1})	k_{cat}/K_m ($s^{-1}\mu M^{-1}$)	K_i (μM)
WT Mn^{2+}	10.1 ± 1.2	58.00±2.95	5.74	205.15 ± 45.1
G376E Mn^{2+}	47.9 ± 1.1	1.31±0.0097	0.027	No Inhibition
G376Q Mn^{2+}	11.3 ± 0.9	7.44±0.22	0.66	501.5 ± 123.0
G376D Mn^{2+}	131.3 ± 3.6	0.48±0.0051	0.0036	No Inhibition
G376N Mn^{2+}	42.0 ± 1.3	1.17±0.016	0.028	804.2 ± 60.4
G376A Mn^{2+}	13.3 ± 0.4	27.92±2.44	2.10	157.4 ± 7.6

Table 3.18: Summary of metal cofactor (Mn^{2+}) kinetic parameters of wild-type vs. variants.

Name	K_m (μM)	k_{cat} (s^{-1})	k_{cat}/K_m ($s^{-1}\mu M^{-1}$)	K_i (μM)
WT PGA	15.7 ± 0.6	39.69±0.54	2.53	No Inhibition
G376E PGA	72.3 ± 3.1	1.17±0.015	0.016	No Inhibition
G376Q PGA	81.5 ± 3.0	6.72±0.16	0.082	No Inhibition
G376D PGA	138.3 ± 4.1	0.51±0.0057	0.0037	No Inhibition
G376N PGA	53.4 ± 1.9	1.52±0.026	0.029	3842.0 ± 2686.5
G376A PGA	16.8 ± 1.0	22.55±0.32	1.34	No Inhibition

Table 3.19: Summary of substrate (PGA) kinetic parameters of wild-type vs. variants.

Name	k_{cat} from Mn experiment	k_{cat} from PGA experiment
Wild-Type	58.00	39.69
G376E	2.20	1.97
G376Q	12.50	11.29
G376D	0.57	0.62
G376N	1.43	1.86
G376A	27.92	22.55

Table 3.20: The fraction dimer corrected k_{cat} values.

3.5.2 Metal cofactor and substrate binding constant comparison

The results in this section were from the preliminary attempts. The results may or may not reflect the actual binding constants.

To obtain the actual binding constant of the metal cofactor and substrate, isothermal titration calorimetry (ITC) was used. This method uses the heat change associated when two molecules interact to determine the binding constant. For each experiment, the concentration of the active site was controlled to be approximately 100 μM. The substrate binding constant was obtained using PEP/PGA equilibrium mix. When the PEP/PGA mix was titrated into the protein sample containing approximately 1 mM $MnCl_2$, the following results were obtained (See Table 3.21). Based on these ITC determined parameters, the binding constants were estimated and listed in Table 3.22.

Name	Wild-Type	G376E
Sites (μM)	96.87	96.63
Chi-Squared	4957	5987
N1	0.5562 ± 0.0601	1.023 ± 0.107
K1	2.665E7 ± 1.476E7	3.359E5 ± 4.545E4
ΔH1	-4975 ± 119.9	-3505 ± 1562
ΔS1	17.3	13.5
N2	0.4352 ± 0.0572	0.0466 ± 0.0997
K2	3.037E6 ± 6.834E5	5.379E5 ± 2.97E4
ΔH2	-3862 ± 318.1	-1.475E5 ± 3.281E5
ΔS2	17.3	-468.5

Table 3.21: ITC determined substrate-binding parameters of wild-type yeast enolase vs. variants.

Name	Wild-Type	G376E
N1	0.5562	1.023
K1 (M^{-1})	2.665E7	3.359E5
N2	0.4352	0.0466
K2 (M^{-1})	3.037E6	5.379E5

Table 3.22: Estimated substrate binding sites fractions and binding constant of wild-type enzyme vs. G376E.

Similarly, the binding constant for the second metal ion was also determined using ITC. A concentrated $MnCl_2$ solution was titrated into samples containing approximately 100 μM active sites and 100 μM of phosphonoacetohydroxamate (PhAH), a tight binding inhibitor. The protein samples were passed through chelex briefly to remove excess metal ions prior to PhAH addition. The results obtained are shown in Figure 3.25 and Table 3.23. Based on these results, the dissociation constant of second metal ion was determined and shown in Table 3.24.

The condition of the protein during the ITC experiment was determined using AUC and is shown in section 3.3.2 (Table 3.11).

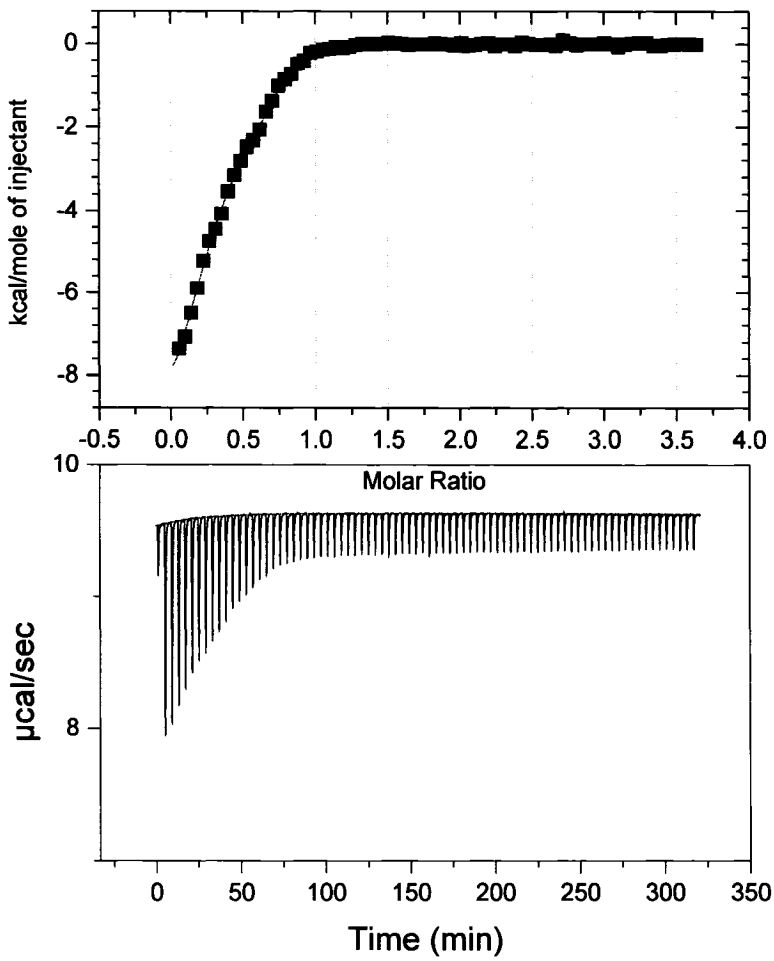

Figure 3.25: Sample ITC graph of G376E Mn^{2+} titration. The experiment was preformed at 25 °C. The results were fitted to two sites model. The graph was generated using MicroCal Origin 5.0 software.

Name	Wild-Type	G376E	G376Q	G376D	G376N
Sites (μM)	99.6	98.27	87.68	89.70	96.61
Chi-Squared	32679	2448.9	2494.2	7150.3	20230.2
N1	-	0.5247 ± 0.0206	0.6241 ± 0.0027	0.2142 ± 0.0724	0.4968 ± 0.0075
K1	-	6.191E5 ± 9.833E4	8.447E5 ± 4.384E4	1.908E5 ± 7.661E4	1.52E6 ± 3.36E5
ΔH1	-	-680.0 ± 514.0	-4890 ± 47.13	-5343 ± 3413	-3729 ± 277.4
ΔS1	-	24.22	10.73	6.25	15.79
N2	0.7729 ± 0.0026	0.2290 ± 0.0099	0.1851 ± 0.0013	0.6557 ± 0.0818	0.4925 ± 0.0094
K2	3.662E6 ± 3.878E5	2.524E6 ± 4.122E5	3.524E7 ± 2.13E6	1.886E6 ± 1.051E6	2.764E7 ± 5.997E6
ΔH2	-1.218E4 ± 76.3	-1.206E4 ± 1275	-1.421E4 ± 99.5	-1.244E4 ± 123.9	-1.084E4 ± 146.2
ΔS2	-10.82	-11.13	-13.07	-13.01	-2.29

Table 3.23: ITC determined second metal ion binding parameters of wild-type yeast enolase vs. variants.

Name	Wild-Type	G376E	G376Q	G376D	G376N
N1	-	0.5247	0.6241	0.2142	0.4968
K1 (M^{-1})	-	6.191E5	8.447E5	1.908E5	1.52E6
N2	0.7729	0.2290	0.1851	0.6557	0.4925
K2 (M^{-1})	3.662E6	2.524E6	3.524E7	1.886E6	2.764E7

Table 3.24: Estimated second metal ion binding sites fractions and binding constant of wild-type vs. variants.

Chapter 4 Discussion

4.1 Why do we want to study Gly376 substitutions in yeast enolase?

Due to the catalytic importance of glycolytic pathway enzymes, deficiencies of such proteins are rare. To date, there are approximately a dozen different cases identified in human, each affecting a specific aspect of glycolysis. For example, hereditary fructose intolerance is a disease caused by mutations in Aldolase B gene, which is potentially lethal as it affects fructose metabolism. The most commonly affected residue in Aldolase B deficiency was at Ala149, which was mutated into a proline. The study of this A149P mutant protein showed that although it is not one of the catalytic residues, it has affected the local structural environment and the adjacent catalytic residue function (Arg148) (*73, 74*).

To date, the case described in Section 1.4.1 is the only case of human enolase deficiency, and very little is known about the effect of the mutations. Aside from the mutations identified in the patient's gene, the immunoblotting results reveal that there was no or very low amount of β-enolase isozyme in the patient's muscle tissues. Although both α- and β-enolase genes are expressed in muscle tissues, ββ-enolase accounts for over 90% of the enolase activity in muscle. The glycolysis is turned on during anaerobic exercise to produce ATP. On the contrary, it is turned off in resting state. Instead, muscle can oxidize fatty acids for energy, which does not involve enolase catalysis. This explains why the patient had exercise-induced myalgias and general muscle fatigue. To complicate the problem further, the patient was a heterozygous mutation carrier, expressing two differently mutated forms of ββ-enolase isozyme in his

muscle. This project focuses on one of the mutations, while another colleague is working on the other mutation.

The authors who found this disease suggest that the protein product from mutated DNA may be more susceptible towards proteolysis, and that due to the location of G374E (human ββ-enolase number system), it is likely to have modified the protein's secondary structure. To further understand the various observations made on the patient, we decided to introduce the mutations into yeast enolase. Although there are some differences between yeast and human enolase amino acid sequences, most of the key structural characteristics are conserved. Moreover, unlike *Homo sapiens* enolases, the yeast enolase has a well-defined crystal structure. We are attempting to use yeast enolase to determine the effect of Gly376 mutation on protein structure, stability and enzymatic activity.

4.2 General purification procedures involved in this project

Purification schemes for wild-type recombinant yeast enolase and Gly376 mutants are now well established based on previous work. The proteins purified using these methods have high yield and good purity. In general, four liters of cells grown over 14 hour period usually results in over 200-300 mg of protein. This is in agreement of previously reported purification results (*32, 64*).

The G376 variants were introduced using QuickChange method. The DNA sequencing results confirmed the presence of the desired substitution; no other undesired mutations were found. Although, some silent mutations were identified, they were also present in the wild-type recombinant plasmid. The purification of wild-type enzyme was done similarly to previous work (*64*), but in some case, colleagues from our laboratory

claim that only one ion-exchange column (Q-sepharose) is required to obtain pure enzyme. This observation is yet to be verified. The mutants with the same overall charge as the wild-type were expressed and purified the same way as wild-type enzyme. The variants with one charge less than wild-type, however, follow a different purification procedure. There was no purification achieved when Q-sepharose column was used after ammonium sulfate salting out. The wild-type protein at pH 7.4 has a net-charge of approximately – 4.9, while the net charge of G376E, G376D are approximately – 5.9 (calculated base on amino acid composition). Being a strong anion resin, the Q-sepharose would retain these two mutants more strongly than wild-type enzyme, which would result in poor separations. However, by reversing the column order, the CM-sepharose (a weak cation resin) column was able to purify these two mutants nicely, because they are less positively charged at pH 6.0 than wild-type enzyme. A small drawback to this procedure is the smaller capacity of CM-sepharose resin and the large amount of material absorbs at 260 nm present in the pooled protein, the latter which can be removed easily using a small Q-sepharose column. The SDS-PAGE results showed no noticeable bands from impurities. The Q-ToF mass spectroscopy did not detect any signal from impurities as well.

The activities of the variant proteins were found to be severely depressed during purification. The preliminary assay shows the specific activity of G376E was approximately 0.01% of that of the wild-type enzyme. It was therefore not possible to construct a purification summary based on total protein and total activity. Utilization of activity assay to track the elution of variant protein was not possible. Instead, the elution was monitored solely by OD_{280}, OD_{260}, with the support of SDS-PAGE. There were a

few possible reasons proposed on loss of activity at this stage of project: 1) the mutation has affected the subunit interface and resulted in largely dissociated protein, which is the inactive form of the protein; 2) the stabilities of the variants are greatly altered such that they are denatured during purification or laboratory manipulations; 3) substitutions at Gly376 have affected the catalytic site structure and thus the enzymatic reaction, so that the k_{cat} of the variants are greatly decreased. Further investigations were performed to examine each of these possibilities.

4.3 The effect of Gly376 mutations on protein structure

Due to unavailability of the crystal structures of the variants, their structural characteristics were examined through spectroscopic techniques. By using different techniques, one may compare the spectroscopic characteristics of wild-type and variants to gain insights into any structural differences.

All Gly376 variants purified to date have similar secondary structural absorption pattern according to far-UV (peptide) CD (see Figure 3.8). Although some small intensity differences were observed in the spectra, these are likely due to concentration difference, or even to differences in cell positioning. As the protein concentration was lowered to 0.1 mg/mL, the peptide CD spectrum of wild-type and mutant were nearly superimposable. Furthermore, the absorption pattern of α-helices can be observed at 209 nm and 222 nm regions. The other types of secondary structural absorption were hard to detect, because the signal to noise ratio is dramatically increased below 205 nm due to our buffer system. The use of software to determine the percentage was therefore not possible. The far-UV

CD results suggest that the variant proteins are folded, and the overall secondary structures were the same as that of wild-type enzyme.

The 4th derivative UV spectroscopy and near-UV (aromatic) CD methods were used to probe the changes in tertiary structure. The aromatic residues of yeast enolase are shown in Figure 4.0. The spectra differed greatly between the variants and wild-type enzyme. Unlike second derivative UV spectra, which is particularly good to detect changes in tyrosine environment (*62*), the 4th derivative UV spectra reveals more detailed changes in all three types of aromatic amino acids (*70*). Moreover, the absorbance maxima of the fourth derivative spectrum corresponds to original zero order spectrum, which makes it more ideal in probing aromatic residue environment changes. The phenylalanine fourth derivative spectrum is characterized in region of 260–270 nm; the tyrosine is in region of 270–290 nm; the tryptophan absorbs in 280–295 nm region. The yeast enolase fourth derivative UV spectrum is mainly characterized between 280 – 300 nm region as the region below 280 nm becomes complicated to analyze. In general, as the environment of the aromatic residues in a protein becomes more polar, the intensity of the spectrum decreases and the absorption maxima shift to a lower wavelength. This is what has been observed in our experiment. As shown in Figure 3.9, most of the 4th derivative spectra of the variants are different than that of wild-type dimer or monomer. The ratios of two major peak-troughs at 293-296 nm and 284-288 nm regions were decreased as shown in Table 3.3. Furthermore, a slight blue shift of the spectra was also observed for variants other than G376A. As suggested earlier in this section, the secondary structure of the variants are preserved; assuming their fourth derivative UV properties are the same as the wild-type enzyme, spectra of the variants were compared to

that of wild-type monomer and dimer. The result suggests that the variant proteins might be dissociated. The degree of dissociation is as follow: G376I > G376Q > G376E > G376D > G376N > G376A. This property seems to depend on the size of the amino acid substitution. Moreover, the environment of the aromatic residues of the variants in 0.3 M NaOAc is more polar than in TEM buffer alone. Some possible explanations of this observation are: 1) although NaOAc is a kosmotrope, a structure maker, its ionic strength may have weakened the variant subunit interaction. As a result, the fraction monomer was increased; 2) the fourth derivative UV characteristics of the variants are different than that of wild-type enzyme. All in all, this observation will be further examined using near-UV CD spectroscopy.

The near-UV CD probes tertiary structure difference in a slightly different manner than fourth derivative UV. The near-UV CD signal is based on the symmetry of the aromatic residues in protein. For instance, if the protein is a molten globule stage, the near-UV CD signal is near zero. The near-UV CD signal distributions of the aromatic residues are similar to that in UV: phenylalanine's signal is between 250-270 nm, tyrosine signal is between 270-290 nm, and lastly the tryptophan signal is between 280-300 nm. The disulfide bond also absorbs weakly in 250-350 nm region, but there are none present in yeast enolase. The phenylalanine gives the lowest intensity, while the tryptophan gives the highest due to its symmetry. Generally, when the yeast enolase dissociates, the spectrum intensity increases and loses some defined shape in 270-290 nm region. The difference spectrum of wild-type dimer and monomer has the shape of a tryptophan spectrum. It is likely that the major signal contribution in this observation is coming from the Trp56 at the subunit interface. As shown in Figure 3.10, the spectral

intensities of the variants were increased except G376A. This result is in agreement of observations made in fourth derivative UV experiment that the variant proteins are dissociating. The percentage dissociation calculated based on near-UV CD however, was clearly different than fourth derivative UV result, though the trend of most dissociated to least dissociated remained similar. Furthermore, the near-UV CD results suggest that there is a greater fraction of dimers when the mutant protein is in 0.3 M NaOAc. Since both of the spectroscopic techniques used here depend on the environment of the chromophore, it is hard to draw conclusions regarding quaternary structure. The mutations introduced may have influenced the environment of the protein's chromophores, resulting in the spectra of the native, dimeric variant proteins being different from that of wild-type enolase. To determine whether the variants are dissociated, analytical ultracentrifugation experiments were conducted.

As stated in the section 3.2.3, whether based on absorbance or interference, the sedimentation coefficients ($S_{20,W}$) from AUC experiments directly reflect the molecular mass and shape. The sedimentation coefficient of yeast enolase dimer and monomer has been determined using commercial enzymes. By comparing the sedimentation coefficients of the variants to wild-type enzyme, we may accurately estimate the fraction of dimer and monomer in an enolase sample. The data were all analyzed using DCDT+ 2.0 (*75*) in the same fashion to minimize the error. The difficulty faced in this type of experiment is to analyze a sample in rapid equilibrium. Unlike single species or non-interactive multiple species samples, the plot of the graph of an equilibrium sample is not symmetrical. This in turn may result in higher percentage error, and even incorrect result. Similar to fourth derivative UV and near-UV CD results, the sedimentation coefficients

of the mutants are in between that of wild-type monomer and dimer. The percentage dissociation ranged from ~48% (G376Q) to ~0% (G376A). The substitutions of similar size had similar sedimentation coefficients: G376E, Q, I values were between 43% to 48, G376D, N values were in range of 27% to 17%, and G376A had very similar value as wild-type dimer. The percentage dissociation determined this way was generally lower than fourth derivative UV results. The near-UV CD results however, were in agreement with AUC result in terms of G376Q, D, N, and A variants. Clearly, the mutations have altered the environments of some aromatic residue of the resulting proteins. That is, even in their "native" dimeric form, the variants may not have the same 4^{th} derivative UV spectra as wild-type. Furthermore, E and I substitutions appear to have altered the environments of some aromatic residues, and the protein may yield different "native" near-UV CD spectra.

All in all, although the secondary structures of the variants are likely being conserved, the tertiary structure is probably different than that of wild-type enzyme. The substitutions at Gly376 have affected the polarity of some aromatic residues and/or their environments. Moreover, the "native" spectra for some mutants may be different than that of wild-type enzyme. Lastly, the mutant protein is evidently partially dissociated (except G376A) according to three different approaches. But how much is the binding weakened? Could one shift the mutant monomer-dimer equilibrium to produce fully dimeric protein? These questions will be discussed in the next section.

Figure 4.0: Aromatic residue distribution in yeast enolase. Highlighted in red are the tryptophan residues, and blue are the tyrosine residues. The green shows the Gly376 position. The image was generated using Rastop and 1one.pdb from RCSB Protein Data Bank.

4.4 Dissociation and efforts to shift mutant equilibrium towards dimer

The dissociation constants of the mutant protein were calculated based on the fraction monomer obtained in AUC experiments. The wild-type enzyme has a dissociation constant of 1-3 x 10^{-8} M (see Table 3.7), but G376E, Q, and I's dissociation constant is increased by ~1000-fold, thus indicating severely weakened subunit interaction. As for G376D and N, possibly due to smaller substitution size, the dissociation constant is increased by 80- to 100-fold. As mentioned in the introduction, the Gly376 is in proximity of residues involved in hydrogen bonding at the subunit interface. By having a larger side chain substituted at this position, the local structural environment must have changed, thus disrupting some hydrogen bonding system. However, the affect of the substitution is probably limited to its immediate proximity and most of the enzyme remains in its native structure. The partial differences in structure may have resulted in bad "fit" at the subunit interface, and led to weaker affinity.

In an effort to shift the equilibrium of the variant proteins towards the dimeric form, different buffer conditions were tested. For example: A) increase osmolarity (*76*) (15% glycerol); B) use of kosmotropic salt (NaOAc); C) increase the concentration of protein; D) increase the metal cofactor and add substrate, etc. All of the above conditions should promote dimer formation. The osmotic pressure favors dimerization by reducing the hydration at the subunit interface; the OAc is a salt from Hofmeister series that helps in forming structures; the higher protein concentration increases the fraction dimer in the sample; the natural substrate and cofactor usually stabilizes the native form of an enzyme. All conditions tested above had positive effect and shifted the equilibrium towards a dimer-like spectrum. However, none produced spectra that resembles the wild-type dimer.

On the contrary, using another Hofmeister series salt, $NaClO_4$, a chaotrope that disrupts structure, we managed to obtain monomer-like near-UV CD spectra. The resulting spectral peaks were more intense than observed for the wild-type monomer, which again suggests that the "native" G376E CD spectrum is different than that of wild-type enzyme.

In later stage of the project, we tested the affect of Mn^{2+}, a non-natural metal cofactor, on the monomer-dimer equilibrium. It is found that, when G376E is bound with Mn^{2+}, the fraction monomer is decreased by ~25%. This is probably due to affinity of Mn^{2+} at the active site. By having a tighter binding metal ion at the catalytic site, the dimerization is favored, thus increasing the fraction dimer is the sample. Furthermore, by increasing protein concentration (~5 mg/mL), using Mn^{2+} and a mixture of substrate and product, a dimer like sedimentation coefficient and near-UV spectrum were obtained. Replacing the substrate and product with a more tightly binding inhibitor resulted in similar results. Although these experiments were not performed with the wild-type enzyme in same buffer condition, the shift in equilibrium in this experiment was the most significant to date. It is concluded that, by stabilizing the active form of enzyme, it is possible to shift the G376E monomer-dimer equilibrium towards dimer.

4.5 The stability of the Gly376 mutants

In the original article describing the disease, it is proposed that the substitutions at Gly376 alters the secondary structure, and changes the susceptibility of enzyme towards proteolysis. Here we will discuss how the stabilities of the variants were affected by the substitution.

First, the chemical stabilities of the variants were tested using urea. Far-UV CD was the primary tool used to monitor this process. The fluorescence data (not shown) gave similar changes as in the CD experiments. While the CD monitors denaturation by loss of secondary structure, the fluorescence tracks the shift of emission λ_{max} and fluorescence intensity and overall spectrum shape (integrating the area under spectrum). By exciting the samples at 280 and 295 nm separately, one may observe tyrosine and tryptophan fluorescence contributions, or tryptophan fluorescence emission alone. Although it is a nice approach in theory, the fluorescence experiment had a few difficulties. First, the fluorescence intensity change between the sample at 0 M and 8 M urea was relatively small (~ 70 for 280 excitation and ~ 50 for 295 nm excitation), and the noise between repeated scans can be as high as 10. The noise to signal ratio was too high. Secondly, the fluorescence intensity depends heavily on fluorophores concentration in a sample. A small difference in protein concentration may lead to wrong result, which makes sample manipulation difficult. Lastly, each set of fluorescence data must be further corrected, as the emission intensity of the fluorophores are influenced by urea concentration directly. The far-UV CD experiment on the other hand, provided low signal to noise ratio and was much more reproducible. Therefore, it was the primary tool used to construct the denaturation curve.

Urea is a product in mammalian protein metabolism; it is formed in liver and secreted by kidney. It is main component of the urine, but it is also used to moisturize our skins. Although the mechanism is still not totally clear, the urea disturbs the non-covalent interactions in a protein. As the urea concentration increase, the protein is unfolded. We believe that at 8 M urea, our protein is fully denatured.

The urea denaturation curves of G376E, Q, and I reveal that the secondary structure of the proteins are not changing up to ~ 1 M urea. In terms of curve shapes, the curves of the variants resemble that of wild-type enzyme closely. The mid urea concentrations ($[urea]_{1/2}$) of the mutants are only lowered by 0.1 – 0.4 M.. Although rabbit ββ-enolase was not tested, we hoped that the change in chemical stability due to the mutation would be small as well. Moreover, even though the secondary structure is not altered, the tertiary structure is changing at 1 M or lower urea concentration according to some near-UV CD spectra collected at this concentration range (See Figure 3.17). Furthermore, the AUC results reveal that due to weakened subunit interaction, the G376E is nearly monomeric when it is incubated in 0.8 M urea (See Table 3.10). The wild-type enzyme however, is barely dissociating up to 1.2 M urea. This suggests that the G376E and wild-type enzyme are under going different denaturation processes. G376E protein is dissociated prior to denaturation. On the other hand, the wild-type enzyme dissociates while unfolding. The wild-type yeast enolase must be following a multi-step denaturation pattern.

The thermal stability is just as important as chemical stability. The thermal denaturation process is again monitored using far-UV CD. All of the normalized thermal denaturation curves had similar shapes, suggesting all proteins undergo the same type of denaturation process. The denaturation temperatures of variants are ~ 3 to 6 °C lower than that of wild-type enzyme. The denaturation temperature had no direct correlation with the dissociation constant. Similar to chemical stability results, the variants may again be dissociated prior to denaturation. Some evidence from previous equilibrium experiment shows that temperature increase may affect the quaternary structure of G376E

(not shown). When G376E was incubated in 15% glycerol and TEM buffer at different temperatures (15 to 35 °C), the near-UV CD showed some increases in intensity, which suggested dissociation. It is to our surprise that the denaturation temperature of G376A dropped so dramatically. It was expected that G376A would be more like wild-type enzyme due to the small substitution. The mutation at Gly376 may be one of the key residues keeping the local structural environment intact.

As no solid conclusion was drawn based on chemical and thermal denaturation, proteolytic susceptibilities of the mutants were tested. Often, this method is used to determine protein amino acid sequence or to identify the boundary between different domains. We are using it to determine the structural stability of the wild-type and variant proteins. Trypsin, which cleaves at arginine and lysine residues, was chosen. There are total of 51 arginine and lysine residues, therefore on statistic average, there would be one cut site every nine amino acids. This allows us to cover most of the regions of the protein. In our project, the limited proteolysis method was used, because we want to determine the most solvent exposed region in the protein. As result, most of the variant proteins were cleaved into three major pieces, revealing two major regions where the structures are different (See Figure 4.1). This result was different from expected. Originally, we had proposed that the digestion sites would be at the subunit interface, because only the monomeric species were digested in the experiments for wild-type enzyme. This reveals a new fact the wild-type monomeric structure is much different than that of the dimer. This may explain why monomers cannot catalyze the enolase reaction.

First of all, according to the digestion result, for dimeric wild-type enzyme, both sites are well buried within the surface of the protein. The backbones were not accessible

to trypsin proteases, whereas dissociating the protein allowed cleavage. To explain this observation, we need to examine the structure near these sites closely. The Arg49 is located on the first loop, which extends from the active site to subunit interface, and it contains active site residue Ser39 and Trp56 that is hydrogen bonded to the other subunit. It is also known that the loop is mobile without the substrate and second metal ion, but it is protected against proteolysis when protein is a dimer. However, upon dissociation, the hydrogen bonding at the interface is disrupted. The loop may become more mobile than it was in dimeric enzyme, thus lead to increased susceptibility.

The Arg329 on the other hand is the third residue on helix H9 (*11, 14*). It is part of a rigid secondary structure, and involved in forming the unique enolase catalytic site topology. It is not near any loops involved in catalysis, nor it is close to subunit interface (See Figure 4.1). The cleavage at this site suggests that in the process of protein dissociation, the structural difference is not limited to quaternary and tertiary, but also secondary. It is possible that some of the secondary structures may become loose or lost, exposing residues that are normally buried in the surface.

It is now definitive that the variant proteins are more susceptible towards proteolysis. However, the mutation has not directly exposed the cleavage sites of enolase. Instead, substitutions at Gly376 weaken the subunit interaction, resulting in greater dissociation of the proteins, which has lead to increased susceptibility to proteolysis. Moreover, the decreased T_m value may have affected the monomer-dimer equilibrium as well, resulting in increased monomer fraction at higher temperature (>15 °C). It may help explain the absence of ββ-enolase in patient's muscle tissues, since the amino acids at the cut site are conserved in human ββ-enolase as well.

To determine the size of trypsin exposed sites and the possibility of other exposed regions, we have tested the susceptibility of G376E with a series of proteases: chymotrypsin, elastase, endoproteainase glu-c, and pepsin (*68*). As shown in Table 4.1, the amino acid sequence near the trypsin cleavage sites can be potential cleavage target for these proteases. Figure 3.22 shows that other than trypsin, only chymotrypsin digestion has yielded some major bands. The elastase and glu-c results showed a very small band below the native protein, which suggested possible weakly exposed cut sites (the position of these cleavage sites are still to be determined). This result is unexpected since the proteases tested covered a wide range of amino acids candidates, none of the proteases were able to yield fragments similar to that of the trypsin digestion. This suggests that the exposure of the amino acid backbone is very precise and limited to a small region.

Cleavage Site #	**Sequence near the trypsin cut site**
1 (near amino acid 49)	VHEALEM-**R**-DGDKSKW
2 (near amino acid 329)	LTVTNPK-**R**-IATAIEK

Table 4.1: The amino acid sequences near the trypsin cut sites. The cut side residue is highlighted in bold.

To extrapolate our results to ββ-enolase, we have tested the trypsin susceptibility of monomeric ββ-enolase from rabbit, which has ~97% sequence identity to the human enzyme. The results, however, have failed to demonstrate direct cleavage (See Figure 4.2). Although the total amount of protein is constantly decreasing over the time of the experiment, there were no visible bands corresponding to the proposed fragments. The rabbit muscle ββ-enolase is harder to dissociate than the yeast enzyme. ββ-enolase requires over night incubation in 0.3 M $NaClO_4$. Perhaps the protein was not monomeric

when the digestion experiment was conducted. It is also possible that the structure of the ββ-enolase is slightly different than that of yeast. As seen in yeast enolase digestion, the exposure of the amino acid backbone was very precise and limited. The difference in amino acid sequence between yeast and ββ-enolase may have led to different amino acid exposure. The ββ-enolase monomer needs to be tested by other proteases in order to draw a conclusion.

Figure 4.1: Two trypsin cut sites and the Gly376 positions. Arg49 is in red, Arg329 is in blue, Gly376 is in green. The image was generated using RasTop and 1one.pdb from RCSB Protein Data Bank.

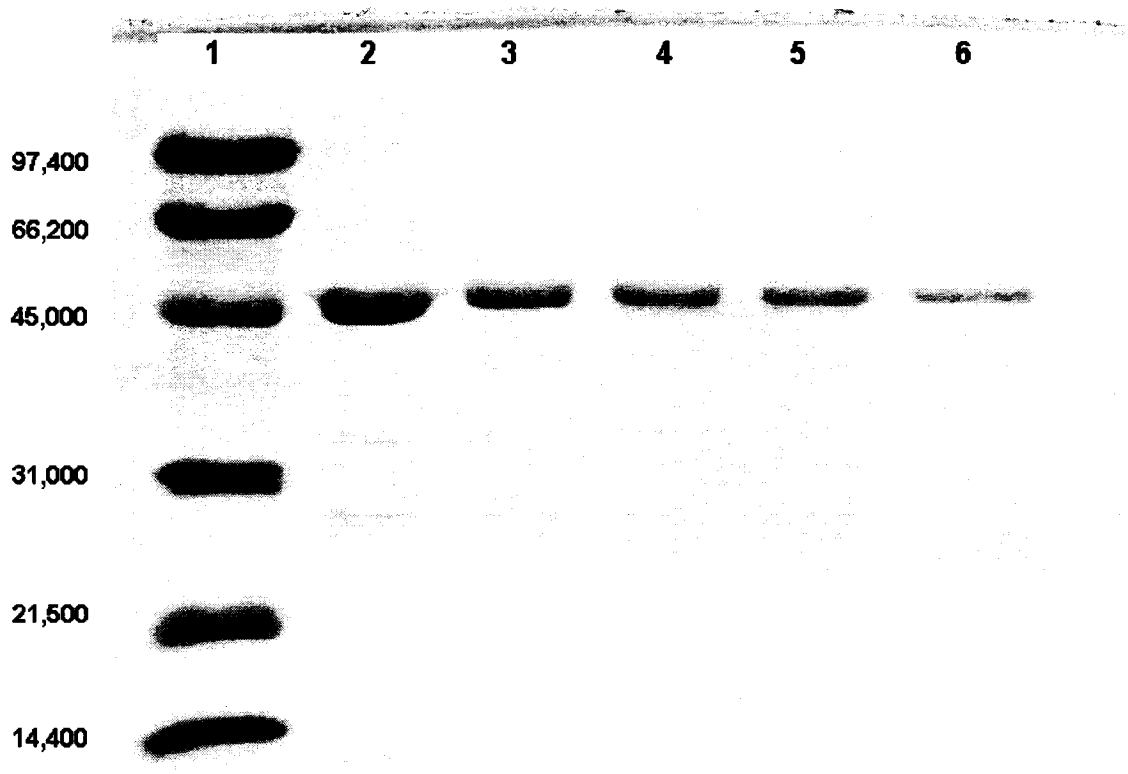

Figure 4.2: Rabbit muscle ββ-enolase monomer digestion results. 1) low-range molecular marker, 2) undigested sample, 3) digested sample after 1 hour, 4) digested sample after 2 hours, 5) digested sample after 4 hours, 6) digested sample after 6 hours. The rabbit muscle ββ-enolase used in this experiment had been purified by colleagues.

4.6 The effect of substitutions at position 376 on catalysis and metal, substrate binding

The effect of the substitutions at Gly376 on subunit interface stability was significant. The increase in the fraction of monomer led to unstable proteins. In the preliminary assay studies, G376E's k_{cat} was approximately 0.01% of that of wild-type enzyme. In order to obtain kinetic information on the variants, a different buffer system that promotes dimerization was necessary. By testing different buffer conditions, a new buffer containing 25 mM Mes-Tris and 0.25 M KOAc, was utilized in kinetic experiments. As shown in Table 3.17, under this assay condition, a majority of the variant proteins are in their dimeric form, and measurable activities were recorded.

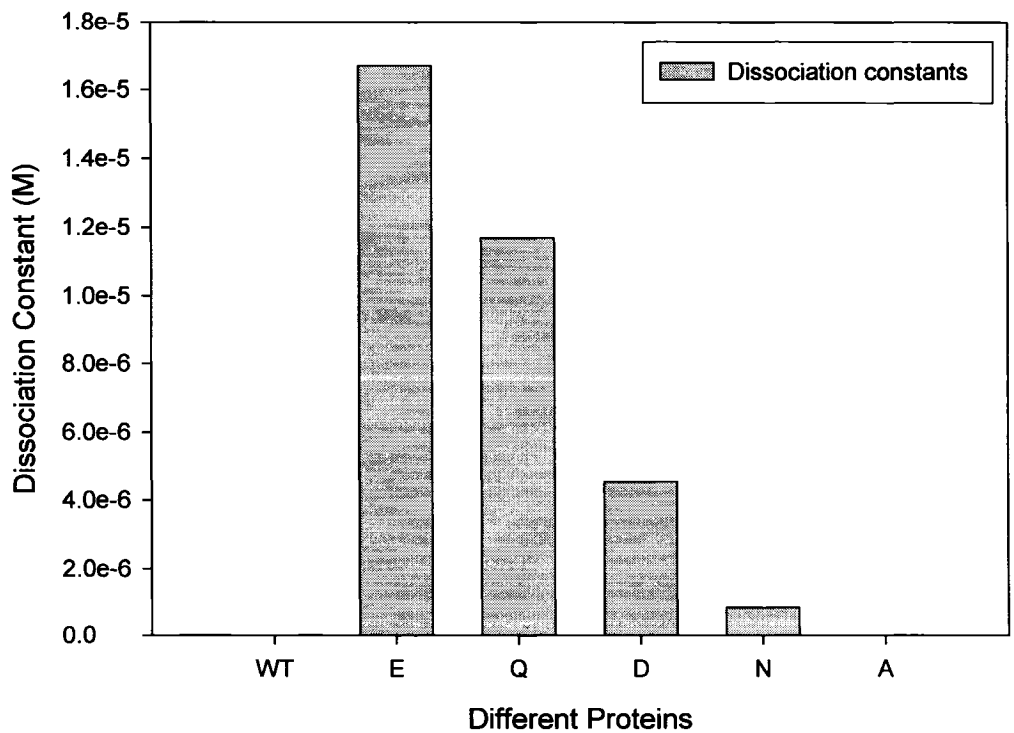

Figure 4.3: Bar graph of dissociation constants of wild-type and variants. The dissociation constant of wild-type and G376A is approximately 1 x 10^{-8} M, and was out of graph axis scale.

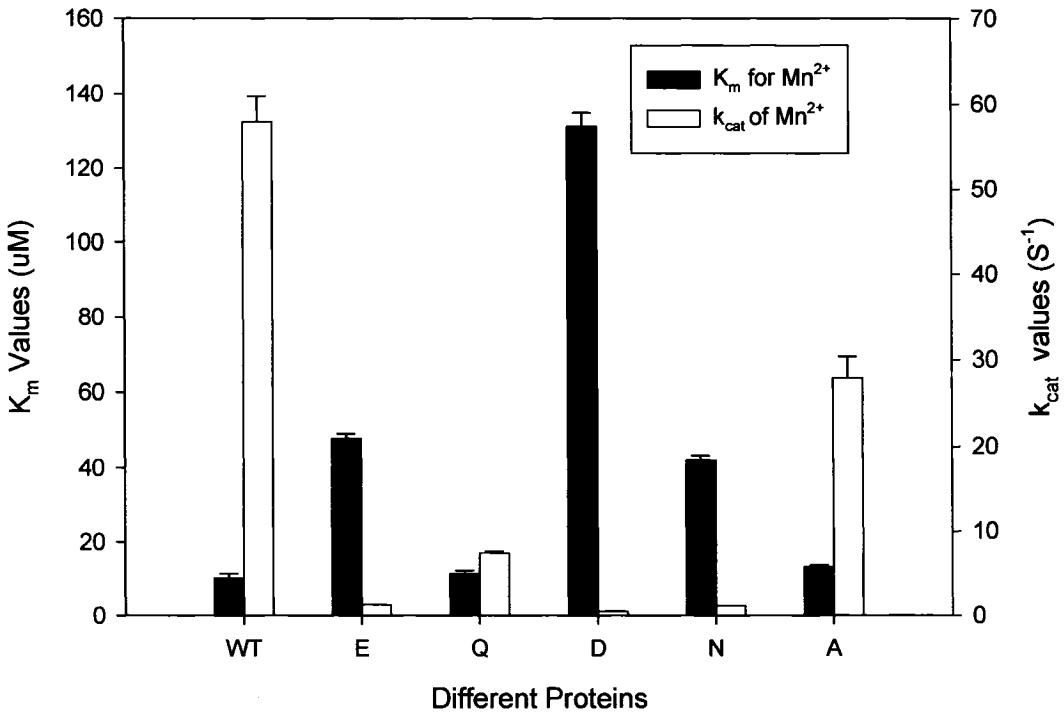

Figure 4.4: Bar graph of kinetic parameters obtained by varying Mn^{2+} concentration.

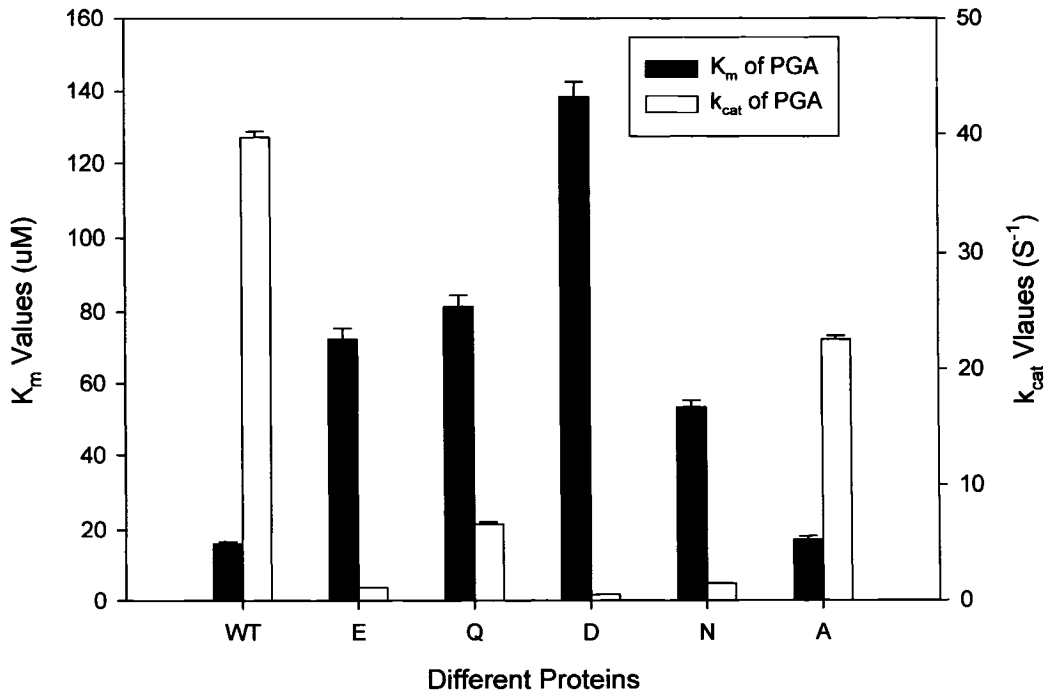

Figure 4.5: Bar graph of kinetic parameters obtained by varying PGA concentration.

As shown in Figure 4.3, the subunit interface stability is stabilized as the size of the substitution decreases. Therefore, the percentage of active dimeric form of enolase enzyme is proportionally increased. However, the turnover number (k_{cat}) and substrate/metal ion affinities (K_m) were not affected the same way. Clearly, the loss of catalytic efficiency was not due to the higher dissociation constant.

All of the variants, regardless of amino acid size, charge, and polarity, had lower substrate/metal ion affinities and/or turnover number than that of wild-type enzyme. Although the kinetic parameters of the variants seemed random at first, some general trend were observed. 1) Small non-polar substitution gave rise to kinetic parameters similar to that of wild-type enzyme. 2) Substitutions without the negative charge had higher activity. 3) When the side chain of the variant was shortened by one carbon, the activity decreased (E to D, Q to N).

As shown on Figure 4.4 and 4.5, the K_m values from both metal and substrate are generally higher for the variants than for wild-type enzyme. Only G376Q and G376A had a K_m value for metal like wild-type enzyme. Although the K_m value was not fully dependent on the size of amino acid substitution, G376Q result was puzzling. The result of G376A was as expected; being the smallest amino acid substitution, it had the smallest effect on the local conformation and enzyme catalysis. Due to the distance of the residue 376 from the groups involved in first metal binding, we believed that the mutation would mainly affect the second metal binding constant. The backbone of Gly376 is hydrogen bonded to Ser36 of the first mobile loop, which also contains Ser39, the only residue interacting with second metal ion. In fact, the result of G376D and N were different then predicted: their K_m values were higher than observed with G376E and Q. As seen in

structural analysis, G376D and N have more dimer like structure than E and Q. The orientation of the side chain may again be responsible, such that the side chain is disturbing the hydrogen bonding with the Ser36 loop, and affecting Ser39's metal binding ability. The K_m values of the variants from PGA saturation curves were increased by a similar ratio (~5- to 10-fold increase) as seen in the kinetic experiments varying metal concentration. The exception is the G376Q protein; it seems to possess an affinity towards Mn^{2+} like wild-type, but a weak affinity towards PGA. It is not clear how it may affect one aspect without affecting the other. However, it is clear that the substitutions at Gly376 affect affinities of both metal and substrate.

The turnover numbers (k_{cat}) obtained from both the metal and substrate saturation curves were significantly lower; in some cases the catalytic efficiency (k_{cat}/K_m) is 1500 fold less than that of wild-type enzyme. Surprisingly, even G376A's k_{cat} value was decreased by 2-fold. Since G376A protein exhibited wild-type-like spectroscopic characteristics, and affinity constants. The difference must originate from catalytic steps. It is not clear, at this stage, which catalytic step is affected, but it maybe the OH^- elimination step. As mentioned in the introduction, amino acid His373 is involved in hydrogen bonding network with the water molecule between Glu168 and Glu211. It is possible that the mutation at Gly376 affects the backbone flexibility and in turn affecting the catalysis.

The study of metal ion and substrate binding were faced with many difficulties. Being a method using the heat change associated in molecular interaction, ITC experiments need to be planned carefully. The number of processes or type of interaction

present in an experiment must be controlled to be minimal at all time. Some of our experiment may have introduced more than one factor that affected the heat change.

To study the first metal ion binding, the yeast enolase must be metal-free. This requires the removal of the metal ions from the active site. However, according to the work of B.H. Lee et. al, the first metal ion binds very tightly with a binding constant of 0.7 μM (*49*). To date, we have tested a few different methods reported previously to make wild-type yeast apo-enolase. None of them have shown an ITC result that suggests the protein was metal-free. It is our conclusion, that either the first metal ion was not removed or trace metal ions were introduced during the experiment. Furthermore, attempts to use Co^{2+} UV spectral changes to study metal binding failed as well (*77, 78*), perhaps due to the metal ion environment in yeast enolase. The signal changes were very small and could not be quantitated.

To study the substrate binding, we have tried a few different approaches. First of all, a substrate analogue, phosphonoacetic acid was used. The signal to noise ratio of this experiment was extremely high due to the interaction between this compound and metal ions. Others in the laboratory have tested the binding experiment of PhAH to enzyme in the presence of 1 mM Mn^{2+}, but the binding of PhAh was too tight to yield a reliable binding constant. Lastly, we have tried to use a mixture of natural substrate and product to titrate the Mn^{2+} containing enzyme sample. The wild-type enzyme yielded promising stoichiometry and two binding constants (see Table 3.21 and Table 3.22). We proposed that the wild-type is binding PGA and PEP with different affinity. However, when titrated separately, the ratio of bound species does not correspond to the PGA/PEP equilibrium ratio. It would be interesting, to test the PGA or PEP binding under

conditions where the metal ion concentration is limited. The data of G376E, although fit to a two-sites model, shows the stoichiometry of the second site is very small and assumed to be negligible (See Table 3.21). The binding constant however, is 10- to 100-fold lower compared to that of wild-type enzyme. Results of G376Q, D, and N ITC experiments are not presented since they did not make any sense. It is possible that the binding of the substrate is greatly altered, so that other interactions such as metal-PGA interaction became dominant.

The study of second metal ion binding in the presence of PhAH has yielded some promising results. Although the wild-type fits to a one-site model nicely, the mutants data could not. Instead, two-sites model was used and the values were listed in Table 3.23. The parameters of wild-type enzyme were similar to that of second site of the variants. The stoichiometry of the sites differs between wild-type and variant enzymes, and the binding constants obtained in this experiment were also different. While G376E, D have shown similar binding constants as that of wild-type enzyme (1~2 folds weaker binding), G376Q, N's binding constants were increased (tighter binding) by a factor of 10 (See Figure 4.6).

Based on the preliminary binding studies, the second metal ion binding is approximately the same or tighter, and the PGA/PEP binding is significantly weaker. The tighter binding of second metal ion can be explained by the hydrogen bonding property of the variant amino acid backbone and Ser36. If the backbone was in a orientation that pulls Ser36 inward, the mobility of the first loop might be more limited, thus bringing the Ser39 closer to the second metal ion. The weaker PGA/PEP binding of G376E can be

explained by the size of the mutant side chain. It is possible that the glutamic acid side chain is interfering with the substrate/product binding.

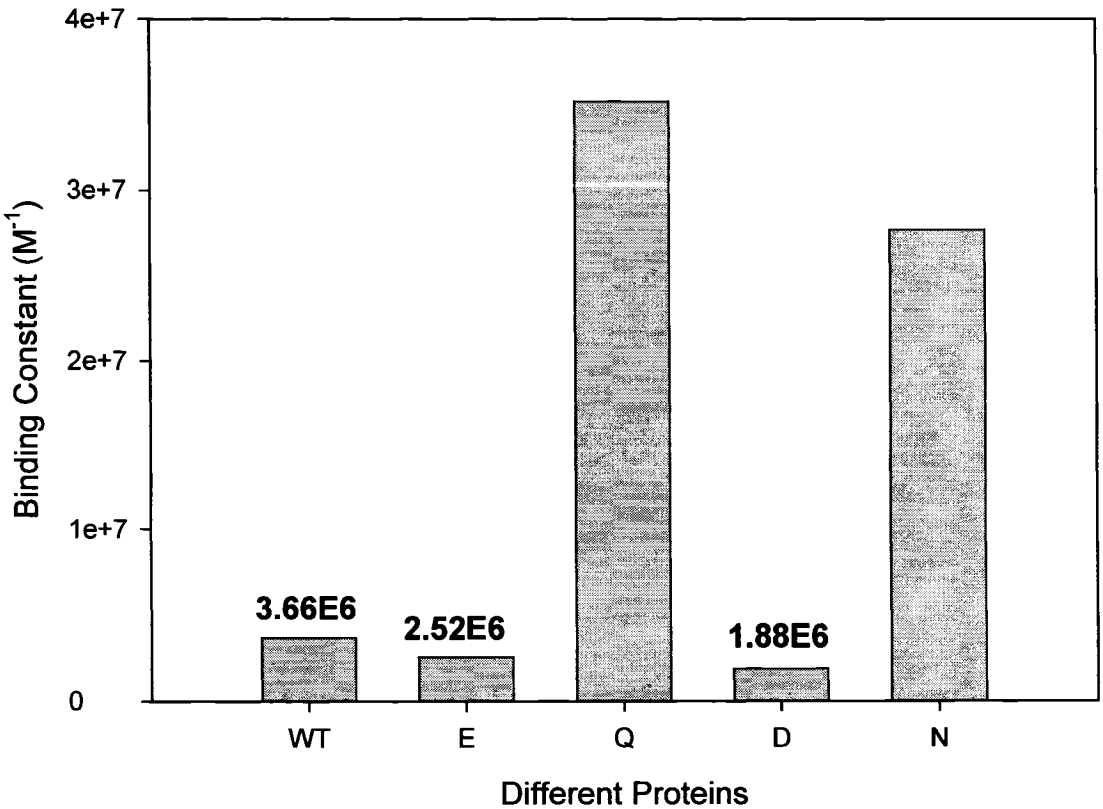

Figure 4.6: Bar graph of second metal binding constants.

Chapter 5

Conclusions and Future Works

As demonstrated in the result section, most of the goals set in the beginning of this project were met. Efficient protocols of wild-type and variants purification are now well established. Although the overall secondary structure possibly remains same as wild-type enzyme, the local environment near the amino acid 376 is most likely altered. The dissociation constants of dimeric variants enolase to increase significantly, and they seemed to be related with the size of the amino acid substituted at position 376. As result, variants were more susceptible towards proteolytic cleavage because of the increased amount of monomeric protein. However, the chemical and thermal stabilities of the variants are not very different than that of wild-type protein. The kinetic studies showed increased in K_m values, and significantly decreased k_{cat}. The catalytic efficiency is greatly decreased, suggesting rate-limiting step is possibly changed. Although still preliminary, the ITC results showed weaker substrate binding and same or tighter second metal ion binding constant. It may aide in explaining the decreased k_{cat} values. This project managed to show some of the effects of mutations at amino acid 376, in terms of protein structure, stability and catalysis.

Some work required to complete this project includes the followings:

1) Obtain crystal structure of the original mutant to verify the assumptions made based on spectroscopic techniques.
2) Perform more proteolytic digestion experiment on mutant to determine the other exposed regions in yeast enolase.

3) Perform proteolytic digestion experiment on ββ-enolase from rabbit using a variety of proteases.
4) Design more ITC experiment that gives more reliable results.
5) Kinetic experiment to determine which catalytic step is affected by the substitution at Gly376, such as kinetic isotope effect studies.

References

1. Wold, F. (1971) Enolase, in *The enzymes* (Boyer, P. D., Ed.) 3rd ed., pp 499-538, Academic Press, New York.
2. Warburg, O. C., Walter. (1942) Isolation and crystallization of enolase, *Biochemische Zeitschrift 310*, 384-421.
3. Fothergrill-Gilmore, L. A. (1986) in *Multidomain Proteins: Structure and Evolution* (Hardie, D. G., and Coggins, J.R., Ed.), pp 85-174, Elsevier Science Publishing Co. Inc., New York.
4. Chin, C. C. Q. (1990) The primary structure of rabbit muscle enolase, *J. Protein Chem. 9*, 427-432.
5. Holland, M. J., Holland, J.P., Thill, G.P., Jackson, K.A. (1981) The primary structure of two yeast enolase genes. Homology between the 5' noncoding flanking regions of yeast enolase and glyceraldehyde-3-phosphate dehydrogenase genes., *J. Biol. Chem. 256*, 1385-1395.
6. Chin, C. C. Q., Brewer, J.M., and Wold, F. (1981) The amino acid sequence of yeast enolase, *J. Biol. Chem. 256*, 1377-1384.
7. Chin, C. C. Q., Brewer, J.M., Eckard, E, Wold, F. (1981) The amino acid sequence of yeast enolase. Preparation and Characterization of peptides produced by chemical and enzymatic fragmentation., *J. Biol. Chem. 256*, 1370-1376.
8. McAlister, L., M. J. Holland. (1982) Targeted deletion of a yeast enolase structural gene. Identification and isolation of yeast enolase isozymes., *J. Biol. Chem. 257*, 7181-7188.
9. C. Kent Brown, P. L. K., Susan Mattingly, Kevin Slates, Patrick J. Calie, William W. Farrar. (1998) A Model of the quaternary structure of enolases, based on structural and evolutionary analysis of the octameric enolase from bacillus subtilis., *J. Protein Chem. 17*, 855-866.
10. Brewer, J. M. (1981) Yeast enolase: Mechanism of activation by metal ions., *CRC critical reviews in biochemistry 11*, 209-254.
11. Lebioda, L., Stec, B., Brewer, J.M. (1989) The structure of yeast enolase at 2.25 Å resolution. An 8-fold $\alpha+\beta$ barrel with a novel $\alpha\alpha\beta\beta(\alpha\beta)_6$ topology., *J. Biol. Chem. 264*, 3685-3693.
12. Larsen, T. M., Wedekind, J.E., Rayment, I., Reed, G.H. (1996) A carboxylate oxygen of the substrate bridges the magnesium ions at the active site of enolase: structure of the yeast enzyme complexed with the equilibrium mixture of 2-phosphoglycerate and phosphoenolpyruvate at 1.8 Å resolution., *Biochemistry 35*, 4349-4358.
13. Duquerroy, S., Camus, C., Janin, J. (1995) X-ray structure and catalytic mechanism of lobster enolase., *Biochemistry 34*, 12513-12523.
14. Kuhnel, K., Luisi, B. (2001) Crystal structure of the *Escherichia coli* RNA degradosome component enolase, *J. Mol. Biol. 313*, 583-592.
15. Chai, G., Brewer, J., Lovelace, L., Aoki, T., Minor, W., Lebioda, L. (2004) Expression, purification and the 1.8 Å resolution crystal structure of human neuron specific enolase., *J. Mol. Biol. 341*, 1015-1021.

16. Stec, B., Lebioda, I. (1990) Refined structure of yeast apo-enolase at 2.25 Å resolution, *J. Mol. Biol. 211*, 235-248.
17. Lebioda, L., Stec, B.,. (1991) Mechanism of enolase: The crystal structure of enolase-Mg^{2+}-2phosphoglycerate/phosphoenolpyruvate complex at 2.2 Å resolution., *Biochemistry 30*, 2817-2822.
18. Poyner, R. R., Larsen, T.M., Wong, S.W., Reed, G.H. (2002) Functional and structural changes due to a serine to alanine mutation in the active site flap of enolase., *Arch. Biochem. Biophys. 401*, 155-163.
19. Brewer, J. M., Glover, C.V., Holland, M.J., Lebioda, L. (1998) Significance of the enzyme properties of yeast S39A enolase to the catalytic mechanism., *Biochim. Biophys. Acta. 1383*, 351-357.
20. Wedekind, J. E., Poyner, R.E., Reed, G.H., Rayment, I. (1994) Chelation of serine 39 to Mg^{2+} latches a gate at the active site of enolase: Structure of the bis (Mg^{2+}) complex of yeast enolase and the intermediate analogue phosphonoacetohydroxamate at 2.7 Å resolution., *Biochemistry 33*, 9333-9342.
21. Zhang, E., Brewer, J.M., Minor, W., Carreira, L.A., Lebioada, L. (1997) Mechanism of enolase: The crystal structure of asymmetric dimer enolase-2-phospho-D-glycerate/enolase-phosphoenolpyruvate at 2.0 Å resolution., *Biochemistry 35*, 12526-12534.
22. Brewer, J. M., Holland, M.J., Lebioda, L. (2000) The H159A mutant of yeast enolase 1 has significant activity., *Biochem. Biophys. Res. Commun. 276*, 1199-1202.
23. Vinarov, D., Nowak, T. (1999) Role of His 159 in yeast enolase catalysis., *Biochemistry 38*, 12138-12149.
24. Poyner, R. R., Cleland, W.W., Reed, G.H. (2001) Role of metal ions in catalsis by enolase: An ordered kinetic mechanism for a single substrate enzyme., *Biochemistry 40*, 8009-8017.
25. Sangadala, V. S., Glover, C.V.C., Robson, R.L., Holland, M.J., Lebioda, L., Brewer, J.M. (1995) Preparation by site-directed mutagenesis and characterization of E211Q mutant of yeast enolase 1., *Biochim. Biophys. Acta. 1251*, 23-31.
26. Dino Vo, E. C., Boyer, P.D. (1971) Isotopic probes of the enolase reaction mechanism., *J. Biol. Chem. 246*, 4586-4593.
27. Stubbe, J., Abeles, R.H. (1980) Mechanism of action of enolase: Effect of the beta-hydroxy group on the rate of dissociation of the alpha-carbon-hydrogen bond., *Biochemistry 19*, 5505-5512.
28. Reed, G. H., Poyner, R.R., Larsen, T.M., Wedekind, J.E., Rayment, I. (1996) Structural and mechanistic studies of enolase, *Curr. Opin. Struct. Biol. 6*, 736-743.
29. Anderson, S. A., Anderson, V.E., Knowles, J.R. (1994) Primary and secondary kinetic isotope effects as probes of the mechanism of yeast enolase., *Biochemistry 33*, 10545-10555.
30. Kornblatt, M. J. (1996) The mechanism of rabbit muscle enolase: Identification of the rate-limiting steps and the site of Li^{+} inhibition site., *Arch. Biochem. Biophys. 330*, 12-18.
31. Cohn, M., Pearson, J.E., Rose, I.A. (1970) Nuclear magnetic resonance assignment of the vinyl hydrogen of phosphoenolpyruvate. Stereochemistry of the enolase reaction., *J. Am. Chem. Soc. 92*, 4095-4098.

32. Poyner, R. R., Laughlin, T., Sowa, G.A., Reed, G.H. (1996) Toward identification of acid/base catalysts in the active site of enolase: Comparison of the properties of K345A, E168Q, and E211Q variants., *Biochemistry 35*, 1692-1699.
33. Brewer, J. M. (1985) Specificity and mechanism of action of metal ions in yeast enolase, *FEBS Letters 182*, 8-14.
34. Brewer, J., Robsn, R.L., Glover, C.V.C., Holland, M.J., Lebioda, L. (1993) Preparation and characterization of the E168Q site-directed mutant of yeast enolase 1., *Proteins. Struct. Funct. Genet. 17*, 426-434.
35. Anderson, V. E., Weiss, P.M., Cleland, W.W. (1984) Reaction intermediate analogues for enolase, *Biochemistry 23*, 2779-2786.
36. Brewer, J. M., Glover, C.V.C., Holland, M.J., Lebioda, L. (1997) Effect of site-directed mutagenesis of His373 of yeast enolase on some of its pysical and enzymatic properties., *Biochim. Biophys. Acta. 1340*, 88-96.
37. Collins, K. M., Brewer, J.M. (1982) Circular dichroism (CD) studies on yeast enolase: Activation by divalent cations., *J. Inorg. Biochem. 17*, 15-28.
38. Brewer, J. M., Collins, K.M. (1982) Studies of the role of catalytic and conformational metals in producing enzymatic activity in yeast enolase., *J. Inorg. Biochem. 13*, 151-164.
39. Faller, L. D., Baroudy, B.M., Johnson, A.M., Ewall, R.X. (1977) Magnesium ion requirements for yeast enolase activity., *Biochemistry 16*, 3864-3869.
40. Brewer, J. M., Carreira, L.A., Collins, K.M., Duvall, M.C., Cohen, C., DerVartanian, D.V. (1983) Studies of activating and non-activating metal ion binding to yeast enolase., *J. Inorg. Biochem. 19*, 255-267.
41. Spencer, S. G., Brewer, J.M., Ellis, P.E. (1985) Cadmium (II)-113 NMR studies of the mechanism of metal ion activation of yeast enolase., *J. Inorg. Biochem. 24*, 47-57.
42. Chien, J. C., Westhead, E.W. (1971) Electron paramagnetic resonance study of the interaction of yeast enolase with activating metal ions., *Biochemistry 10*, 3198-3203.
43. Zhang, E., Hatada, M., Brewer, J.M., Lebioda, L. (1994) Catalytic metal ion binding in enolase; The crystal structure of an enolase-Mn^{2+}-phosphonoacetohydroxamate complex at 2.4 Å resolution., *Biochemistry 33*, 6295-6300.
44. Spencer, S. G., Brewer, J.M. (1984) Activation of yeast enolase by Cd (II), *J. Inorg. Biochem. 20*, 39-52.
45. Sinha, U., Brewer, J.M. (1984) Cu (II) activates yeast enolase, *J. Inorg. Biochem. 22*, 175-177.
46. Wang, S., Scott, R.A., Lebioda, L., Zhou, Z.H., Brewer, J.M. (1995) An x-ray absorption spectroscopy study of the interactions of Ni^{2+} with yeast enolase., *J. Inorg. Biochem. 58*, 209-221.
47. Rose., S. L., Dickinson, C., Westhead, E.W. (1984) Kinetic and physical properties of Co^{2+} enolase., *J. Biol. Chem. 259*, 4405-4413.
48. Lebioda, L., Stec, B., Brewer, J.M., Tykarska, E. (1991) Inhibition of enolase: The crystal structure of enolase-Ca2+-phosphoglycerate and enolase-Zn2+-phosphoglycolate complexes at 2.2 Å resolution., *Biochemistry 30*, 2823-2827.

49. Lee, B. H., Nowak, T. (1982) Influence of pH on the Mn^{2+} activation of and bind to yeast enolase: A functional study., *Biochemistry 31*, 2165-2171.
50. Elliott, J. I., Brewer, J.M. (1980) Binding of inhibitory metals to yeast enolase., *J. Inorg. Biochem. 12*, 323-334.
51. da Silva Giotto, M. T., Hannaert, V., Vertommen, D., de A S Navarro, M.V., Rider, M.H., Michels, P.A., Garratt, R.C., Rigden, D.J. (2003) The crystal structure of *Trypanosoma brucei* enolase: visualisation of the inhibitory metal binding site III and potential as target for selective, irreversible inhibition., *J. Mol. Biol. 331*, 653-665.
52. Kornblatt, M. J., Musil, R. (1990) The inhibition of yeast enolase by Li^{+} and Na^{+}. *Arch. Biochem. Biophys. 277*, 301-305.
53. Kornblatt, M. J., Klugerman, A. (1989) Characterization of the enolase isozymes of rabbit brain: Kinetic differences between mammalian and yeast enolase., *Biochem. Cell. Biol. 67*, 103-107.
54. Brewer, J. M., Faini, G.J., Wu, C.A., Goss, L.P., Carreira, L.A., Wojcik, R. (1978) Characterization of the subunit dissociation of yeast enolase. Physical aspects of protein interactions., pp 57-78, Elsevier/North-Holland, Amsterdam.
55. Brewer, J. M., Weber, G. (1968) The reversible dissociation of yeast enolase., *Proc. Natl. Acad. Sci. USA 59*, 216-223.
56. Brewer, J. M. (1969) Interactions of potassium chloride and acetate with yeast enolase., *Arch. Biochem. Biophys. 134*, 59-66.
57. Trepanier, D., Wong, C., Kornblatt, M.J. (1990) The salt-induced dissociation and inactivation of mammalian enolase: Evidence for the formation of active monomers., *Arch. Biochem. Biophys. 283*, 271-277.
58. Kornblatt, M. J., Al-Ghanim, A., Kornblatt, J.A.K. (1996) The effect of sodium perchlorate on rabbit muscle enolase. Spectral characterization of monomer., *Eur. J. Biochem. 236*, 78-84.
59. Keresztes-Nagy, S., & Orman, R. (1971) Dissociation of yeast enolase into active monomers, *Biochemistry 10*, 2506-2508.
60. Holleman, W. H. (1973) The use of absorption optics to measure dissociation of yeast enolase into enzymatically active monomers., *Biochim. Biophys. Acta. 327*, 176-185.
61. Kornblatt, M. J., Lange, R., Balny, C. (2004) Use of hydrostatic pressure to produce 'native' monomers of yeast enolase., *Eur. J. Biochem. 271*, 3897-3904.
62. Kornblatt, J. A., Kornblatt, M.J., Hui Bon Hoa, G. (1982) Second derivative spectroscopy of enolase at high hydrostatic pressure: An approach to the study of macromolecular interactions., *Biochemistry 34*, 1218-1223.
63. Comi GP, F. F., Lucchiari S, Bordoni A, Prelle A, Jann S, Keller A, Ciscato P, Galbiati S, Chiveri L, Torrente Y, Scarlato G, Bresolin N. (2001) Beta-enolase deficiency, a new metabolic myopathy of distal glycolysis, *Annals of Neurology 50*, 202-207.
64. Padovani, A. (2003) Characterization of subunit interactions versus catalysis in yeast enolase, in *Chemistry and Biochemistry*, p 155, Concordia University, Montreal.
65. Kreig, P., Melton, Doug. (1991) Nucleic acid sequencing and mutagenesis, in *Protocols and Application Guide* 2nd ed., pp 106-107, Promega Corporation.

66. Sambrook, F., Maniatis (1090) *Molecular Cloning*, Cold Spring Harbor Laboratory Press.
67. Sambrook, F., Maniatis (1989) *Molecular Cloning*, Cold Spring Harbor Laboratory Press.
68. Carrey, N. A. M. a. E. A. (1997) Peptide Mapping, in *Protein structure. A practical approach.* (Creighton, T. E., Ed.) Second Edition ed., pp 117-149, IRL Press at Oxford University Press, New York.
69. Sims, P. A. R., G.H. (2005) Method for the enzymatic synthesis of 2-phospho-D-glycerate from adenosine 5'-triphosphate and D-glycerate via D-glycerate-2-kinase., *J. Mol. Catal. B. 32*, 77-81.
70. Lange, R., Frank, J., Saldana, J-L., Balny, C. (1996) Fourth derivative UV-spectroscopy of proteins under high pressure I. Factors affecting the fourth derivative spectrum of the aromatic amino acids., *Eur. Biophys. J. 24*, 277-283.
71. Strickland, E. H. (1974) Aromatic contribution to circular dichroism spectra of proteins., *CRC Crit. Rev. Biochem. 2*, 113-175.
72. Ralston, G. (1993) *Introduction to analytical ultracentrifugation, for Beckman Instruments Inc.*
73. A.D. Malay, K. N. A., D.R. Tolan. (2005) Structure of the Thermolabile Mutant Aldolase B, A149P: Molecular Basis of Hereditary Fructose Intolerance, *J. Mol. Biol. 347*, 135-144.
74. A.D. Malay, S. L. P., D.R. Tolan. (2002) The temperature dependence of activity and structure for the most prevalent mutant aldolase B associated with hereditary fructose intolerance, *Arch. Biochem. Biophys. 408*, 295-304.
75. Philo, J. S. (2006) DCDT+, 2.0.5 ed., Thousand Oaks.
76. M.J. Kornblatt, J. A. K., G.H.B.Hoa. (1993) The role of water in the dissociation of enolase, a dimeric enzyme, *Arch. Biochem. Biophys. 306*, 495-500.
77. Rose, S. L., Dickinson, C., Westhead, E.W. (1984) Kinetic and physical properties of Co^{2+} enolase., *J. Biol. Chem. 259*, 4405-4413.
78. John C. Payne, B. W. R., Adam L. Tenderholt, and Hilary Arnold Godwin. (2003) Spectroscopic determination of the binding affinity of zinc to the DNA-binding domains of nuclear hormone receptors, *Biochemistry 42*, 14214-14224.